AEDC-TR-79-1

[redacted]

Vol I

[redacted]

David Hughes

Dup

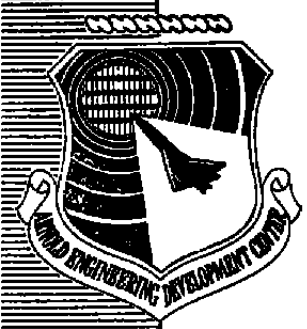

Store Separation Testing Techniques at the Arnold Engineering Development Center

Volume I
An Overview

J. B. Carman, Jr.
ARO, Inc.

August 1980

Final Report for Period October 1, 1978 – September 30, 1979

Approved for public release; distribution unlimited.

[redacted]

[redacted]

ARNOLD ENGINEERING DEVELOPMENT CENTER
ARNOLD AIR FORCE STATION, TENNESSEE
AIR FORCE SYSTEMS COMMAND
UNITED STATES AIR FORCE

NOTICES

When U. S. Government drawings, specifications, or other data are used for any purpose other than a definitely related Government procurement operation, the Government thereby incurs no responsibility nor any obligation whatsoever, and the fact that the Government may have formulated, furnished, or in any way supplied the said drawings, specifications, or other data, is not to be regarded by implication or otherwise, or in any manner licensing the holder or any other person or corporation, or conveying any rights or permission to manufacture, use, or sell any patented invention that may in any way be related thereto.

Qualified users may obtain copies of this report from the Defense Technical Information Center.

References to named commerical products in this report are not to be considered in any sense as an indorsement of the product by the United States Air Force or the Government.

This report has been reviewed by the Office of Public Affairs (PA) and is releasable to the National Technical Information Service (NTIS). At NTIS, it will be available to the general public, including foreign nations.

APPROVAL STATEMENT

This report has been reviewed and approved.

ALVIN R. OBAL, Captain, CF
Project Manager
Directorate of Technology

Approved for publication:

FOR THE COMMANDER

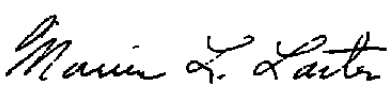

MARION L. LASTER
Director of Technology
Deputy for Operations

REPORT DOCUMENTATION PAGE	READ INSTRUCTIONS BEFORE COMPLETING FORM
1 REPORT NUMBER: AEDC-TR-79-1	2 GOVT ACCESSION NO. / 3. RECIPIENT'S CATALOG NUMBER
4 TITLE (and Subtitle): STORE SEPARATION TESTING TECHNIQUES AT THE ARNOLD ENGINEERING DEVELOPMENT CENTER, VOLUME I: AN OVERVIEW	5 TYPE OF REPORT & PERIOD COVERED: Final Report - October 1, 1978 - September 30, 1979 / 6 PERFORMING ORG. REPORT NUMBER
7 AUTHOR(s): J. B. Carman, Jr., ARO, Inc., a Sverdrup Corporation Company	8. CONTRACT OR GRANT NUMBER(s)
9 PERFORMING ORGANIZATION NAME AND ADDRESS: Arnold Engineering Development Center/DOT, Air Force Systems Command, Arnold Air Force Station, Tennessee 37389	10. PROGRAM ELEMENT, PROJECT, TASK AREA & WORK UNIT NUMBERS: Program Element 65807F
11 CONTROLLING OFFICE NAME AND ADDRESS: Arnold Engineering Development Center/DOS, Air Force Systems Command, Arnold Air Force Station, Tennessee 37389	12 REPORT DATE: August 1980 / 13. NUMBER OF PAGES: 88
14 MONITORING AGENCY NAME & ADDRESS(if different from Controlling Office)	15 SECURITY CLASS. (of this report): UNCLASSIFIED / 15a. DECLASSIFICATION/DOWNGRADING SCHEDULE: N/A

16 DISTRIBUTION STATEMENT (of this Report)

Approved for public release; distribution unlimited.

17 DISTRIBUTION STATEMENT (of the abstract entered in Block 20, if different from Report)

18 SUPPLEMENTARY NOTES

Available in Defense Technical Information Center (DTIC).

19. KEY WORDS (Continue on reverse side if necessary and identify by block number)

store separation
dynamic drop techniques
trajectory computer techniques
captive trajectories
free-drop techniques

20 ABSTRACT (Continue on reverse side if necessary and identify by block number)

The purpose of this report is to describe the formulation and basic composition of several store separation techniques (dynamic drop, wind tunnel computer simulation, and analytical computer simulation) along with the benefits and limitations of each. In the course of the report, guidelines are established for use in formulation of future store separation test and evaluation programs.

DD FORM 1 JAN 73 1473 EDITION OF 1 NOV 65 IS OBSOLETE

PREFACE

The work reported herein was conducted by the Arnold Engineering Development Center (AEDC), Air Force Systems Command (AFSC), at the request of the AEDC/DOT. The AEDC Project Manager was Mr. A. F. Money. The results of the research were obtained by ARO, Inc., AEDC Division (a Sverdrup Corporation Company), operating contractor for the AEDC, AFSC, Arnold Air Force Station, Tennessee, under ARO Project Number P32E-39D. The manuscript was submitted for publication on October 8, 1979.

This report is the first in a series of four volumes entitled "Store Separation Testing Techniques at the Arnold Engineering Development Center." Subtitles of these volumes are as follows:

Volume I	An Overview
Volume II	Description of Captive Trajectory Store Separation Testing in the Aerodynamic Wind Tunnel (4T)
Volume III	Description and Validation of Captive Trajectory Store Separation Testing in the von Kármán Facility
Volume IV	Description of Dynamic Drop Store Separation Testing

CONTENTS

Page

1.0 INTRODUCTION 7
2.0 DYNAMIC DROP TRAJECTORY TECHNIQUES
2.1 General 8
2.2 Three-DOF Equations of Motion 8
2.3 Dynamic Scaling Principles 9
2.4 Trajectory Comparisons 13
2.5 Applications 14
3.0 COMPUTER SIMULATION TRAJECTORY TECHNIQUES
3.1 General 17
3.2 AEDC Trajectory Generation Program 18
3.3 Wind Tunnel Applications 18
3.4 Analytical Applications 24
4.0 CONCLUDING REMARKS 26
REFERENCES 27

ILLUSTRATIONS

Figure

Page

1. Diagram of Trajectory Generation Options 31
2. Three-DOF Coordinate Notation 32
3. Summary of Dynamic Similarity Principles 33
4. Stable Store Aerodynamics 34
5. Aircraft Flow Field for Stable Store 35
6. Froude Scaling with Stable Store 37
7. Heavy Mach Scaling with Stable Store 39
8. Light Mach Scaling with Stable Store 40
9. Comparison of Heavy-Scaled Model and Flight Test Trajectory Data for the F-15 Aircraft, Empty 600-gal Tank, Inboard Pylon, $M_\infty = 0.88$, h = 21K ft 43
10. Simplified Block Diagram of a Trajectory Generation Computer Program 44
11. Positive Directions for the Body-Axis Coordinate System 45

Figure | Page

12. Body/Inertial/Flight Axes Directions for an Aircraft Pullup/Pushover Maneuver 46
13. Isometric Drawing of a Typical Store Separation Installation in Tunnel 4T and a Block Diagram of the Computer Control Loop 47
14. Isometric Drawing of a Typical Store Separation Installation in Tunnels B and C 48
15. Typical Separation Characteristics of a Slender-Finned Bomb from a Supersonic Fighter Aircraft 49
16. Typical Aerodynamic Coefficient Data Obtained on a Slender-Finned Bomb in the Flow Field of a Supersonic Fighter Aircraft 50
17. 40-deg Conical Probe 52
18. Flow-Field Measurements Beneath a Supersonic Fighter Aircraft 53
19. EOGB-II Models 55
20. 0.05-Scale MK-84 LDGP Bomb Model 57
21. Variation of the Zero-Lift Longitudinal Stability Derivatives and Axial-Force Coefficients of a Slender-Finned Bomb with Mach Number 58
22. Effects of Coefficient Corrections on a Typical Trajectory of a Slender-Finned Bomb 59
23. Effect of CTS Rig on Local Mach Number Distribution Obtained from a CTS-Mounted Static Probe 60
24. Typical Variation of Store Aerodynamic Coefficient Data in the Flow Field of a Supersonic Fighter Aircraft 61
25. Effect of Sway Braces on the Comparison of Wind Tunnel and In-Flight Measurements of Captive-Position Store Loads for the MK-83 Low-Drag Bomb, $M_\infty = 0.6$, F-4C Aircraft, Left Inboard Pylon, TER Position 1 62
26. Effect of Sway Braces on Separation Trajectories of the MK-83 Low-Drag Bomb from the F-4C Aircraft, Left Inboard Pylon, TER Station 1, Level Flight, 1,200-lb Ejector Force 63
27. Effect of Pitch-Damping Coefficient Variations on the Trajectory Motion of a Slender-Finned Bomb 64
28. Potential Extension of a Foreshortened Captive Trajectory with the Analytic Simulation Technique 65

APPENDIXES

Page

A. ANGULAR MOMENTUM 67
B. GENERALIZED MOMENT EQUATION AND ANGULAR ACCELERATIONS . 69
C. GENERALIZED FORCE EQUATION AND LINEAR ACCELERATIONS 74
D. FULL-SCALE FORCE AND MOMENT EQUATIONS 78
NOMENCLATURE 79

1.0 INTRODUCTION

As the operational flight speeds of military aircraft have increased, the problems associated with aircraft/store compatibility have increased significantly. Generally, this can be attributed to a large increase in the ratio of store aerodynamic to inertial forces caused by the increased flight speeds and to independent rather than integrated design of aircraft and stores. It is obvious that compatibility for the large number of aircraft/store combinations cannot be determined from full-scale flight tests alone: not only would the costs be prohibitive; the unnecessary risks to the pilot would also be unacceptable. Therefore, certification of aircraft/store load combinations for carriage and release must be obtained by other means and confirmed, as required, by flight tests.

Currently, many facets of aircraft/store compatibility are evaluated and verified from wind tunnel test data obtained on reduced scale models. For instance, aircraft stability, carriage loads, captive separation trajectory, aerodynamic grid survey, flow-field survey, store heat transfer, and dynamic drop separation trajectory tests are routinely conducted in the AEDC wind tunnels. However, this report considers only separation trajectory evaluation.

A separation trajectory can be defined as a time history of the position and attitude of a released store with respect to the aircraft. Separation trajectories generally fall into three categories. First, the released store may undergo a clean separation from the aircraft in a manner that allows a high probability of striking the desired target. Second, the released store may separate cleanly, but an unfavorable aircraft flow field could induce large pitch and/or yaw excursions such that on-board guidance equipment would fail to lock on target (guided weapon) or could so alter the initial ballistics of an unguided weapon as to cause impact well outside the acceptable targeting limits. Third, the aircraft flow field could conceivably cause the released store to "fly" back into the aircraft with potentially disastrous results. Obviously, no store would be certified for release at conditions where any real possibility of an aircraft/store collision existed. It would also be undesirable to release munitions under conditions that precluded any reasonable chance of a successful strike, even though the separations might be clean. Therefore, it is highly desirable, if not imperative, to define release conditions where the risk is lowest and the success probability greatest before flight testing is initiated.

Three basic approaches are available for generating separation trajectories: dynamic drop wind tunnel tests, wind tunnel computer simulations, and analytic computer simulations. The dynamic drop approach is strictly experimental while the computer

simulations may use experimental, semiempirical, or theoretical techniques (see block diagram, Fig. 1). The purpose of this report is to describe several of the options by which store separation characteristics may be generated and discuss the relative merits and shortcomings of each such that guidelines for their general use may be implied. This report is the first in a series of four volumes which describe store separation capabilities at the AEDC. Volumes II and III describe captive trajectory store separation testing in the AEDC Aerodynamic Wind Tunnel (4T) and Supersonic Wind Tunnel (A), respectively. Dynamic drop testing capabilities for all AEDC wind tunnels are given in Volume IV.

2.0 DYNAMIC DROP TRAJECTORY TECHNIQUES

2.1 GENERAL

As previously noted, separation trajectories by the dynamic drop (or free-drop) method must be effected experimentally. However, because of the nonsteady-state nature of the tests, it is necessary to simulate not only the applied forces, but also the inertial response of the store to these forces (Ref. 1). The aerodynamic forces can be simulated on a geometrically scaled model if the compressibility and viscous airstream effects are reproduced. The principles of dynamic similitude for reduced scale models are not new and have been well documented (e.g., Refs. 1 through 3). However, the method shown by Marshall (Ref. 1) will be used to establish the dynamic relationships for this report.

2.2 THREE-DOF EQUATIONS OF MOTION

By using simplified (three degrees of freedom) equations of motion and an earth-oriented coordinate system (see Fig. 2), the forces and moments on the store are described as:

$$m\ddot{X} = -\left[C_{A,t}\cos\theta + C_N \sin\theta\right] q_\infty A + F_{E1}\sin\theta \tag{1}$$

$$m\ddot{Z} = -\left[C_N \cos\theta - C_{A,t}\sin\theta\right] q_\infty A + F_{E1}\cos\theta + Wt \tag{2}$$

$$I_{YY}\ddot{\theta} = \left[C_m + C_{m_q}\left(\frac{\ell_1\dot{\theta}}{2V_\infty}\right)\right] q_\infty A\ell_1 - F_{E1}X_{E1} \tag{3}$$

If the angular motion is small and if flow-field spatial variations in streamline inclination and curvature can be represented by incremental values of angle of attack and pitching-moment coefficient, respectively, then the aerodynamic coefficients may be described as:

$$C_N = C_{N_\alpha}\left(\theta + \frac{\dot{Z}}{V_\infty} + \Lambda\alpha_s\right) \tag{4}$$

$$C_m = C_{m_\alpha}\left(\theta + \frac{\dot{Z}}{V_\infty} + \Delta\alpha_s\right) + \Delta C_m \tag{5}$$

$$\left.\begin{aligned} C_{A,t} &= \text{Constant} \\ C_{m_{\dot{q}}} &= \text{Constant} \\ C_{N_\alpha} &= \text{Constant} \\ C_{m_\alpha} &= \text{Constant} \end{aligned}\right\} \tag{6}$$

After the coefficient relationships are substituted, the motion equations become:

$$\frac{\ddot{X}}{g} = -\left[C_{A,t}\cos\theta + C_{N_\alpha}\left(\theta + \frac{\dot{Z}}{V_\infty} + \Delta\alpha_s\right)\sin\theta\right]\frac{q_\infty A}{mg} + \left(\frac{F_{E1}}{mg}\right)\sin\theta \tag{7}$$

$$\frac{\ddot{Z}}{g} = 1 - \left[C_{N_\alpha}\left(\theta + \frac{\dot{Z}}{V_\infty} + \Delta\alpha_s\right)\cos\theta - C_{A,t}\sin\theta\right]\frac{q_\infty A}{mg} + \left(\frac{F_{E1}}{mg}\right)\cos\theta \tag{8}$$

$$\ddot{\theta} = \left[C_{m_\alpha}\left(\theta + \frac{\dot{Z}}{V_\infty} + \Delta\alpha_s\right) + C_{m_q}\left(\frac{\ell_1\dot{\theta}}{2V_\infty}\right) + \Delta C_m\right]\frac{q_\infty A\ell_1}{I_{YY}} - \frac{F_{E1}X_{E1}}{I_{YY}} \tag{9}$$

2.3 DYNAMIC SCALING PRINCIPLES

From an examination of the previous three equations, one can deduce the dynamic simulation relationships which will produce comparable motion on model and full-scale stores. From the requirement of linear geometric scaling of stores and aircraft models (where λ is the scale factor), the relationships are as follows:

$$\left.\begin{aligned} A' &= A\lambda^2 & \theta' &= \theta \\ \ell_1' &= \ell_1\lambda & X_{cg}' &= X_{cg}\lambda \\ X' &= X\lambda & X_{E1}' &= X_{E1}\lambda \\ Z' &= Z\lambda \end{aligned}\right\} \tag{10}$$

where primed quantities represent model quantities.

If compressibility and viscous effects in the airstream are matched on the geometrically scaled models, then:

$$\left.\begin{aligned} C'_{N_\alpha} &= C_{N_\alpha} & C'_{A,t} &= C_{A,t} \\ C'_{m_\alpha} &= C_{m_\alpha} & C'_{m_q} &= C_{m_q} \end{aligned}\right\} \tag{11}$$

From the requirement that full- and model-scale values of $(\ddot{X}/g)$, $(\ddot{Z}/g)$ and $\ddot{\theta}$ be equal, the full- and model-scale values of the parameters $(\dot{Z}/V_\infty)$, $(q_\infty A/mg)$, (F_{E1}/mg), $(\ell_1\dot{\theta}/2V_\infty)$, $(q_\infty A\,\ell_1/I_{YY})$, and $(F_{E1}\,X_{E1}/I_{YY})$ must also be equal. The relationships of time, velocity (and Mach number), mass, inertia, and ejector force, respectively, are then determined to be:

$$t' = t\sqrt{\lambda(g/g')} \tag{12}$$

$$V'_\infty = V_\infty \sqrt{\lambda(g'/g)} \tag{13}$$

$$M'_\infty = M_\infty \sqrt{\lambda(g'/g)\,(T_\infty/T'_\infty)} \tag{14}$$

$$m' = m(\rho'_\infty/\rho_\infty)\,(V'_\infty/V_\infty)^2(g/g')\lambda^2 \tag{15}$$

$$I'_{YY} = I_{YY}(\rho'_\infty/\rho_\infty)\,(V'_\infty/V_\infty)^2(g/g')\lambda^4 \tag{16}$$

$$F'_{E1} = F_{E1}(\rho'_\infty/\rho_\infty)\,(V'_\infty/V_\infty)^2\,\lambda^2 \tag{17}$$

Noting that $g' = g$ and substituting the velocity relationship into the other equations gives

$$t' = t\sqrt{\lambda} \tag{18}$$

$$V'_\infty = V_\infty\sqrt{\lambda} \tag{19}$$

$$M'_\infty = M_\infty \sqrt{\lambda(T_\infty/T'_\infty)} \tag{20}$$

$$m' = m(\rho'_\infty/\rho_\infty)\lambda^3 \tag{21}$$

$$I'_{YY} = I_{YY}(\rho'_\infty/\rho_\infty)\lambda^5 \tag{22}$$

$$F'_{E1} = F_{E1}(\rho'_\infty/\rho_\infty)\lambda^3 \tag{23}$$

Equations (18) through (23) are generally referred to as the "Froude scaling" relationships because the velocity scaling is equivalent to the hydrodynamic Froude number.

As noted, the only stipulations for the Froude scaling principles are linear geometric scaling and aerodynamic coefficient equality. These, in turn, lead to the reduced velocity requirement (assuming $g' = g$) on the scaled models. As long as full-scale flight conditions are low subsonic, these relationships are compatible and valid. However, with the onset of significant airstream compressibility effects, model-scale aerodynamic data obtained at reduced velocity may no longer be equal to the full-scale values. Therefore, the useful test range of the Froude relationships is restricted to low subsonic flight conditions.

To insure aerodynamics matching, compromise simulation methods have been developed which require Mach number equality at the expense of another parameter. These Mach scaling techniques are commonly known as the "heavy" and "light" scaling principles. For heavy scaling, which is probably the most widely used scaling technique, the quantities $(\dot{Z}/V_\infty)$ and $(\ell_1\dot{\theta}/2V_\infty)$ are removed from the simulation. The relationships for heavy scaling which are changed from Froude scaling are then (assuming $g' = g$):

$$M'_\infty = M_\infty \tag{24}$$

$$V'_\infty = V_\infty \sqrt{(T'_\infty/T_\infty)} \tag{25}$$

$$m' = m(q'_\infty/q_\infty)\lambda^2 \tag{26}$$

$$I'_{YY} = I_{YY}(q'_\infty/q_\infty)\lambda^4 \tag{27}$$

$$F'_{E1} = F_{E1}(q'_\infty/q_\infty)\lambda^2 \tag{28}$$

The connotation "heavy scaling" may be deduced from the mass relationship. All else being equal, the mass of the heavy-scaled models will be larger than that for Froude-scaled models by a factor of $(1/\lambda)$ because of the increased velocity requirement. Because of the relaxed velocity ratio simulation, the heavy scaling principles do not properly account for induced angle of attack or aerodynamic damping effects. The amplitude of the angular motions will be too large because of reduced damping, and linear position will be affected by the dependence of the aerodynamic coefficients on angle of attack. However, previous work (Ref. 2) has indicated that the angle-of-attack error is never greater than 10 percent and that the damping error is of small consequence in studying body motion immediately after release, unless the rate of decay of oscillation is important.

When the angular motion response is deemed important, the light scaling principles may be used. Light scaling retains the velocity ratio simulations by assuming that the gravitational constant of the model-scale experiment may be arbitrarily increased, such that:

$$g' = g\left(\frac{V'_\infty}{V_\infty}\right)^2 \Big/ \lambda \tag{29}$$

The scaling relationships for light scaling which are changed from Froude scaling are then:

$$M'_\infty = M_\infty \tag{30}$$

$$V'_\infty = V_\infty \sqrt{T'_\infty / T_\infty} \tag{31}$$

$$F'_{E1} = F_{E1}(q'_\infty / q_\infty)\lambda^2 \tag{32}$$

$$t' = t\left[\lambda/(V'_\infty/V_\infty)\right] \tag{33}$$

The connotation "light scaling" is derived from the equality of the mass ratio with Froude scaling. Unless the increased gravitational requirement can be effected with a magnetic field (Ref. 4) or perhaps by accelerating the aircraft away from the store after separation occurs, the model will, in reality, be subjected to the gravitational acceleration "g" rather than "g'". The vertical acceleration will then be deficient by the amount

$$\Delta g' = g' - g = g\left[\frac{(V'_\infty/V_\infty)^2}{\lambda} - 1\right] \tag{34}$$

Consequently, vertical displacement will be too small. Up to the end of the ejector stroke, the correct motion can be produced with an increased ejector force such that:

$$\Delta F'_{E1} = m'\Delta g' \tag{35}$$

$$X'_{E1} = X_{E1}\lambda\left[F'_{E1}/(F'_{E1} + \Delta F'_{E1})\right] \tag{36}$$

Even so, with the gravitational acceleration deficient throughout the remainder of the trajectory, the risk of premature collision is increased. To avoid this possibility, the ejector force could be further augmented such that a velocity simulation match would be effected at a point in the flow field other than the end of the ejector stroke (typically one-half store length away from carriage). However, the velocity ratio simulation would be lost on either side of the match point.

Marshall (Ref. 1) has shown the feasibility of the augmented ejector force concept for light scaling and also has developed a correction factor which may be applied to the model-scale trajectory to account for insufficient gravity and the increased ejector force. The correction is an empirical relation which adjusts the model-scale vertical displacement curve and is defined as:

$$\Delta Z' = \tfrac{1}{2}(\Delta g')\,(t')^2 - \tfrac{1}{2}\left(\frac{\Delta F'_{E1}}{m'}\right)(t')^2 \qquad \text{for } (t' < t'_E) \tag{37}$$

$$\Delta Z' = \tfrac{1}{2}(\Delta g')\,(t')^2 - \tfrac{1}{2}\left(\frac{\Delta F'_{E1}}{m'}\right)(t'_E)\,(2t' - t'_E) \qquad \text{for } (t' \geq t'_E) \tag{38}$$

As may be seen, use of the correction requires that the time at the end of the ejector stroke (t'_E) be known. If, however, the value of (t'_E) is unknown, it can be estimated if one assumes no aerodynamic forces during ejector action. The resulting error in the corrected displacements typically will be on the order of 2 percent (Ref. 1).

2.4 TRAJECTORY COMPARISONS

To assess the relative merits and disadvantages of the dynamic scaling techniques, direct comparison of trajectories by each of the techniques with full-scale flight test trajectory results would be desirable. However, in the absence of flight test data, analytical trajectories were generated using the 3-DOF equations of motion of Section 2.2 (Ref. 1). (For reference, the Froude, heavy, and light scaling principles are summarized in Fig. 3). For full-scale flight conditions of $M_\infty = 0.95$ and altitude of 6,000 ft, trajectories were calculated on a 2,000-lb store (large, slender, finned bomb) using aerodynamic data as typically expected for the store and aircraft flow field (see Figs. 4 and 5, respectively). Using the same motion equations and aerodynamic data (except as noted), trajectories were then calculated for wind tunnel models which were designed according to each set of scaling laws and for the following conditions:

$$\left.\begin{aligned} \lambda &= 0.05 & q'_\infty &= 50 \text{ psf (Froude)} \\ T'_t &= 570^\circ\text{R} & q'_\infty &= 200 \text{ psf (Heavy)} \\ & & q'_\infty &= 600 \text{ psf (Light)} \end{aligned}\right\} \tag{39}$$

These trajectory results are presented in Figs. 6 through 8. When the transonic aerodynamic coefficient data of the full-scale store were used with the Froude-scaled model (Fig. 6a), the

model motion reproduced that of the full-scale store exactly. However, using transonic aerodynamic characteristics at the reduced velocity required for Froude scaling effectively ignores changes in aerodynamics between compressible and incompressible flow. When typical subsonic aerodynamic data are used with the Froude-scaled models (See Figs. 4 and 5), differences in full- and model-scale trajectories are large (Fig. 6b).

The heavy scaling trajectory data indicate an underdamped pitch oscillation for the model-scale trajectory because of incorrect velocity scaling (Fig. 7). However, the agreement obtained between full- and model-scale trajectory data is quite reasonable for the angular motion and quite good for the linear motions. The conclusions drawn from the heavy-scaled analytical data are confirmed by wind tunnel and flight test results from the F-15 aircraft (see Fig. 9 and Ref. 5).

Calculated trajectories for light-scaled models were determined for three conditions: (1) no ejector augmentation (Fig. 8a), (2) ejector force increased by the amount necessary to offset gravitational deficiency during the ejector stroke (see Section 2.3 and Fig. 8b), and (3) ejector force augmented by three times the amount used in the preceding case which provided the velocity simulation match near one-half body length from carriage (Fig. 8c). For all three cases, the angular motion of the full-scale trajectory was well matched by the model data, but, as expected, vertical position was considerably in error. However, when the vertical position correction factor (Ref. 1) was applied to the model data, agreement was quite reasonable. It should be noted that for all three scaling principles, similar trends were exhibited in trajectory data calculated for an unstable store of the 750-lb class (Ref. 1) such that the stable store results are not considered unique.

2.5 APPLICATIONS

The choice among the available techniques for the design of dynamic drop models is not an easy one. From a purely analytical standpoint, the selection of Froude scaling would be desirable since full-scale motion is reproduced exactly within the limits of the simulation. However, as previously mentioned, to choose Froude scaling with confidence would require almost certain knowledge that the store aerodynamic coefficients were invariant with Mach number. Unfortunately, experience has shown that aerodynamic data obtained around typical carriage locations at transonic and supersonic speeds will almost certainly be Mach number dependent; this condition effectively eliminates the choice of Froude scaling for many applications.

The trajectory data of Figs. 7 and 9 seem to substantiate the usual choice of heavy scaling as the alternative to Froude scaling. In all but the most demanding analyses, expected differences between model- and full-scale trajectory data would surely be within

acceptable limits. However, there are some practical problems inherent in this technique. The large model mass requirement quite often necessitates the use of high density materials such as tungsten, gold, iridium, or platinum in model fabrication. Disadvantages of these materials generally include one or more of the following: they are 1) not readily available, 2) difficult to machine, or 3) very expensive. Reduction of the dynamic pressure for the wind tunnel experiment could alleviate the high mass requirement somewhat but only at the further expense of the Reynolds number simulation.

A viable scaling alternative is the light scaling technique since it has been demonstrated (Ref. 1) that position error from insufficient vertical acceleration can be corrected. However, to establish the proper experimental parameters, a general knowledge of store behavior must be obtained in advance. Unfortunately, one of the primary reasons for free-drop testing is that a nonuniform and largely undefined aerodynamic flow field surrounds an aircraft at transonic and supersonic speeds. An additional disadvantage of this technique is that implementation of a large augmented ejector force on small-scale models may generate a completely new set of design problems which are comparable in complexity to those of heavy scaling.

The previous arguments have been confined to the relative merits and shortcomings of each of the dynamic drop techniques when compared to the others. However, the advantages and disadvantages of the dynamic drop experiment with respect to other trajectory acquisition techniques must also be considered in any practical applications. Some of the characteristics of the dynamic drop technique which may be considered advantageous are as follows:

1. Test results are valid within the limits of the scaling relationships.

2. Since no modifications are required on the reduced-scale stores to accommodate balance/sting combinations, no errors in the trajectory data will be introduced from anomalies in aerodynamic data caused by either configurational compromise or sting interference.

3. For weapons bay releases, trajectories may be initiated from the carriage position.

4. There are no hardware restraints to obstruct the motion of tumbling stores.

5. Several types of staged release separations can be simulated (for instance, pivoting fuel tank).

6. The dynamic drop technique is particularly suited for simulation of complicated loading separations such as multiple racks with a full or partial complement of stores.

7. Multiple or ripple releases can be accomplished.

Some of the characteristics of the dynamic drop technique which might be considered disadvantageous are as follows:

1. The use of a wind tunnel facility is required, and facility productivity must be considered in resource management. For the AEDC Aerodynamic Wind Tunnel (4T) and Propulsion Wind Tunnel (16T), approximately 1-1/2 to 2 drops per test hour can be accomplished for a single drop mode. Because of the model injection system of the AEDC Supersonic Wind Tunnel (A), it is estimated that 3 to 4 drops per test hour could be accomplished. (When multiple drops can be made during one run, productivity is correspondingly increased for all AEDC tunnels.)

2. A separate model is normally required for each trajectory. Although some models may be captured in a reusable state, model-catching screens are generally used only to salvage models for refurbishing and use in subsequent test programs.

3. Some store detail may be lost at reduced scale (for instance, lugs, conduits, radomes, etc.).

4. Models must be designed for the capabilities of the test facility. (This requirement is less critical for a variable density wind tunnel since a range of model weight would be valid for a given set of flight conditions) (see Fig. 3).

5. In the design and fabrication of wind tunnel models, it is often difficult to obtain the correct model inertia, weight, and center of gravity location simultaneously.

6. Only straight and level flight can be simulated. However, in much the same manner that vertical position corrections for insufficient gravity can be made for light scaling (see Section 2.3), corrections could be applied to the axial and vertical position data for first-order effects of climbing or diving flight.

7. Thrusting or active guidance system releases cannot be accomplished. Only jettison trajectories may be simulated.

8. Because of processing and reading requirements of the data film, access to final trajectory data is comparatively slow. Therefore, any decisions required to define test program direction must be based on visual interpretation of fast-processed film data.

To summarize briefly, the overall objectives of any separation analysis will dictate whether the acquisition of dynamic drop trajectory data is desirable. When free-drop trajectories are deemed necessary, selection of the proper scaling technique generally requires compromises. The choice which will be most advantageous to the particular experiment can be made only by familiarity with all the available options. A complete description of how the dynamic drop experimental data are obtained and evaluated at the AEDC is given in Volume IV of this series.

3.0 COMPUTER SIMULATION TRAJECTORY TECHNIQUES

3.1 GENERAL

Separation trajectories can be calculated on high-speed, digital computers if the full-scale forces and moments at any point along the trajectory path and the equations of motion of the released stores are known. A simplified block diagram showing essential elements of a trajectory generation computer program is presented in Fig. 10. The composition within the blocks may vary considerably among different trajectory generation programs depending on the complexity of the specific program, but all trajectory programs must perform in some manner the functions indicated.

Although the equations of motion are universal, the boundary conditions imposed dictate which terms must be retained for the simulation (free or restrained motion, number of degrees of freedom desired, etc.). In addition to the static aerodynamic forces and moments, the full-scale forces and moments in a comprehensive program will include the effects of aerodynamic damping, gravity, ejector forces and moments, thrust, jet damping, reaction forces and moments (to simulate staged release), and control inputs (to simulate active guidance systems, flap deflections, drogue chute deployment, etc.). The accelerations and velocities of the store can be numerically integrated using any of several available methods (Ref. 6). However, the greatest variations in computer simulation trajectory techniques probably exist in the method of defining aerodynamic coefficient data. Basically, two options are available (see Block diagram, Fig. 1). At each point along the trajectory

path, the aerodynamic coefficient data can be measured in the wind tunnel using reduced-scale models and a captive trajectory support (CTS) system or predicted using a flow-field math model. Each method will be described more fully in subsequent sections of this report.

3.2 AEDC TRAJECTORY GENERATION PROGRAM

At the AEDC, a basic trajectory generation package has been developed which can be used in conjunction with either the captive trajectory support systems or flow-field math models for separation trajectory generation. The general composition of this package is outlined as follows. The equations of motion allow for six-degrees-of-freedom movement of the released store and are given in Appendixes A, B, and C (see Fig. 11 for definition of the body-axis system). In addition to free motion releases, the equations include provisions for staged separation (e.g., pivoting fuel tanks, missile rail launches) and for accelerated flight (pullup/pushover aircraft maneuver only, see Fig. 12). Aircraft dive or bank maneuvers are simulated by adjusting the weight components of the store at release. Full-scale force and moment equations for a free-falling store are presented in Appendix D. As may be seen, terms are included to account for each of the items mentioned in Section 3.1. Of the force and moment parameters included, only the aerodynamic damping derivatives are normally assumed to be constant throughout a trajectory. Integration of the accelerations and velocities is accomplished using the Adams-Moulton (predictor-corrector) algorithm with a Runge-Kutta algorithm to start the process (Ref. 6). To permit the trajectory calculations in the corrector loop of the integration process to be made independently of data acquisition, aerodynamic coefficient data (C_Y, C_N, etc.) used in the force and moment calculations are obtained by extrapolation. The extrapolation is accomplished using a second-order polynomial to fit the time history of the last three calculated values of the coefficients. A complete description of the trajectory program is contained in Volume II of this series.

3.3 WIND TUNNEL APPLICATIONS

Much of the initial work in store separation testing was performed by the Naval Ship Research and Development Center (NSRDC) (Refs. 7 and 8). Some of the other wind tunnel facilities which conduct store separation tests include those of the LTV Aerospace Corporation (Ref. 9), the Office National d'Etudes et de Recherches Aérospatiales (ONERA, Ref. 10), the Weapons Systems Research Laboratory (WSRL, Ref. 11), the Cornell Laboratory (Calspan, Ref. 12), and the Aircraft Research Association, LTD, (ARA, Ref. 13).

For store separation testing using computer simulations, two separate and independent support systems are used to support the models. The aircraft model is attached to the tunnel

main support, and the store model is attached to the captive trajectory support (CTS) mechanism, which provides store movement (generally six degrees of freedom) independent of the aircraft model. An isometric drawing of a typical store installation in Tunnel 4T is shown in Fig. 13. The CTS mechanism for Tunnel 4T has been operational since 1968, and the initial description of system operation (Ref. 14) is superseded by Volume II of this series. The CTS mechanism for AEDC Tunnels A, B, and C (Fig. 14) has been operational since 1973, and a description of system operation is contained in Volume III of this series.

Wind tunnel tests which utilize either AEDC CTS system can be conducted in either the trajectory generation or grid mode. In the trajectory mode, the trajectory generation computer program (Section 3.2) is coupled with the CTS system through the facility digital computer in a closed-loop operation (Figs. 10 and 13). After the wind tunnel test conditions are established, aircraft model angle of attack is set, and the store model is located at the carriage position, the trajectory generation process is initiated. Each point along the trajectory is calculated using measured aerodynamic coefficient data and the applicable simulation parameters as inputs to the trajectory program. As each succeeding point is determined, the store model is automatically repositioned through commands to the CTS, and new aerodynamic data inputs are obtained. This process is repeated until trajectory completion. As may be seen, the only essential inputs provided by the wind tunnel for the simulation are the aerodynamic coefficient data. Typical trajectories as obtained in Tunnel 4T are presented in Fig. 15.

In the grid mode, the CTS system is also coupled with the facility digital computer for closed-loop operation. However, in this mode, the store model is automatically positioned by the CTS at selected locations and orientations with respect to the aircraft model (or in the free stream) which are pre-programmed into the computer. Typical aerodynamic coefficient data as obtained in Tunnel 4T are presented in Fig. 16.

In many CTS grid mode applications, the store/balance combination is replaced by a flow angularity probe (Fig. 17). For this case, local flow angles (Fig. 18) are the data output rather than aerodynamic coefficients. As might be expected, most of the experimental data obtained during CTS grid tests are used in the development of flow-field math models for analytical trajectory generation programs. However, at the WSRL (Ref. 11), experimental trajectories are generated using a flow angularity probe rather than a store model/internal balance combination because of the small scale of aircraft and store models required by wind tunnel size (typically, 0.02-scale models are used). The technique is similar to other experimental simulations except that each set of store aerodynamic coefficient data must be calculated using flow angles measured at 12 points along the predicted store centerline location instead of being directly measured with a store model/internal balance combination placed in the same position.

Advantages and disadvantages of wind tunnel computer simulations with respect to other trajectory acquisition techniques must be considered in the choice of techniques. Since this technique is experimental, many areas of concern are hardware related. Some of the advantageous characteristics of the wind tunnel computer simulation technique are as follows:

1. Test results are valid within the limits of the simulation. Herein lies probably the single greatest advantage of this technique (with respect to analytical techniques) in that measured store aerodynamic data are used to determine the trajectory path. The only assumptions regarding store aerodynamic behavior in the aircraft flow field are that Reynolds number and sting interference effects are small.

2. Test results are available at the completion of each trajectory, allowing almost real-time monitoring of the data. This markedly increases the flexibility and effectiveness of the test program since subsequent trajectory selections can be based on test results. When unanticipated trajectory trends make changes in test program direction necessary, the required changes can normally be accomplished quickly and easily.

3. Several parameters can be simulated which cannot be simulated in drop tests. These include aircraft acceleration (pullup/pushover maneuvers), aircraft dive angle, thrust, and active guidance.

4. The number of models required is substantially lower than for drop tests. Also, design and fabrication of the models is not as difficult since only the external shape of the store need be matched.

Several papers have been published which discuss a number of the problem areas associated with wind tunnel trajectory techniques (e.g., Refs. 15 through 17). Some of the characteristics of this technique which might be considered disadvantageous are as follows:

1. The use of a wind tunnel facility is necessary, and facility productivity must be considered in resource management. For example, approximately 4 to 5 trajectories (of 1-sec duration, full-scale time) can be accomplished per test hour in the AEDC wind tunnels. However, for trajectories of shorter duration, the productivity is correspondingly increased.

2. Some store detail may be lost at small scale. For example, comparison of 0.05-and 0.25-scale models of the EOGB-II (Fig. 19) indicates several items

(launch lugs, DME antenna, umbilical fitting, harness fairing, side conduit, wing fences, and flap gaps) which are present on the larger model but not on the smaller. In some cases, lifting surfaces (wings, canards, strakes) on full-scale stores have airfoil shapes, whereas those on small models are normally flat plates of the same planform with shaped leading and trailing edges. Correct alignment of lifting surfaces is also difficult at small scale. Some stores require external shape modification in order to accept a sting-balance combination. This is a particular problem on stores with long, tapering afterbodies such as the MK-84 LDGP (Fig. 20).

Whenever possible, it is desirable to determine the effects of reduced scaling on store aerodynamics. When discrepancies in the free-stream aerodynamic characteristics of different scale models are detected (for whatever reason), corrections can be applied to the small-scale model data during trajectory testing if so desired. For example, agreement among the free-stream data for three different scale slender bomb models (Fig. 21) is quite good at Mach numbers greater than 1, but at subsonic Mach numbers, the center-of-pressure location on the small-scale models is obviously further aft. For the subsonic case, the moment reference point of the small-scale models could be adjusted to bring the static margin more in line with the large-scale model data. However, in implementing this adjustment, it is assumed that aerodynamic effects in the curvilinear aircraft flow field are comparable to those in the free stream, which may or may not be the case. Unpublished AEDC data of D. W. Hill have shown that adjustments to the measured model data can result in substantial changes in trajectory motion (Fig. 22).

3. For sting-mounted models, the influence of the sting on measured aerodynamic data is perhaps always in question, especially at the large sting-to-model diameter ratio (about 0.3 to 0.5) normally required for structural integrity at small scale. Numerous reports have been published documenting sting effects on aerodynamic data (e.g., Refs. 18 through 20). Cahn (Ref. 18) noted that the drag characteristics on models with boattail afterbodies were particularly susceptible to sting effects at transonic Mach numbers and that surface pressure distributions could be altered as far upstream from the base as 40 percent of the length of the model. Changes in the pressure distribution on the store afterbody would almost certainly affect the moment characteristics as well. The data of Ref. 18 also showed that sting interference on drag diminished rapidly as ratio of straight sting length (no flares or bends) to base diameter increased. For a straight sting length of about six base diameters, interference effects were

negligible on most boattail configurations. Adherence to such a criterion for CTS sting-mounted models is not always possible, it is certainly desirable, especially for boattailed stores.

4. The presence of the CTS mechanism may influence store aerodynamic loads. Studies have been made in Tunnel 4T to determine effects of overall sting length (or the proximity of the CTS head with respect to the store cg) on measured aerodynamic data (Hill and Ref. 21). Typical data from Hill are presented in Figs. 23 and 24 which show effects of CTS proximity on wind tunnel Mach number and measured aerodynamic coefficients, respectively. On the basis of these results, a minimum sting length of 24 in. is recommended between the CTS yaw center and model center of gravity.

5. Some detail of the aircraft suspension equipment may be lost at small scale, such as ventilating slots or sway braces on multiple racks or pylons. Dix (Ref. 22) has shown improved correlation of wind tunnel and flight test results for MK-83 carriage loads aerodynamics when sway braces were present on a triple ejection rack (TER) model (Fig. 25). Dix has also determined that the presence of sway braces could sometimes have a significant effect on trajectory motion (Fig. 26). In view of these results, it is desirable to include as much detail as possible on the aircraft model suspension hardware.

6. Foreshortened trajectories usually result for rapidly pitching or tumbling stores because of CTS hardware limitations. The required store position/attitude in the aircraft flow field may cause the store model support sting or CTS to contact the aircraft or its support sting. Also, to set large trajectory attitudes may require a CTS position outside of the physical travel limits even though the store may still be in close proximity to the aircraft.

7. Store rolling capability is sacrificed when many offset and bent sting-support combinations are used in order to provide adequate clearance between the CTS- and aircraft-related hardware. How the loss of this degree of freedom is dealt with in the Tunnel 4T and VKF trajectory programs is contained in Volumes II and III of this series, respectively.

8. The spacing between the store model and suspension equipment at trajectory initiation can affect trajectory results. For a vibration-free environment, a gap between the model surface and suspension equipment of nominally 0.070 in., model scale (approximately 1.4 in., full scale) exists when the store model is

located at the carriage position. This roughly approximates full-scale values. However, because of vibration of the store or aircraft models, it is sometimes necessary to initiate trajectories at a greater distance from the carriage location to prevent premature collisions. Since aerodynamic gradients are usually large near carriage, nonrepresentative trajectories could result. It is generally recommended that the gap between store and aircraft suspension equipment be no greater than 0.150 in., model scale (approximately 3 in., full scale) at trajectory initiation.

9. Correcting the model attitude for angle of attack and sideslip angle induced by the motion of the full-scale store may produce changes in the interference aerodynamics. Because of the aerodynamic angles induced by lateral and vertical velocities of the store cg, the model cannot be positioned at the correct attitude with respect to both the relative wind vector and the aircraft. For the Tunnel 4T trajectory program, the angular position with respect to the relative wind vector was deemed more important, and the store model is positioned accordingly. For the VKF trajectory program, the model-induced angle corrections are recommended, but can be deleted as a program option. Fortunately, store velocities in the aircraft near flow field are usually not large; thus the small corrections for induced angles may result in only minimal errors in interference aerodynamics. At greater distances from carriage, store velocities (hence, induced angles) can be large, but substantial changes in store attitude when it is located in the aircraft far flow field may produce only negligible errors in the interference aerodynamics. The induced angle corrections for the Tunnel 4T and VKF trajectory programs are contained in Volumes II and III of this series, respectively.

10. The aerodynamic damping characteristics of most stores are not well defined even in the free stream and may well be sensitive to position and attitude in the highly nonuniform flow field surrounding a typical aircraft. Because of the lack of knowledge of damping values, aerodynamic damping derivative coefficients are input as constant values in most trajectory programs. However, this disadvantage is not only related to experimental trajectory programs but is a factor in computer simulations in general. Marshall and Summers (Ref. 23) determined that a ±50-percent variation in constant values of damping produced little change in trajectory motion for low amplitude angular excursions. However, Hill has shown that variations in aerodynamic damping can produce large differences in trajectory results for high amplitude angular motion (Fig. 27).

3.4 ANALYTICAL APPLICATIONS

As previously mentioned, the basic difference between analytical and experimental trajectory programs is in the method of definition of the aerodynamic coefficient data. For the analytical technique, aerodynamic characteristics of the released store are extracted from a flow-field math model. The basic options available in the design of such a math model are described in Fig. 1. In general, free-stream aerodynamics are combined with interference aerodynamics induced by the aircraft flow field to define the store total aerodynamic characteristics, which are then input into trajectory calculations. Either theoretical predictions or an empirical data base may be used to define free-stream and interference aerodynamics. However, to make accurate predictions, the flow-field model needs to consider the aerodynamic shape of the aircraft and store, aircraft angle of attack and sideslip angle, aircraft external store loading, free-stream Mach number, and the position and attitude of the store relative to the aircraft.

The formulation of a flow-field math model from an empirical data base is usually accomplished along the following guidelines. The free-stream aerodynamic characteristics are obtained from test data for the largest scale model available, since these data are more likely to be representative of full-scale store aerodynamics. Interference aerodynamics may be determined by the interference coefficient method or the flow angularity method.

In the interference coefficient method, a matrix of aerodynamic data is measured on a small-scale model at selected positions and attitudes in the aircraft flow field which are expected to encompass the subsequent trajectory path. Then free-stream aerodynamics (for the same store model at the same attitude) are subtracted from the flow-field aerodynamics to define the interference coefficients. In the process it is hoped that any effects of loss of detail at small scale on store aerodynamics will be minimized.

In the flow angularity method, flow angles are obtained with a flow angle probe at selected positions in the aircraft flow field. Using the flow angles relative to the store body and lifting surfaces, one can calculate interference aerodynamic coefficients.

Once the interference coefficients have been defined, total store aerodynamics used in the trajectory simulation are determined at each point along the trajectory path by adding the free-stream (function of attitude with respect to the relative wind) and interference (function of position and attitude with respect to the aircraft) contributions. (Although this description is intended primarily for empirical data, a math model using theoretical estimates for the aerodynamic coefficients or aerodynamic flow angles could be assembled in the same manner.)

A number of analytical trajectory programs have been developed for separation analysis. Nielsen Engineering and Research, Inc. (Refs. 24 through 26) used analytic computations such as slender body theory, the vortex-lattice method, and three-dimensional source distributions in the formulation of their flow-field model. Rockwell International (Ref. 27) and the Air Force Armament Laboratory (ADTC/DLJC) (Ref. 28) have developed flow-field models based on the flow angularity method. The ADTC/DLJC (Ref. 29) and Sandia Laboratories (Ref. 30) have developed flow-field math models based on the interference coefficient method. At the AEDC, most analytical trajectory programs use the interference coefficient method. Many other facilities have working analytical trajectory programs; those mentioned were selected simply to illustrate the diversity in the formulation of flow-field math models.

Advantages and disadvantages of the analytical computer simulations with respect to other trajectory acquisition techniques must be considered in their development and use. Some of the characteristics of the analytical computer simulation technique are as follows:

1. When compared to experimental techniques, the cost per trajectory for analytical simulations can be significantly lower. Obviously, considerable engineering and programming expense is involved in the development of an analytical program; however, once a program is developed, large numbers of trajectories can be calculated at a relatively small cost per trajectory.

2. Analytical simulations are quite flexible. Within the limitations of the flow-field model, the influence of a number of parameters may be investigated. In fact, parametric evaluations are ideally suited to this technique.

3. As for the wind tunnel computer technique, several parameters such as aircraft acceleration, aircraft dive angle, thrust, and active guidance can be simulated which cannot be simulated in drop tests.

4. Trajectory results are immediately available. No delays are inherent in this technique which might affect design decisions, flight clearance status, or subsequent analysis effort.

5. Analytical simulations can be accomplished which require no empirical data. However, as evidenced by the Nielsen program (Refs. 24 through 26), development of such simulations may require years of work. A complete description of nonuniform flow fields around complex configurations is not amenable to theoretical techniques at this time.

6. The flow angularity method is perhaps slightly more flexible than the interference coefficient method. Once the aerodynamic flow angles in an aircraft flow field are defined, trajectories for different shaped stores can be determined with minor adjustments to the flow-field calculations, and no additional empirical data are required (assuming the aircraft loading configuration is not altered). However, of all of the analytical flow-field models, those using the incremental coefficient method are probably the easiest to generate.

7. The adaptation of this technique for the extension of experimentally obtained trajectories which were prematurely terminated because of CTS hardware limitations is very feasible (Fig. 28). Development of this capability at the AEDC is currently in progress, and documentation should be completed in the near future. In many cases, extensions of this nature could provide the basis for additional testing or for release certification.

8. It is extremely difficult to develop a comprehensive flow-field model which accurately accounts for all variables. For this reason, the reliability of trajectories generated by analytical programs is not yet on a par with wind tunnel techniques and may be suspect unless demonstrated otherwise. It should be noted that good results have been obtained with this technique in many cases for limited flow-field applications (for example, see Figs. 22 and 27).

4.0 CONCLUDING REMARKS

As the sophistication of modern weaponry is increased and release certification is required at more demanding flight conditions, the complexity of store separation analysis programs must necessarily increase. Thus, more thorough planning will be required to effectively utilize the available prediction techniques in the attainment of overall program objectives. In the formulation of a test program, available resources (manpower for design, model fabrication, programming, and analysis; access to test and computer facilities; dollars; etc.) must be balanced against the advantages and disadvantages of each trajectory technique to arrive at the combination that will accomplish the objectives of the test program in the most timely and efficient manner. Obviously, this combination is almost certain to be unique for each specific application. In the discussion of the trajectory techniques in Sections 2 and 3, an attempt was made to present the benefits and limitations of each in such a way as to demonstrate their truly complementary nature, and, in so doing, to provide information which may be used for guidance in the formulation of future store separation test and evaluation programs. Specifically, use of the analytical simulation technique is encouraged whenever possible to aid in structuring efficient and cost effective wind tunnel test programs so that maximum benefit may be realized from the empirical data.

REFERENCES

1. Marshall, John C. "Analytical Evaluation of the Limitations of the Various Scaling Laws for Freedrop Store Separation Testing." Fourth Aircraft/Stores Compatibility Symposium Proceedings, Vol. 1, October 1977, pp. 197-234.

2. Deitchman, S. J. "Similarity Laws for Dynamic Model Testing." Cornell Aeronautical Laboratories Report No. CAL GC-910-C-14, September 1956.

3. Sandahl, C. A. and Faget, M. A. "Similitude Relations for Free-Model Wind-Tunnel Studies of Store-Dropping Problems." NACA-TN-3907, January 1957.

4. Stephens, T. "Wind Tunnel Simulation of Store Jettison with Magnetic Artificial Gravity." Aircraft/Stores Compatibility Symposium Proceedings, Vol. 3, December 1971, pp. 151-175.

5. Short, C. R., Capt., USAF and Lanterman, B. J. "A Pivot Mechanism to Provide an Extended Jettison Envelope for the F-15 Aircraft." Aircraft/Stores Compatibility Symposium Proceedings, Vol. 2, September 1973, pp. 237-254.

6. Henrici, Peter. *Discrete Variable Methods in Ordinary Differential Equations.* New York, John Wiley and Sons, Inc., 1964.

7. Bamber, M. J. "Two Methods of Obtaining Aircraft Store Trajectories from Wind Tunnel Investigations." Aero Report 970 (AD233198), David Taylor Model Basin, Washington, D. C., January 1960.

8. Nichols, James H., Jr. "A Method for Computing Trajectories of Stores Launched from Aircraft." DTMB-R-1878 (AD612515), David Taylor Model Basin, Washington, D.C., November 1964.

9. Wolfe, J. A. "A Computer-Controlled Wind Tunnel Testing System for Investigation of Aircraft or Booster Separation Problems." Aircraft/Stores Compatibility Symposium Proceedings, Vol. 3, December 1971, pp. 311-338.

10. Coste, Jacques. "Six Degrees of Freedom System for Store Separation Studies in ONERA Wind-Tunnels." Fourth Aircraft/Stores Compatibility Symposium Proceedings, Vol. 1, October 1977, pp. 293-304.

11. Heron, I. C. and Bishop, G. R. "The Software for the Captive Trajectory Yawmeter System." Weapons Systems Research Laboratory, Adelaide, South Australia, Technical Report WSRL-0005-TR, April 1978.

12. Cornell Aeronautical Laboratory Wind Tunnel. "Captive Trajectory Testing." WTO-461, August 1967.

13. Staff of the Aircraft Research Association. "Design Study for the Installation of a Two-Sting Rig for Captive Store Trajectory Simulation in the A.R.A. 9 ft x 8 ft Transonic Wind Tunnel." ARA Model Test Note M.76/1, Volumes 1, 2, and 3, January 1975.

14. Christopher, J. P. and Carleton, W. E. "Captive-Trajectory Store-Separation System of the AEDC-PWT 4-Foot Transonic Tunnel." AEDC-TR-68-200 (AD839743), September 1968.

15. Arnold, R. J., Braud, S. C., Lt., USAF, and Hill, D. W., Jr. "An Investigation of Factors Affecting the Accuracy of the Captive Trajectory Wind Tunnel Technique." Aircraft/Stores Compatibility Symposium Proceedings, Vol. 4, September 1973, pp. 141-177.

16. Arnold, R. J. and Epstein, C. S. "The Uses and Limitations of the Captive Trajectory System in Store Separation Analysis." Aircraft/Stores Compatibility Symposium Proceedings, Vol. 2, December 1971, pp. 307-373.

17. Bottoms, W. C. "Evaluation of the Captive Trajectory Technique of Wind Tunnel Testing for the Prediction of External Stores Flight Separation Trajectories." Aircraft/Stores Compatibility Symposium Proceedings, Vol. 3, December 1971, pp. 229-257.

18. Cahn, Maurice S. "An Experimental Investigation of Sting-Support Effects on Drag and a Comparison with Jet Effects at Transonic Speeds." NACA Report 1353, 1958.

19. Dix, R. E. "Influences of Sting Support on Aerodynamic Loads Acting on Captive Store Models." AEDC-TR-76-1 (ADA022257), March 1976.

20. Tunnell, Phillips J. "An Investigation of Sting-Support Interference on Base Pressure and Forebody Chord Force at Mach Numbers from 0.6 to 1.30." NACA RMA54K16a, January 1955.

21. Luchuk, Wallace and Hill, David W., Jr. "Evaluation of the Aerodynamic Interference of the Tunnel 4T Captive Trajectory System on the Separation Characteristics of the BLU-27 Store." AEDC-TR-76-142 (ADA032063), November 1976.

22. Dix, R. E. "Influences of Sway Braces and Mounting Gaps on the Static Aerodynamic Loading of External Stores." AEDC-TR-77-117 (ADA054963), February 1978.

23. Marshall, J. C. and Summers, W. E. "An Analysis of the Relative Importance of Parameters Required for the Simulation of Store Separation Trajectories." Aircraft/Stores Compatibility Symposium Proceedings, Vol. 2, December 1971, pp. 67-126.

24. Nielsen, Jack N., Goodwin, Frederick K., and Mansfield, Joseph A. "A Calculative Method for Predicting Store Separation Trajectories at Speeds up to the Critical Speed." Aircraft/Stores Compatibility Symposium Proceedings, Vol. IV, November 1969, pp. 4-1 to 4-25.

25. Goodwin, Frederick K., Dillenius, Marnix F. E., and Nielsen, Jack N. "Method of Predicting Loading and Trajectories of Single or TER or MER Mounted Stores on Swept-Wing Aircraft." Aircraft/Stores Compatibility Symposium Proceedings, Vol. 2, December 1971, pp. 231-305.

26. Stahara, S. S. et al. "A Rapid Predictive Method for Three-Dimensional Transonic Flow Fields about Parent Aircraft with Applications to External Stores." Fourth Aircraft/Stores Compatibility Symposium Proceedings, Vol. I, October 1977, pp. 155-195.

27. Blose, Terry G. and Barnes, Ralph M. "Launch Transient Analysis: Essential Element of Air-Launched Weapon Configuration Development." Aircraft/Stores Compatibility Symposium Proceedings, Vol. 1, September 1975, pp. 411-459.

28. Korn, Stephen C., Lt., USAF. "Use of the Flow Angularity Technique for Predicting Store Separation Trajectories." Aircraft/Stores Compatibility Symposium Proceedings, Vol. 2, December 1971, pp. 415-455.

29. Mathews, C. B. et al. "A Technique for Investigating the Launch and Separation of Guided Weapons." Aircraft/Stores Compatibility Symposium Proceedings, Vol. 1, September 1975, pp. 355-410.

30. Everett, Roger N. "A Comparison of Flight Test Results and 6-DOF Calculations Using the Incremental Coefficient Method for Store Releases from the F-111 Weapons Bay." Fourth Aircraft/Stores Compatibility Symposium Proceedings, Vol. 2, October 1977, pp. 813-839.

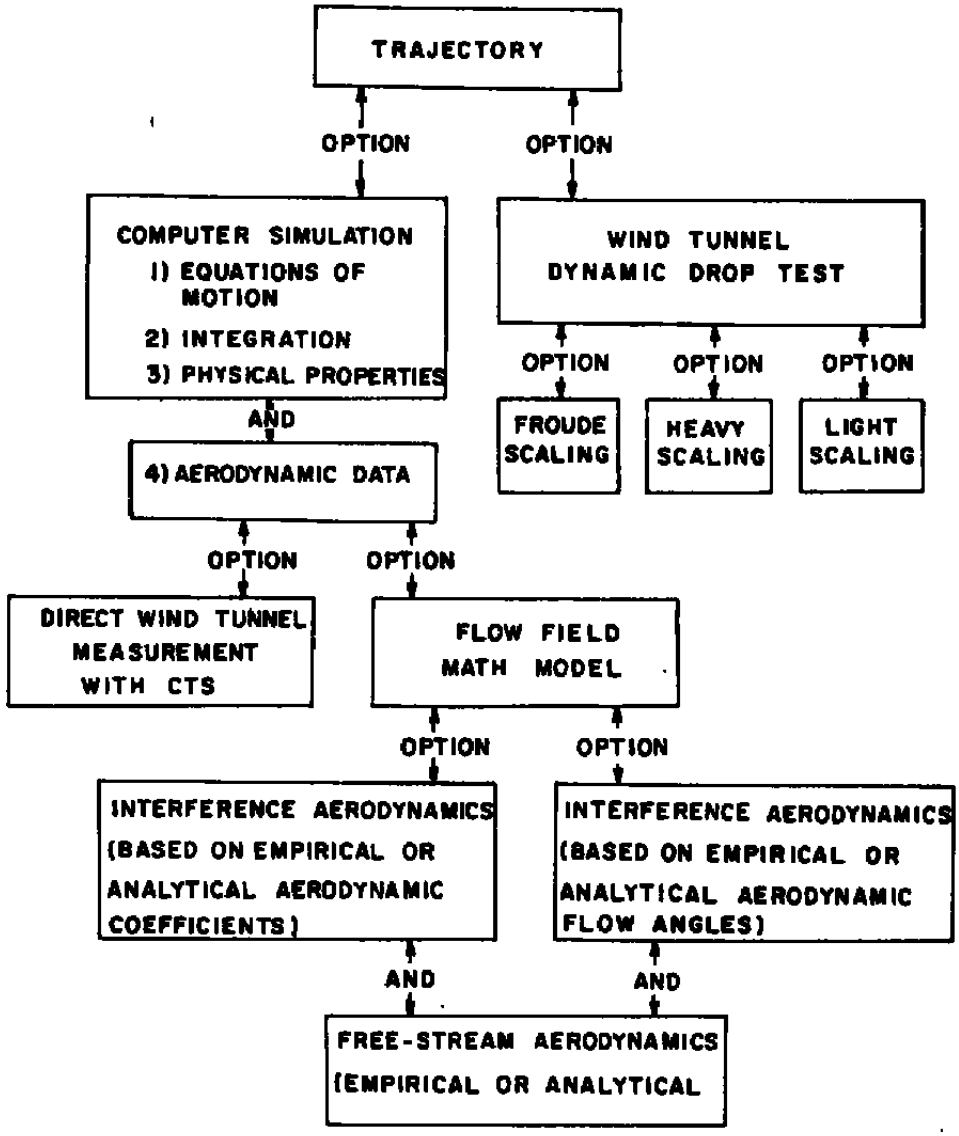

Figure 1. Diagram of trajectory generation options.

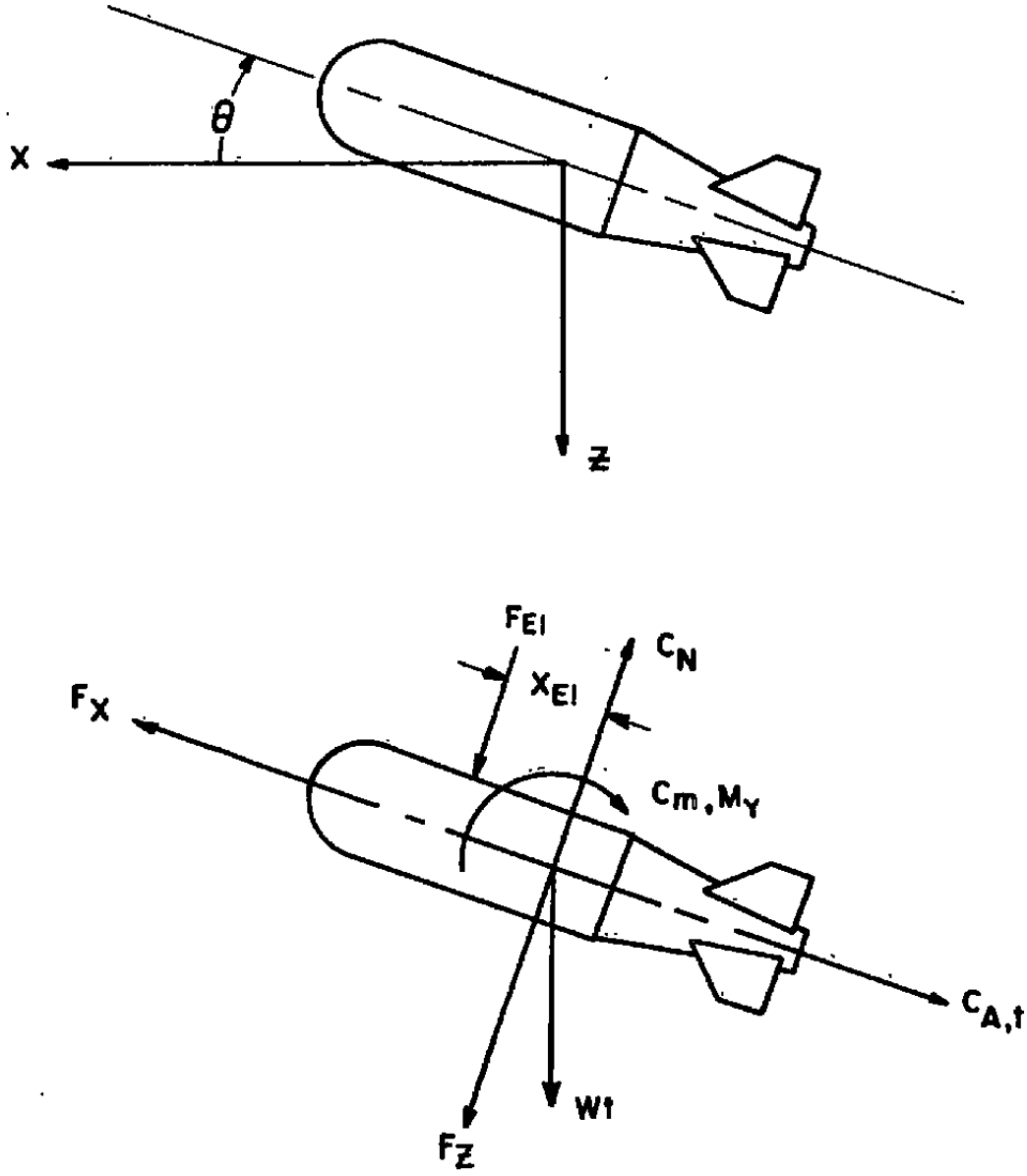

Figure 2. Three-DOF coordinate notation.

Parameter	Scaling Principle		
	Froude	Heavy	Light
A'/A	λ^2	λ^2	λ^2
$\ell_1'/\ell_1, \ell_2'/\ell_2, \ell_3'/\ell_3$	λ	λ	λ
X'/X, Y'/Y, Z'/Z	λ	λ	λ
θ'/θ, ψ'/ψ, ϕ'/ϕ	1	1	1
X_{cg}'/X_{cg}	λ	λ	λ
C_N'/C_N, C_Y'/C_Y, $C_{A,t}'/C_{A,t}$	1	1	1
C_m'/C_m, C_n'/C_n, C_ℓ'/C_ℓ	1	1	1
g'/g	1	1	$(V_\infty'/V_\infty)^2/\lambda$
V_∞'/V_∞	$\sqrt{\lambda}$	$\sqrt{(T_\infty'/T_\infty)}$	$\sqrt{(T_\infty'/T_\infty)}$
M_∞'/M_∞	$\sqrt{\lambda\,(T_\infty/T_\infty')}$	1	1
t'/t	$\sqrt{\lambda}$	$\sqrt{\lambda}$	$\lambda/(V_\infty'/V_\infty)$
m'/m	$(\rho_\infty'/\rho_\infty)\lambda^3$	$(q_\infty'/q_\infty)\lambda^2$	$(\rho_\infty'/\rho_\infty)\lambda^3$
I_{XX}'/I_{XX}, I_{YY}'/I_{YY}, I_{ZZ}'/I_{ZZ}	$(\rho_\infty'/\rho_\infty)\lambda^5$	$(q_\infty'/q_\infty)\lambda^4$	$(\rho_\infty'/\rho_\infty)\lambda^5$
F_{EI}'/F_{EI}	$(\rho_\infty'/\rho_\infty)\lambda^3$	$(q_\infty'/q_\infty)\lambda^2$	$(q_\infty'/q_\infty)\lambda^{2*}$
X_{EI}'/X_{EI}	λ	λ	λ^*

*To augment the ejector force for insufficient gravity up to the end of stroke:

$$\Delta F_{EI}' = m'g\left[\frac{(V_\infty'/V_\infty)^2}{\lambda} - 1\right]$$

$$X_{EI}'/X_{EI} = \lambda[F_{EI}'/(F_{EI}' + \Delta F_{EI}')]$$

Figure 3. Summary of dynamic similarity principles.

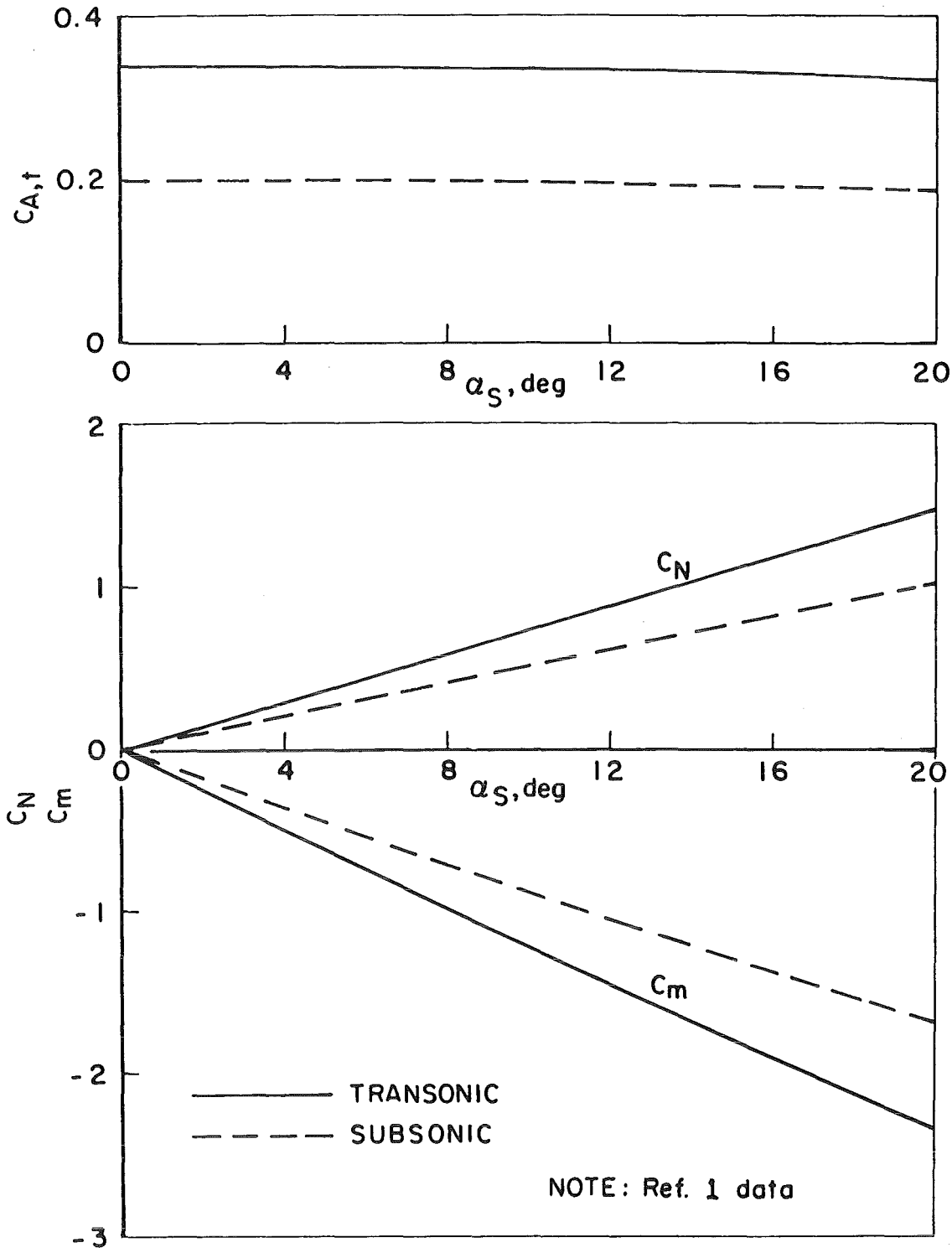

Figure 4. Stable store aerodynamics.

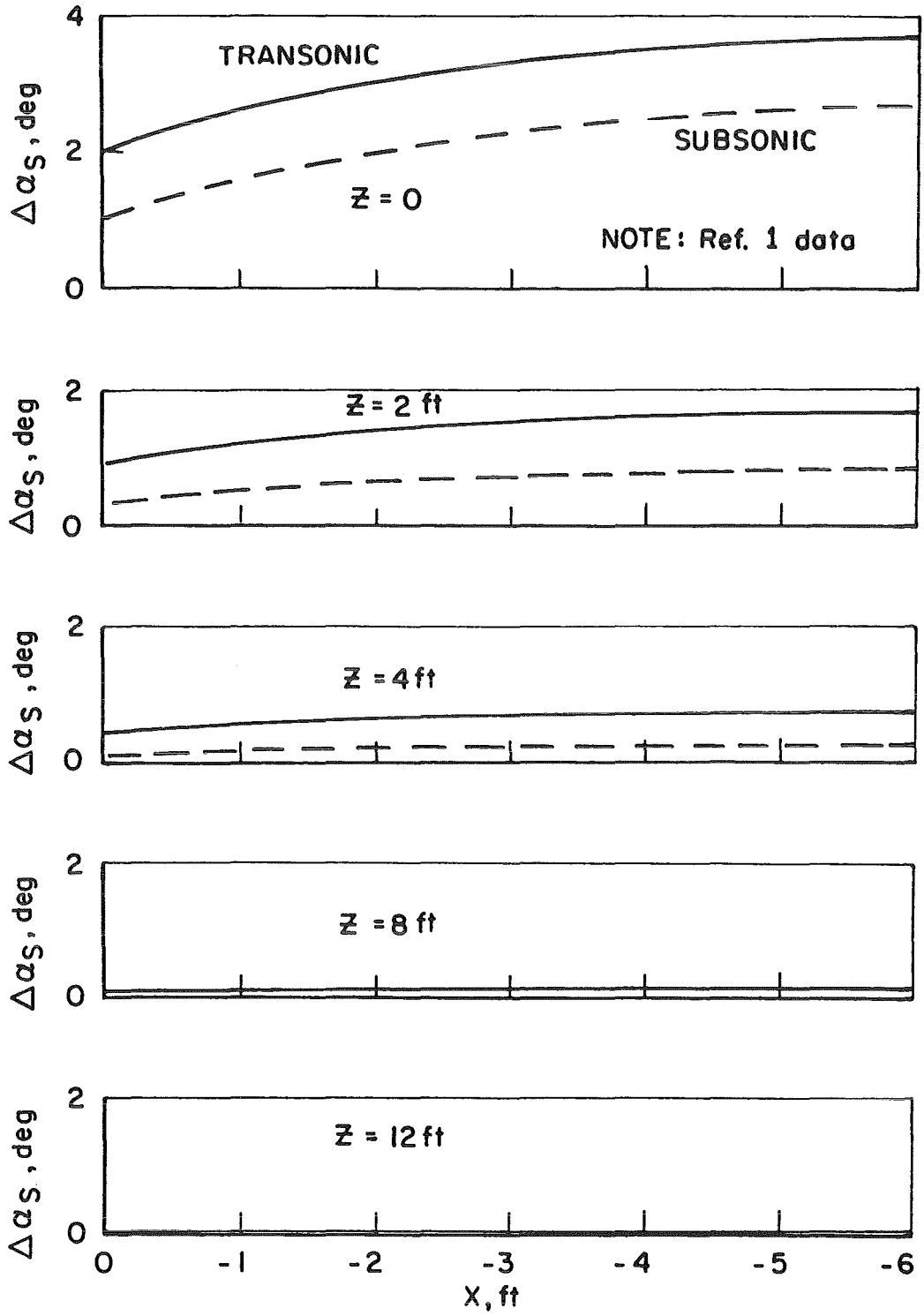

a. Incremental flow angle

Figure 5. Aircraft flow field for stable store.

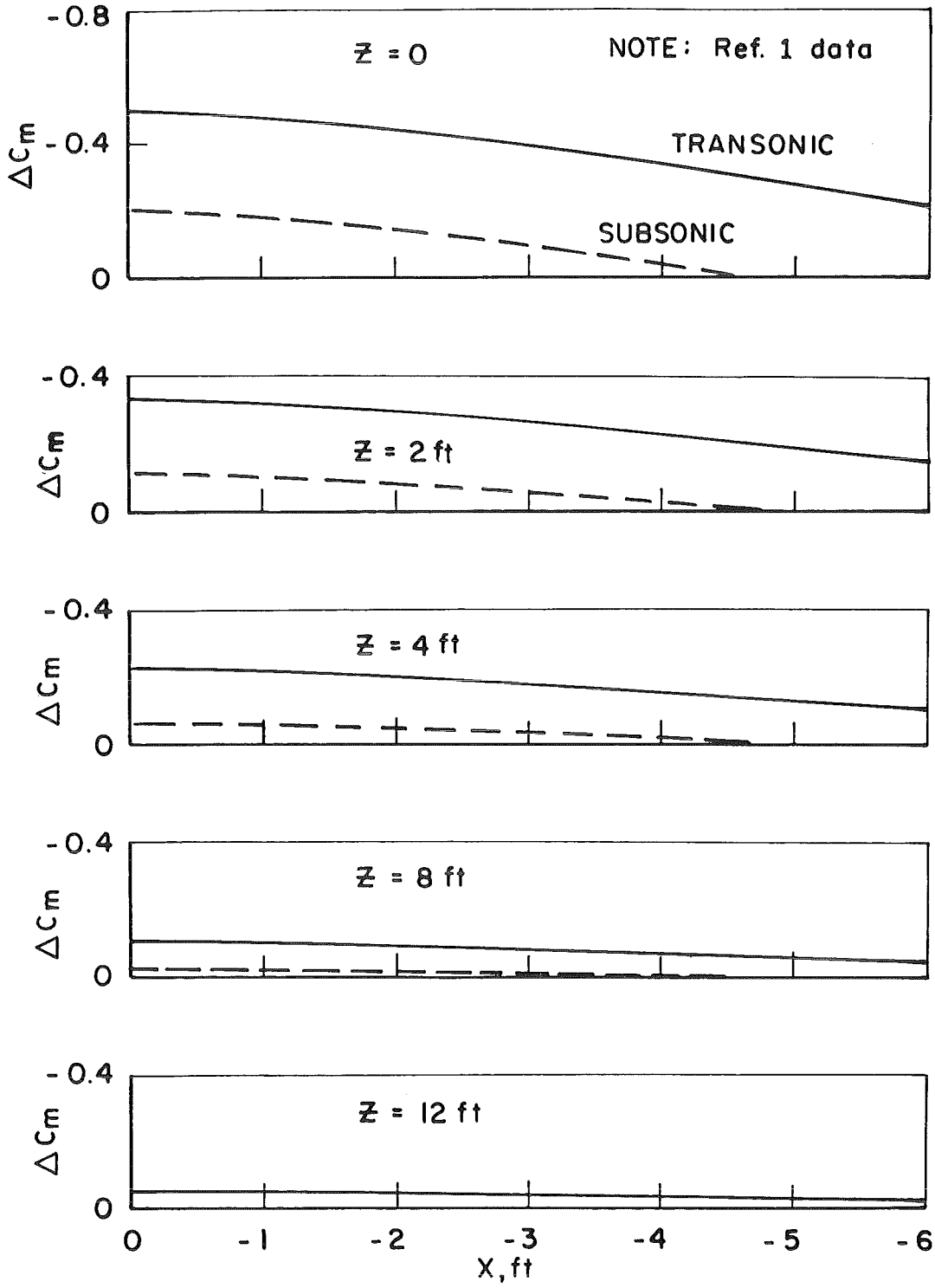

b. Incremental pitching-moment coefficient

Figure 5. Concluded.

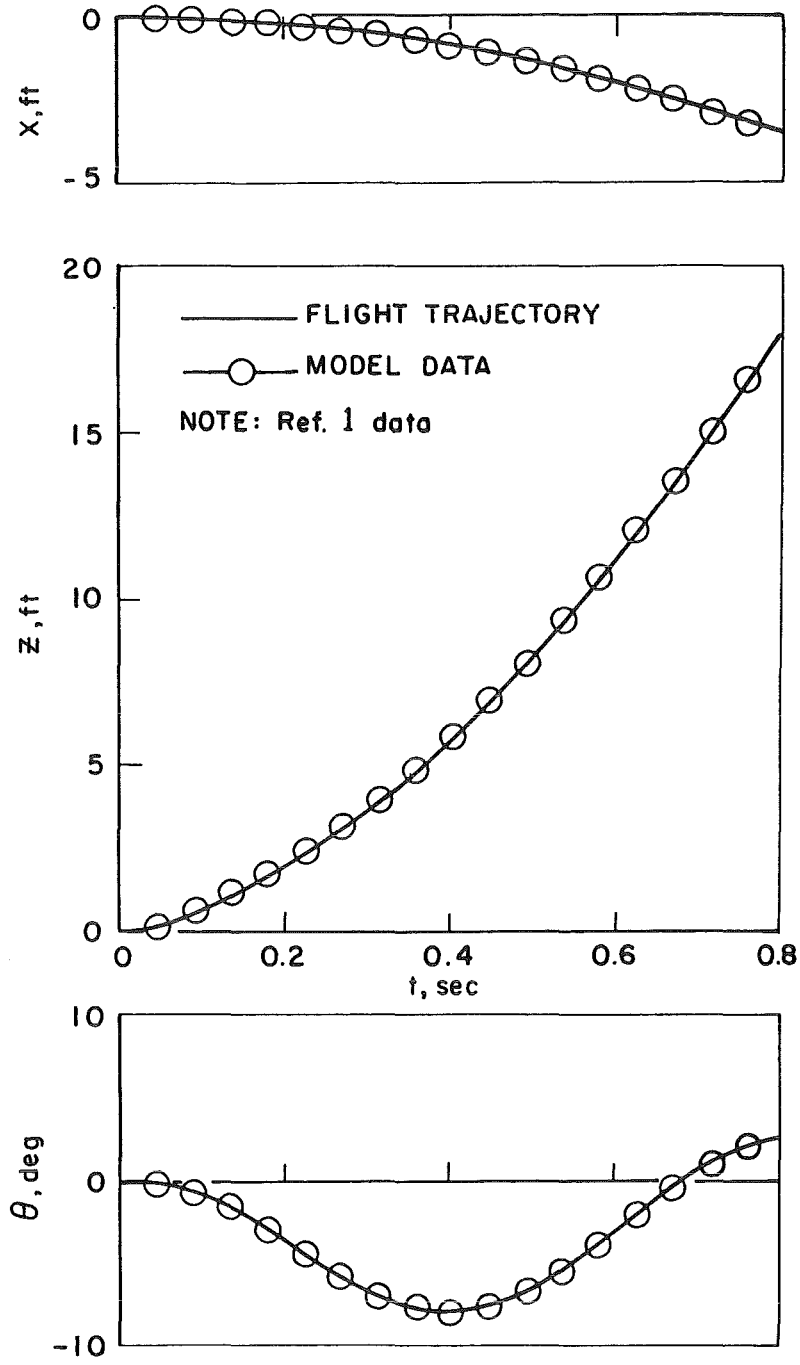

a. Transonic aerodynamics

Figure 6. Froude scaling with stable store.

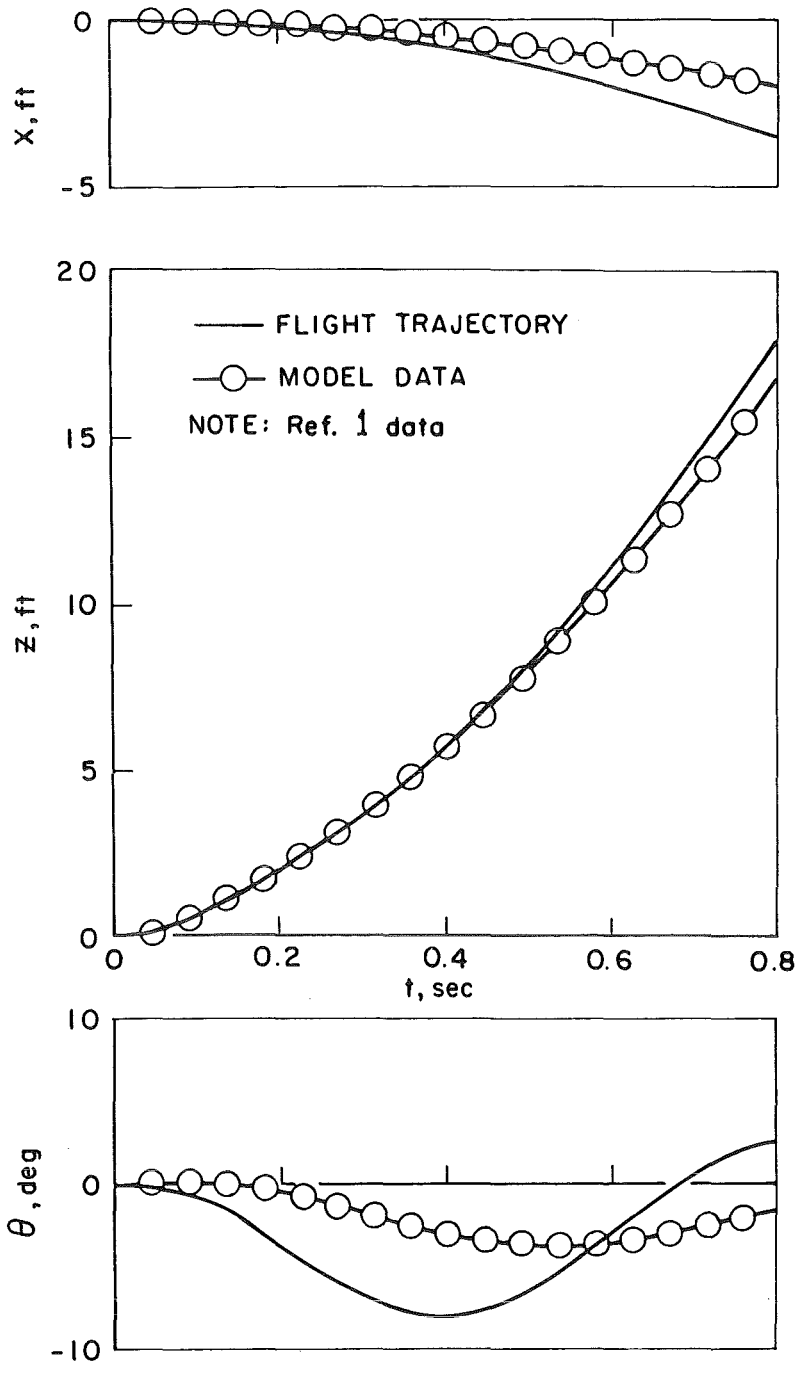

b. Subsonic aerodynamics
Figure 6. Concluded.

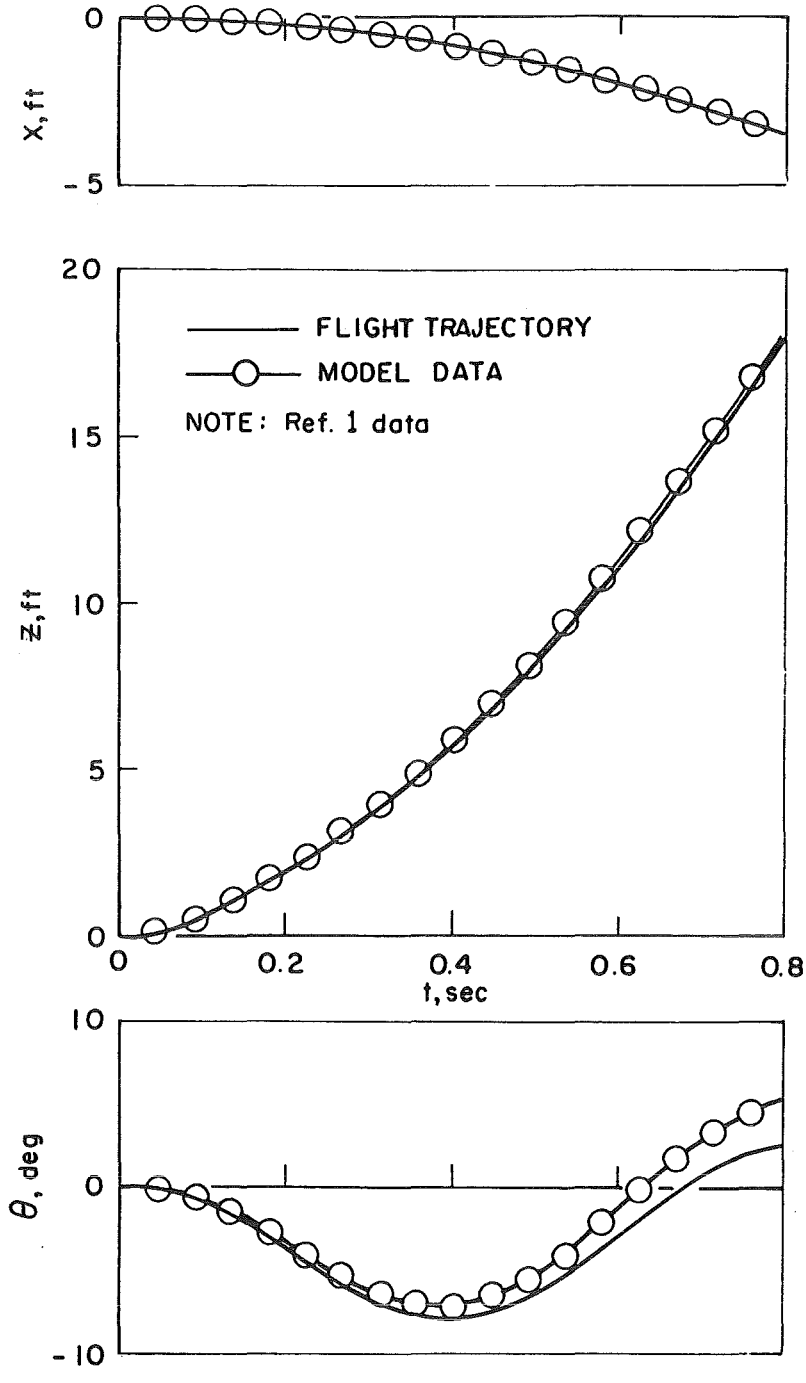

Figure 7. Heavy Mach scaling with stable store.

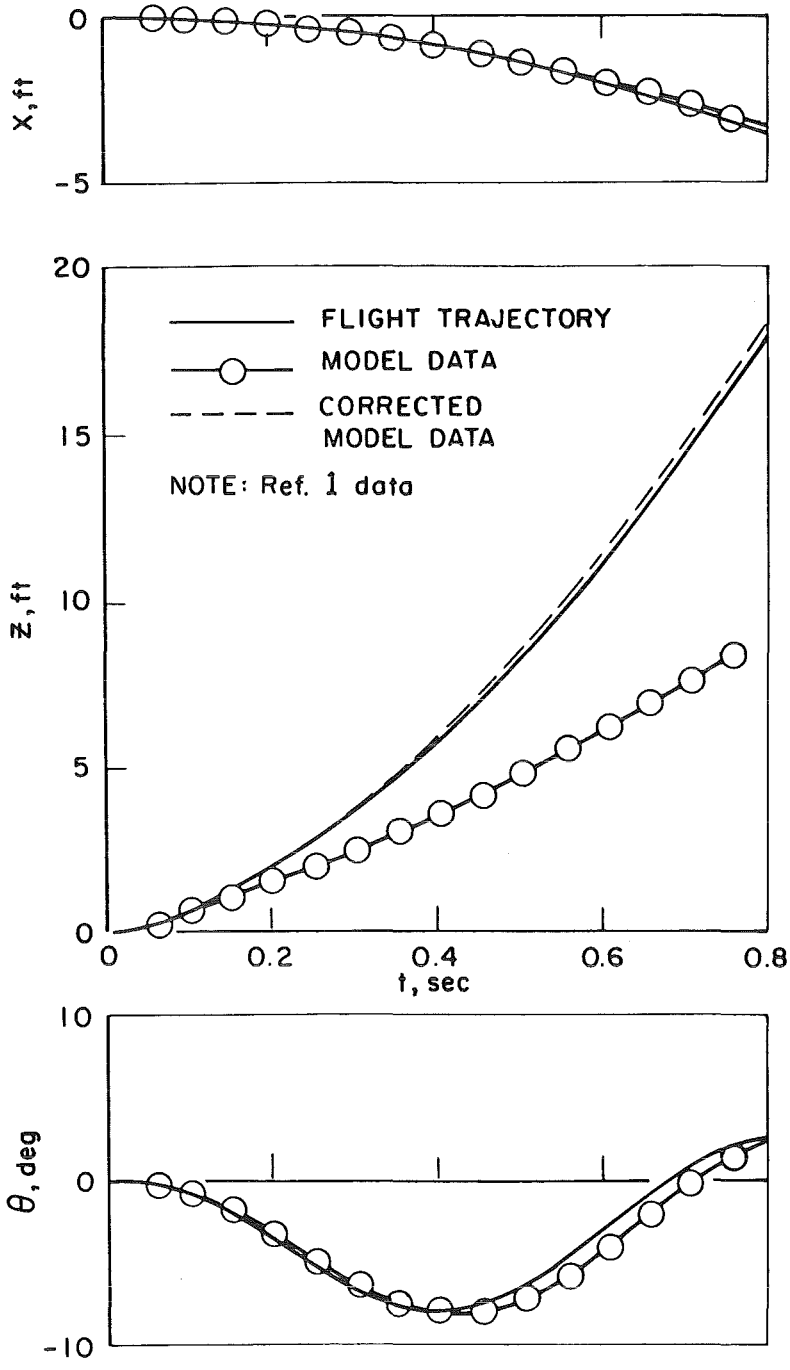

a. $\Delta F'_{E1} = 0$

Figure 8. Light Mach scaling with stable store.

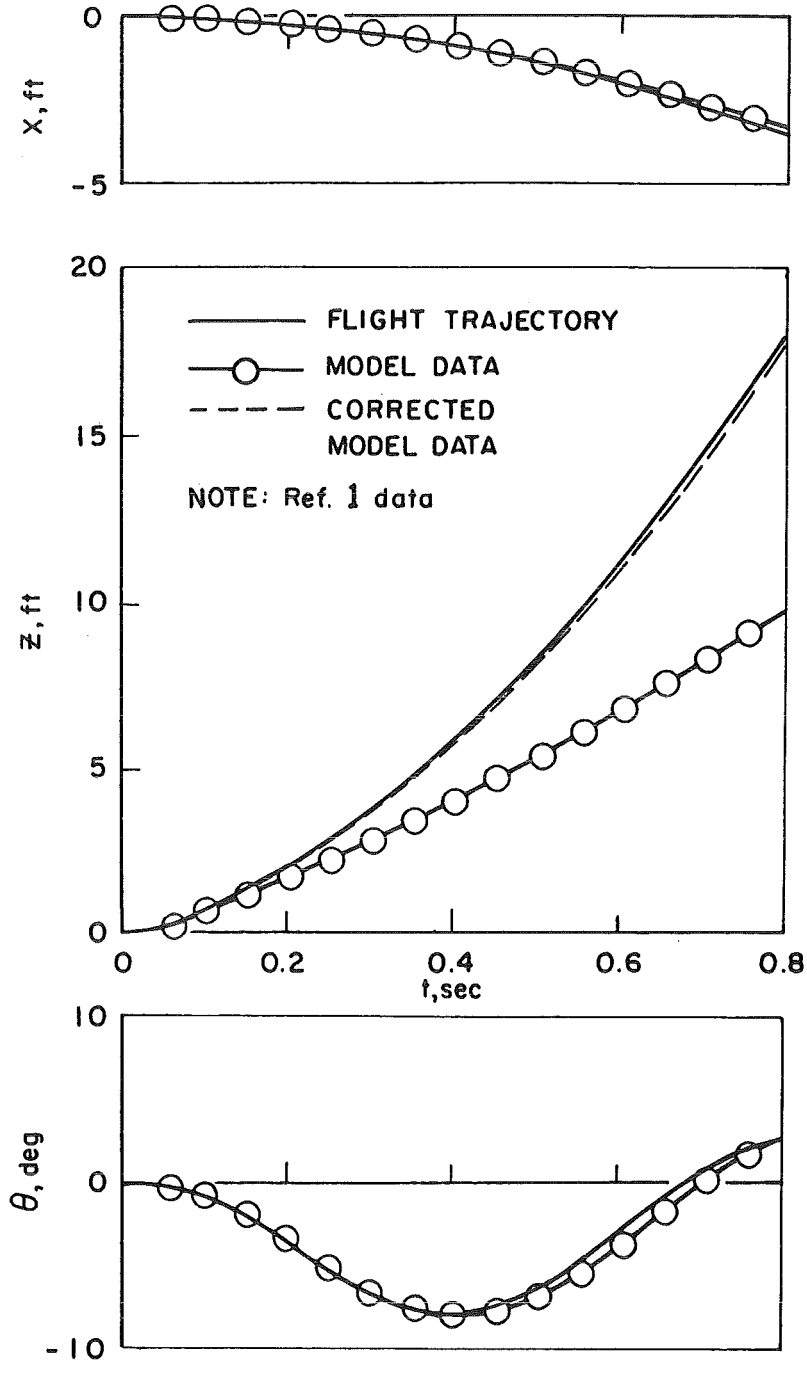

b. $\Delta F'_{E1} = m' (\Delta g')$

Figure 8. Continued.

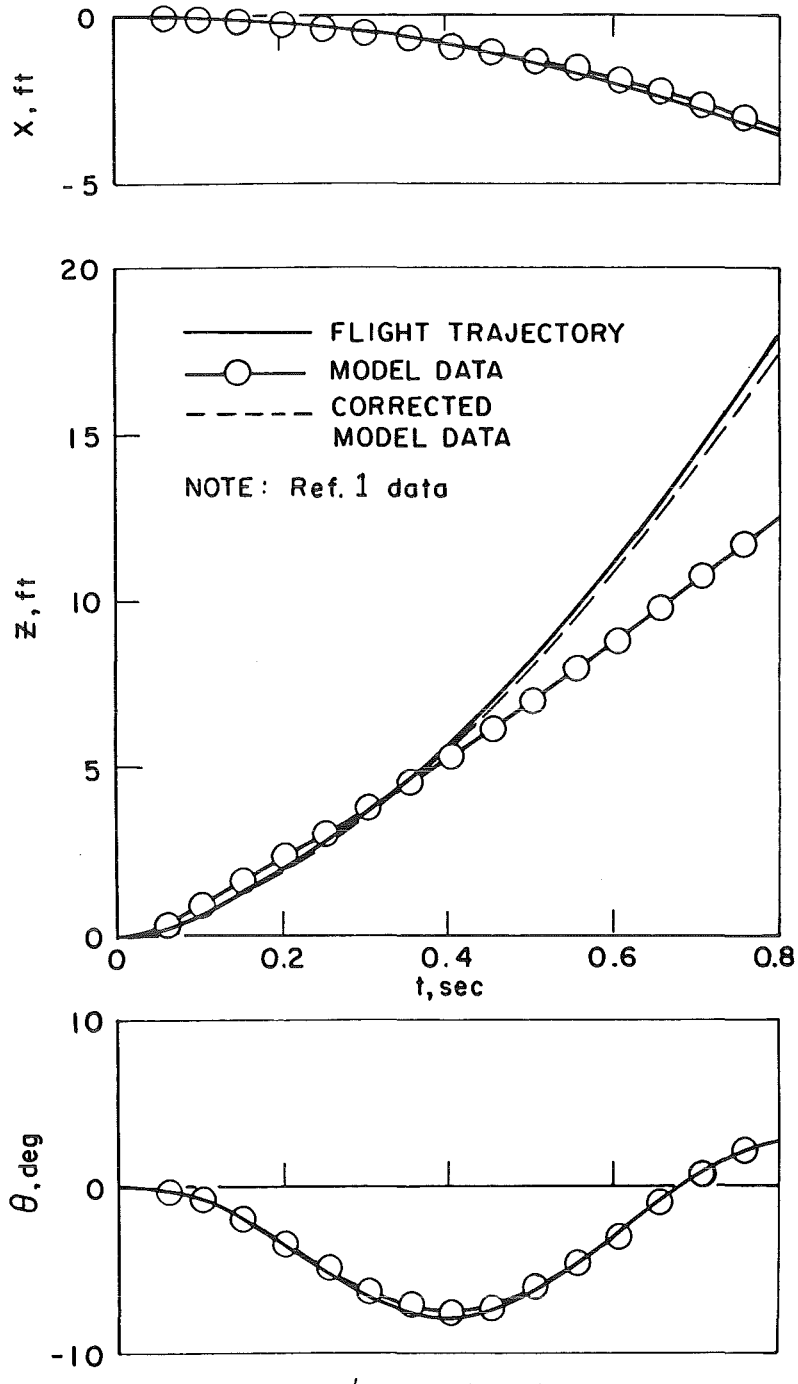

c. $\Delta F'_{E1} = 3m' (\Delta g')$

Figure 8. Concluded.

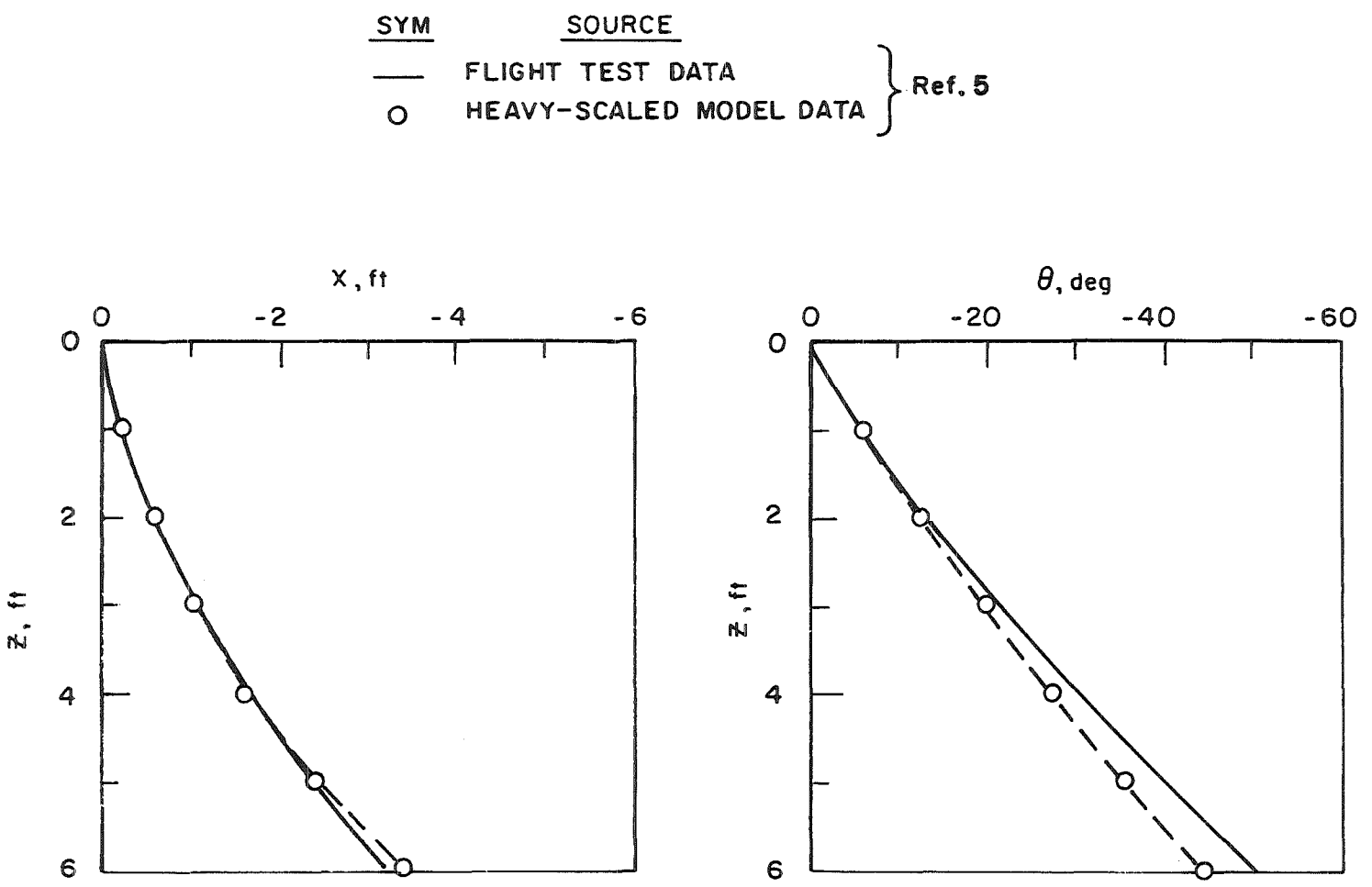

Figure 9. Comparison of heavy-scaled model and flight test trajectory data for the F-15 aircraft, empty 600-gal tank, inboard pylon, M_∞ = 0.88, h = 21K ft.

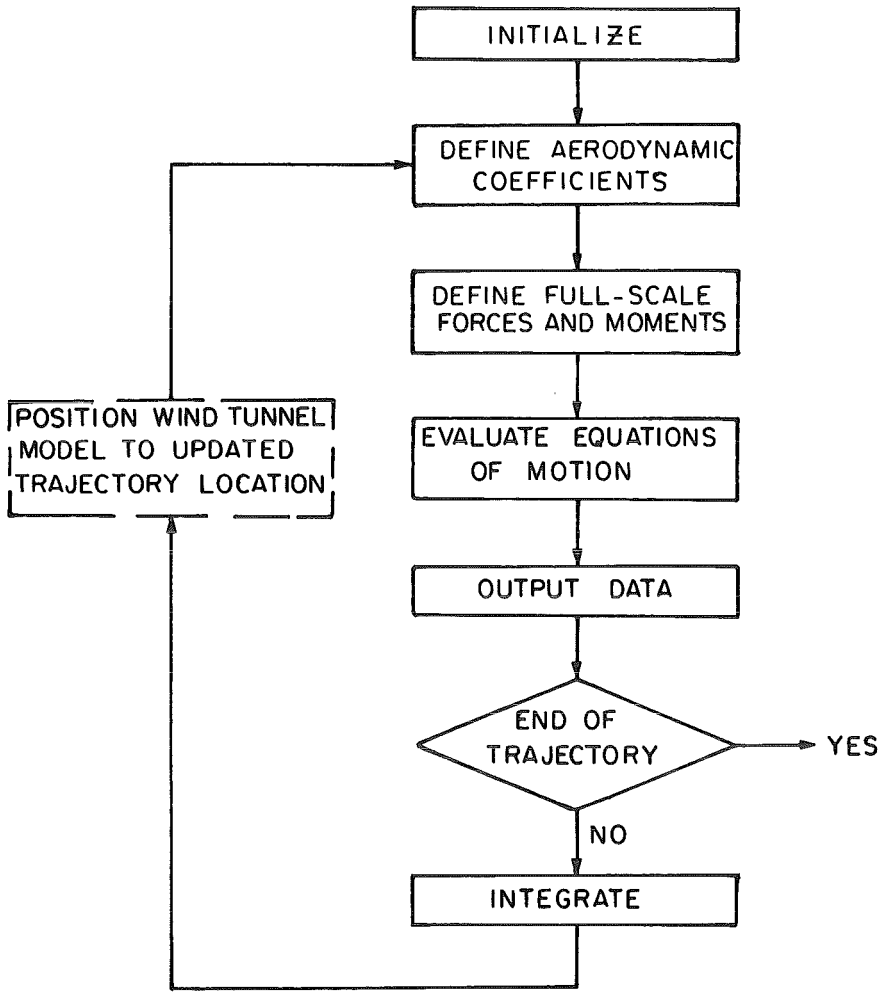

Figure 10. Simplified block diagram of a trajectory generation computer program.

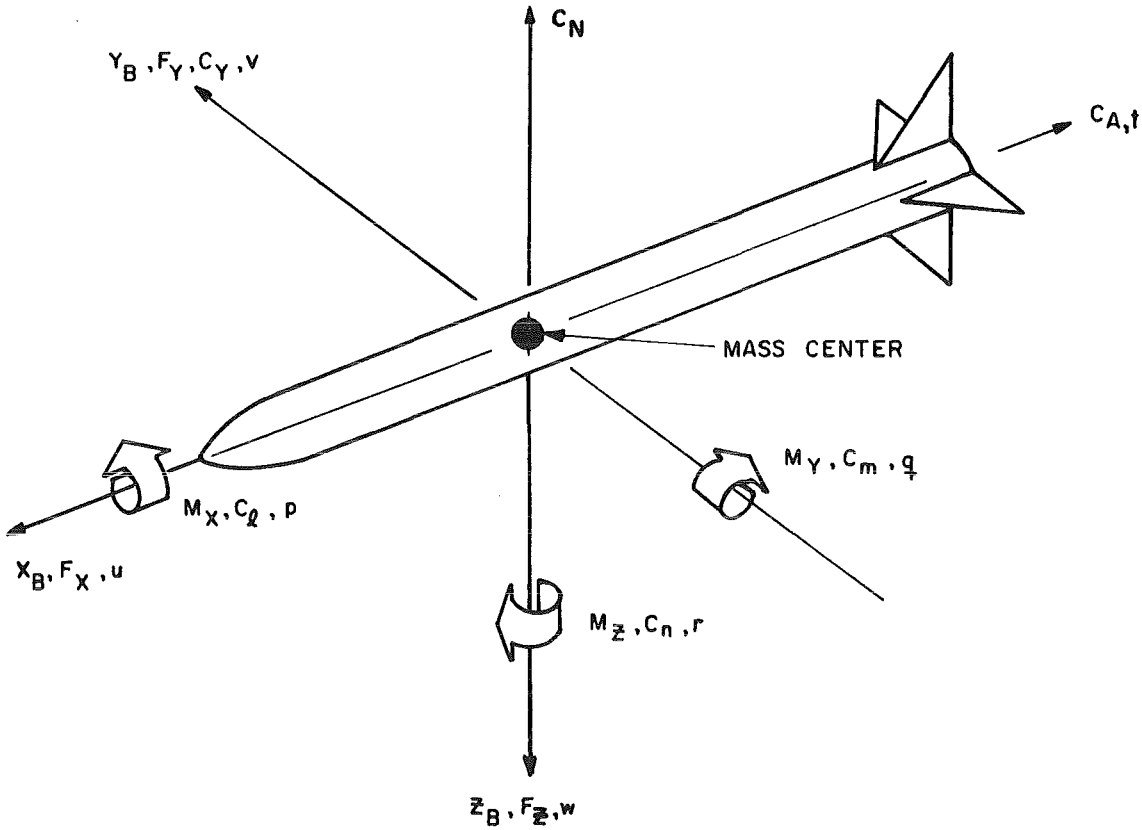

Figure 11. Positive directions for the body-axis coordinate system.

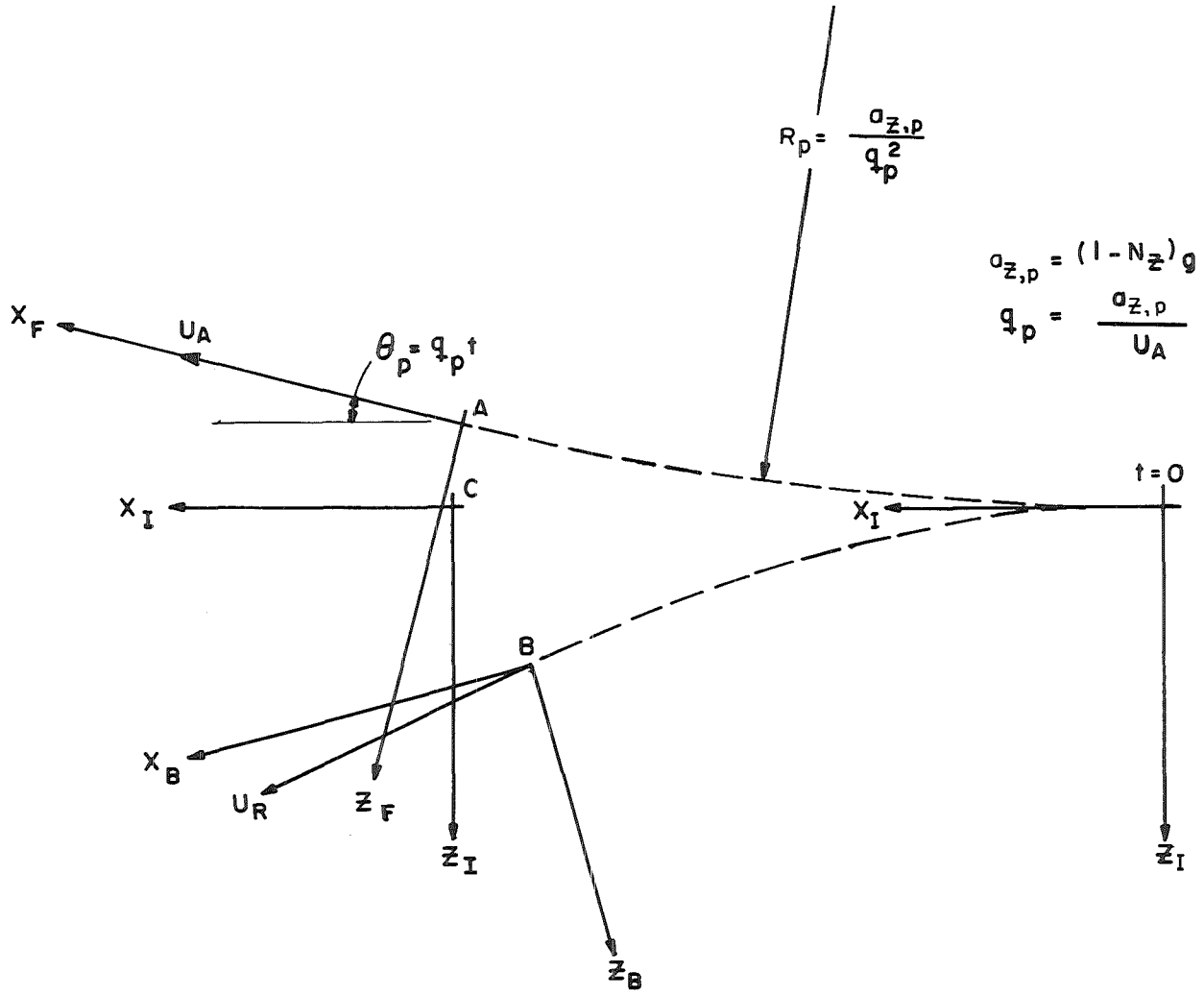

Figure 12. Body/inertial/flight axes directions for an aircraft pullup/pushover maneuver.

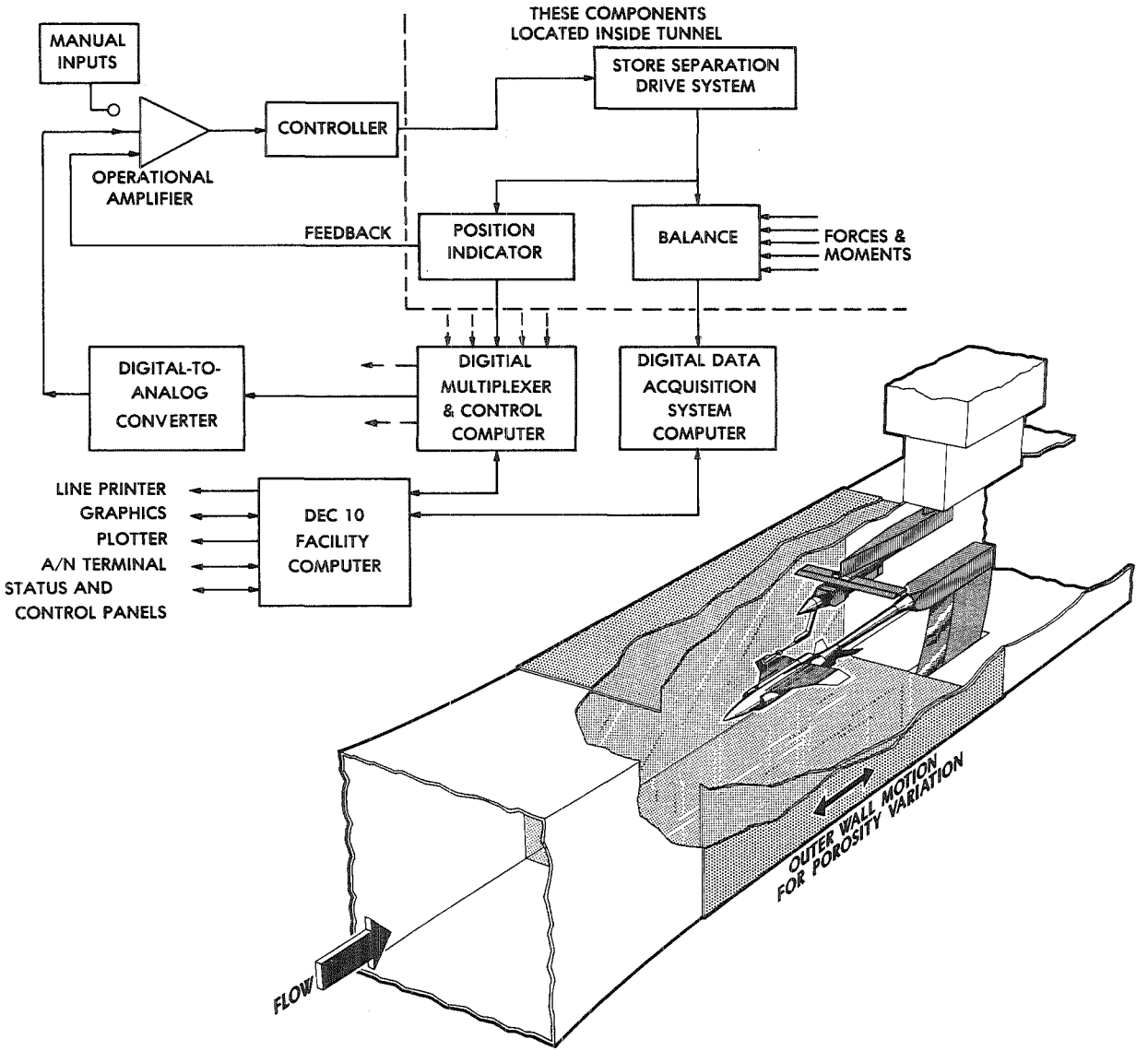

Figure 13. Isometric drawing of a typical store separation installation in Tunnel 4T and a block diagram of the computer control loop.

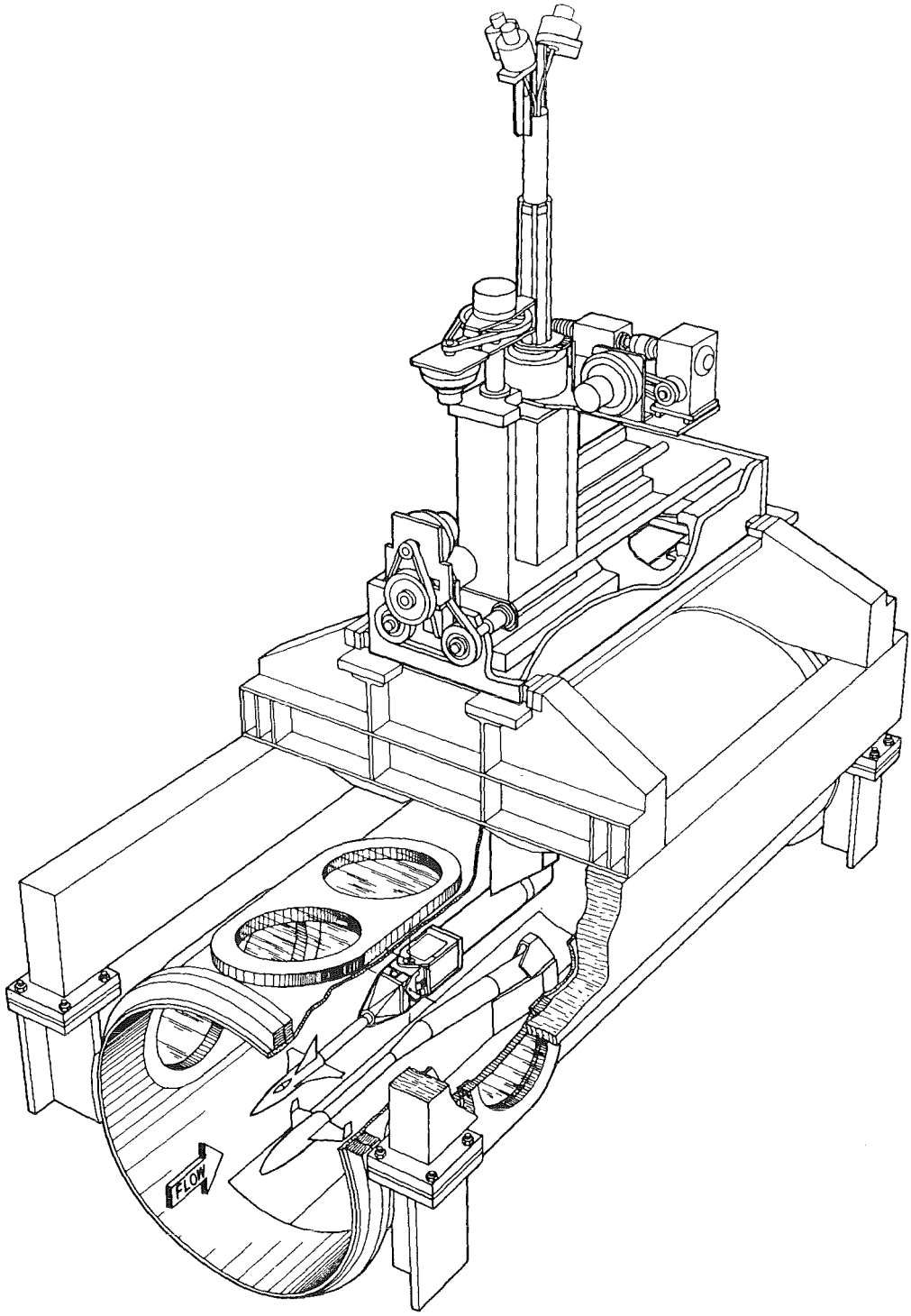

Figure 14. Isometric drawing of a typical store separation installation in Tunnels B and C.

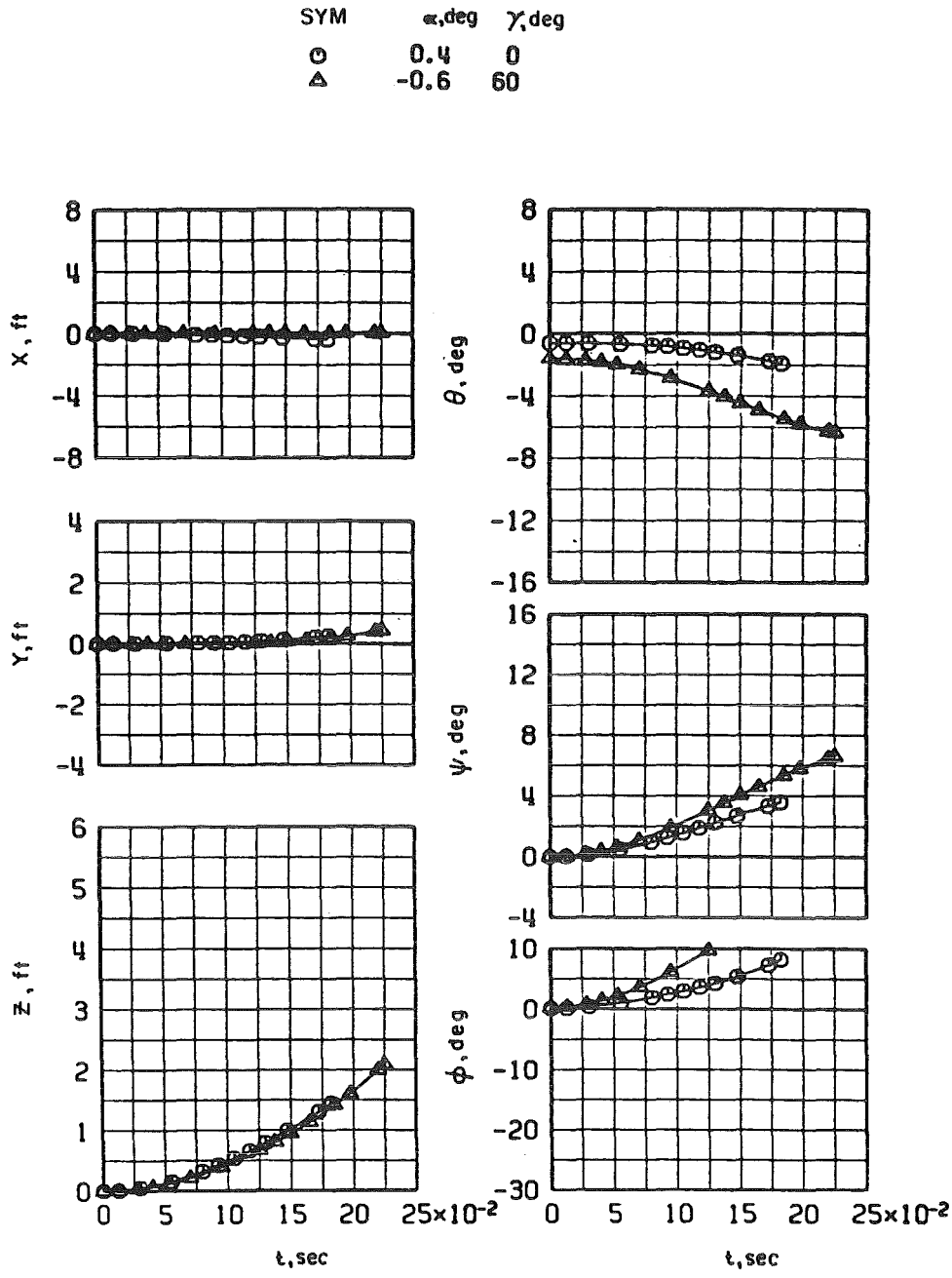

Figure 15. Typical separation characteristics of a slender-finned bomb from a supersonic fighter aircraft.

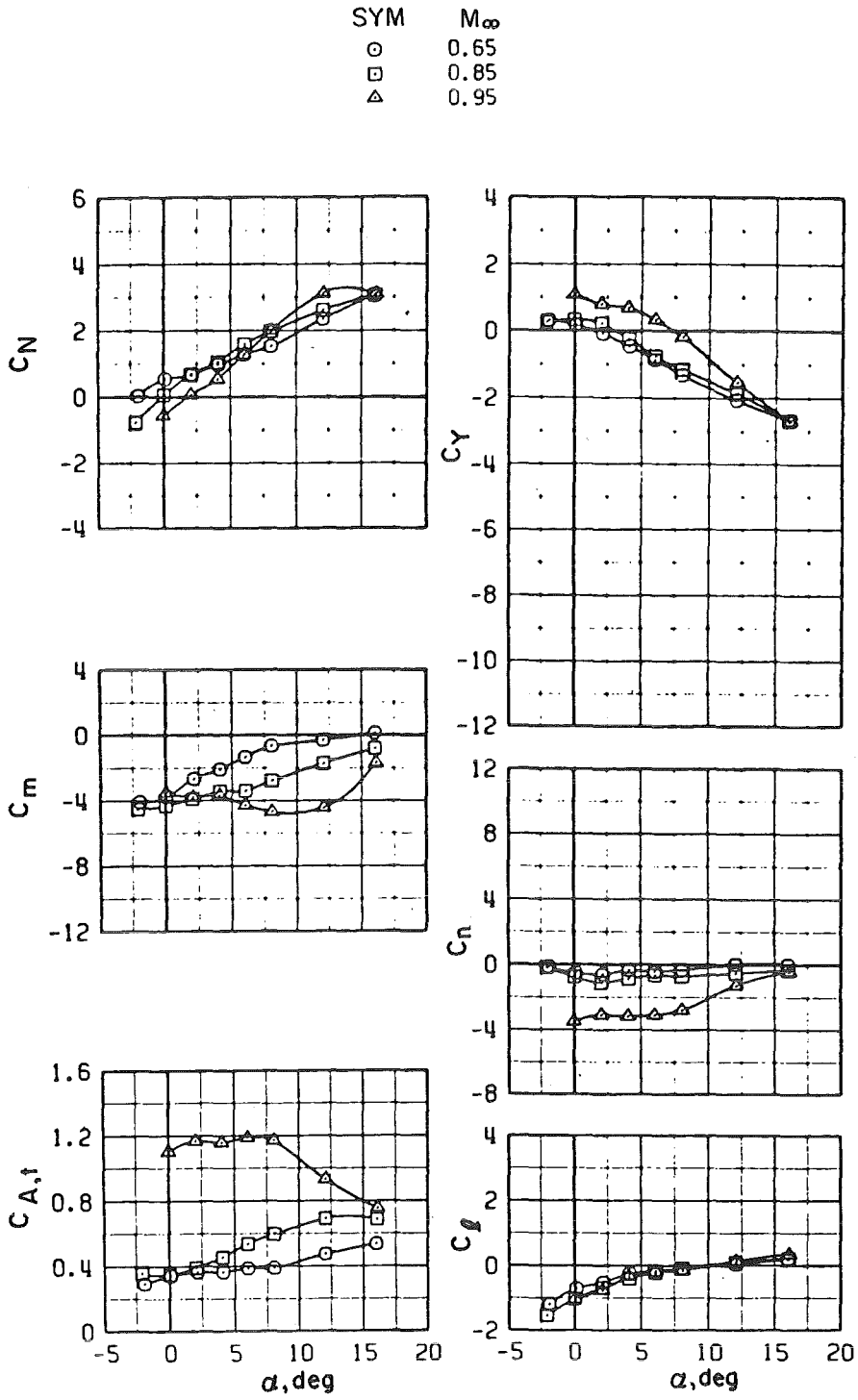

a. Carriage position characteristics

Figure 16. Typical aerodynamic coefficient data obtained on a slender-finned bomb in the flow field of a supersonic fighter aircraft.

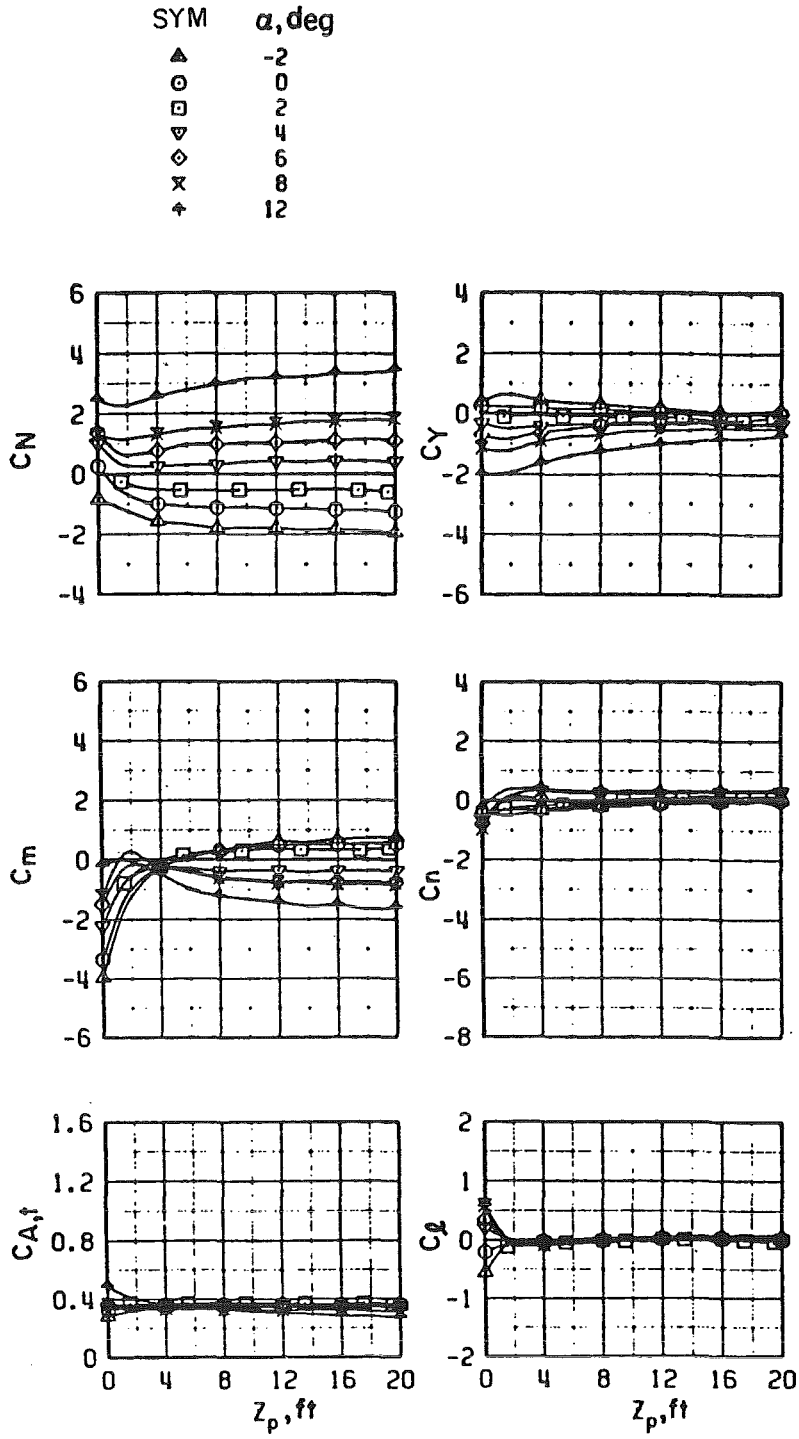

b. Flow-field characteristics
Figure 16. Concluded.

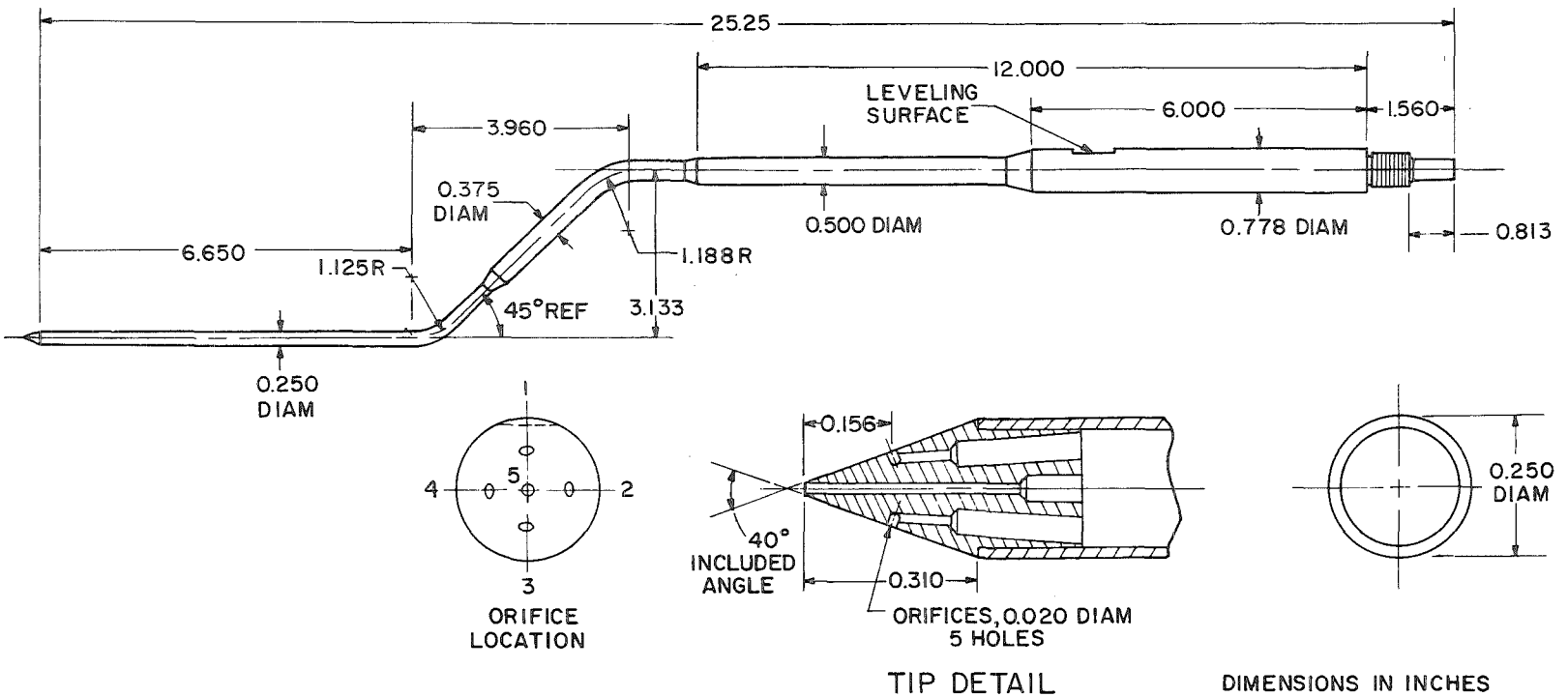

Figure 17. 40-deg conical probe.

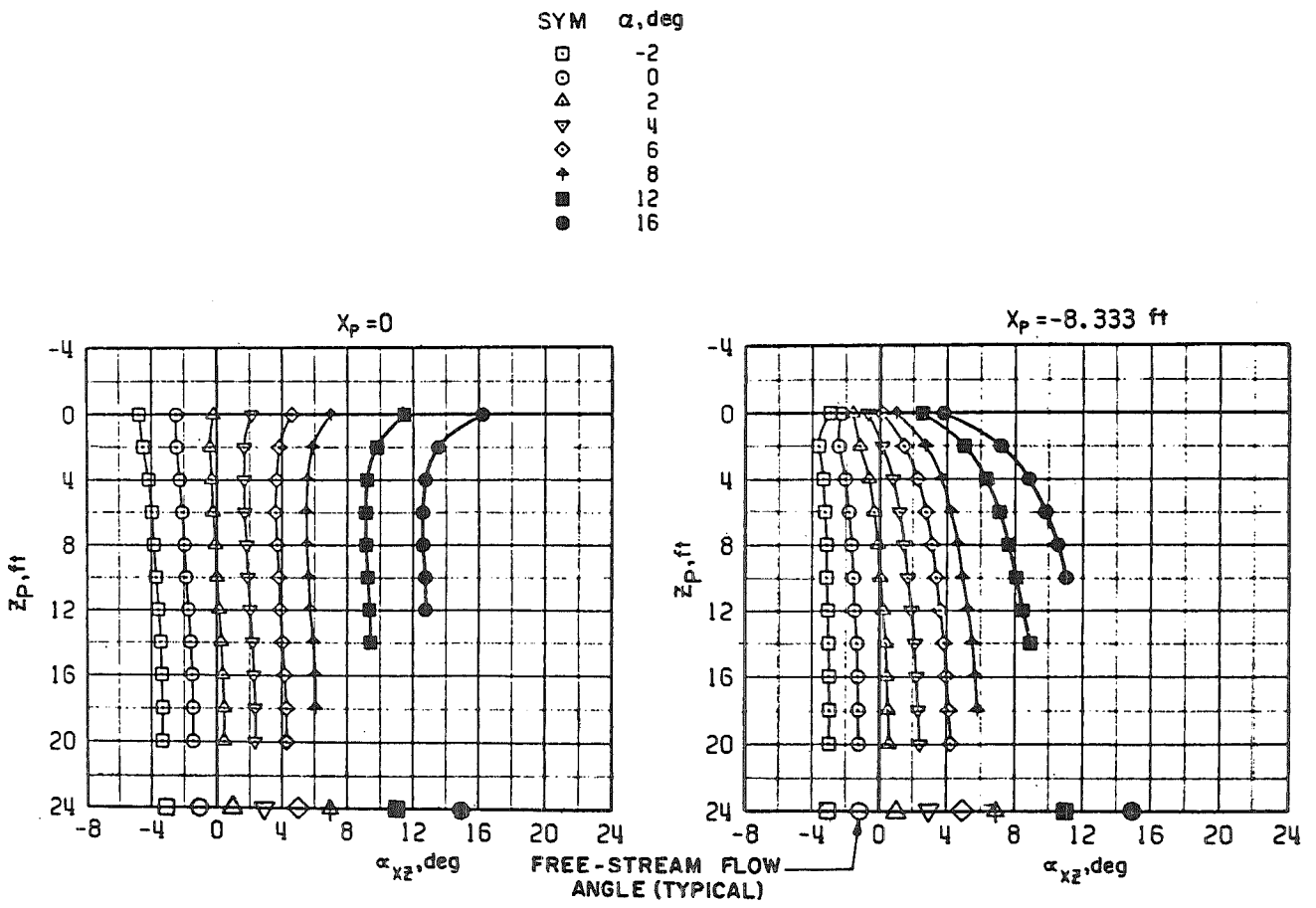

a. Upwash

Figure 18. Flow-field measurements beneath a supersonic fighter aircraft.

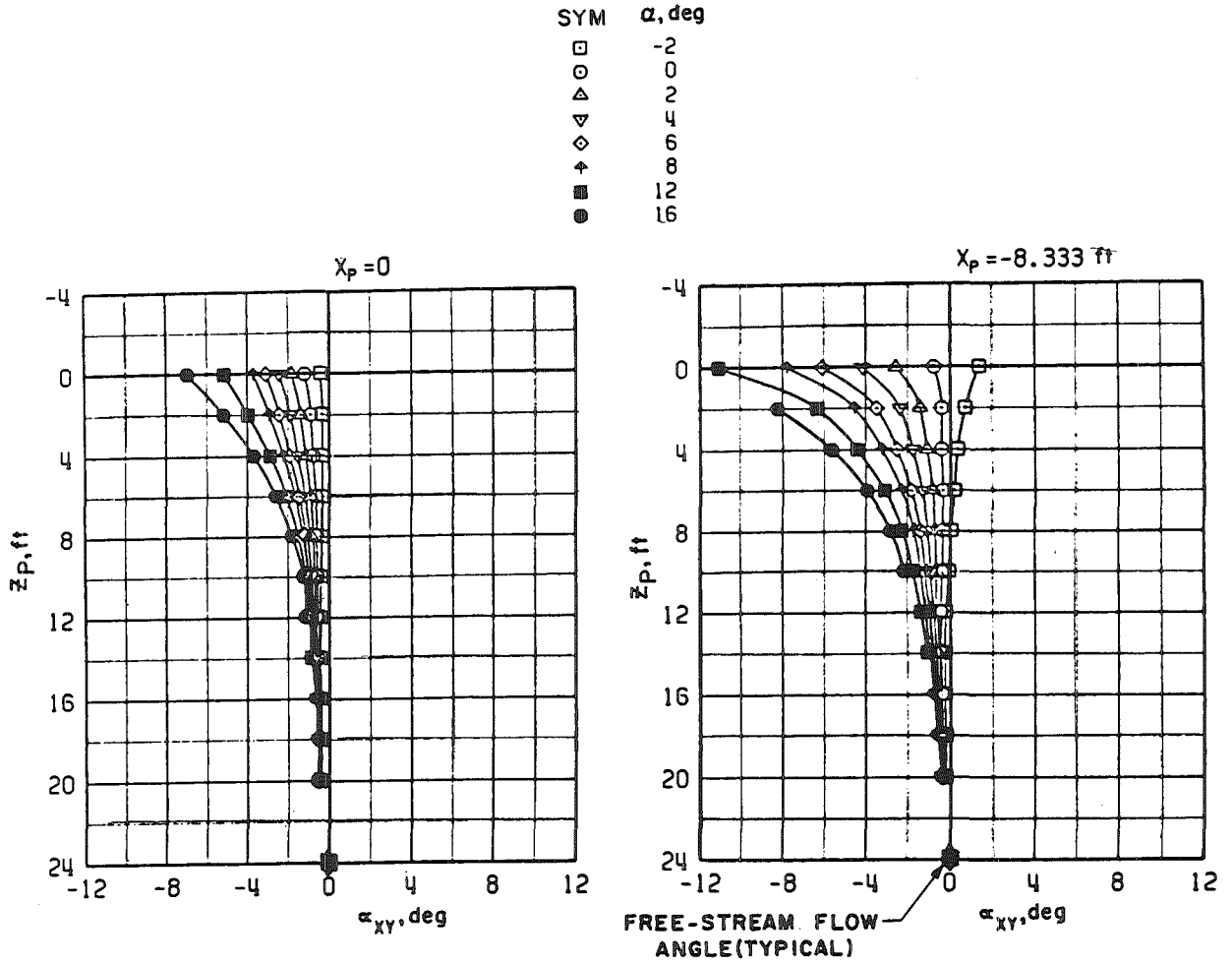

b. Sidewash

Figure 18. Concluded.

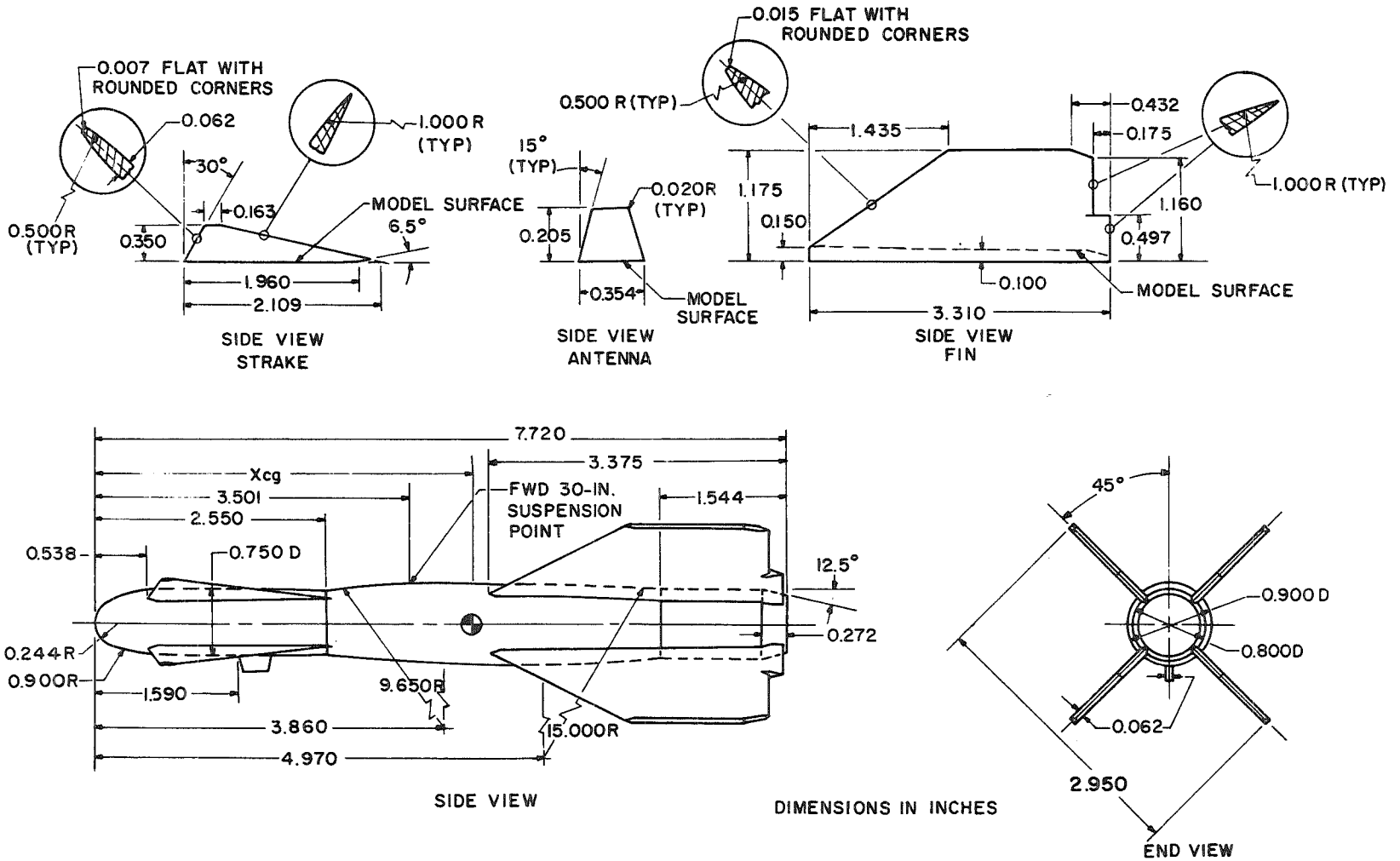

a. 0.05 scale

Figure 19. EOGB-II models.

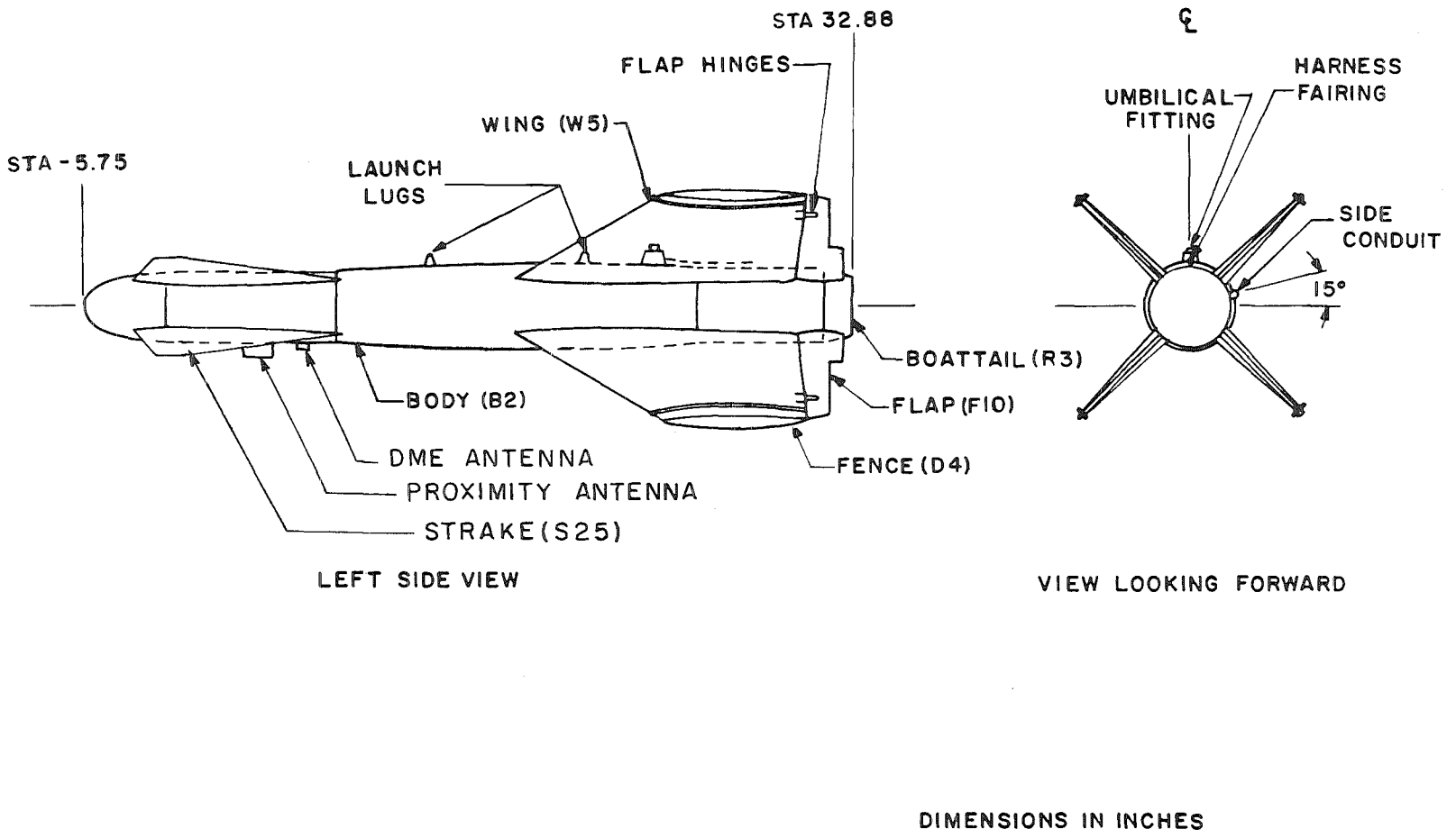

b. 0.25 scale

Figure 19. Concluded.

STA.	DIAM
0.000	0.150
0.212	0.150
0.238	0.231
0.412	0.354
0.612	0.467
0.812	0.556
1.012	0.625
1.212	0.680
1.412	0.730
1.612	0.770
1.812	0.806
2.012	0.838
2.212	0.867
2.412	0.887
2.612	0.896
2.707	0.900
3.821	0.900
4.021	0.897
4.221	0.889
4.421	0.874
4.621	0.856
4.821	0.833
5.021	0.803
5.045	0.800

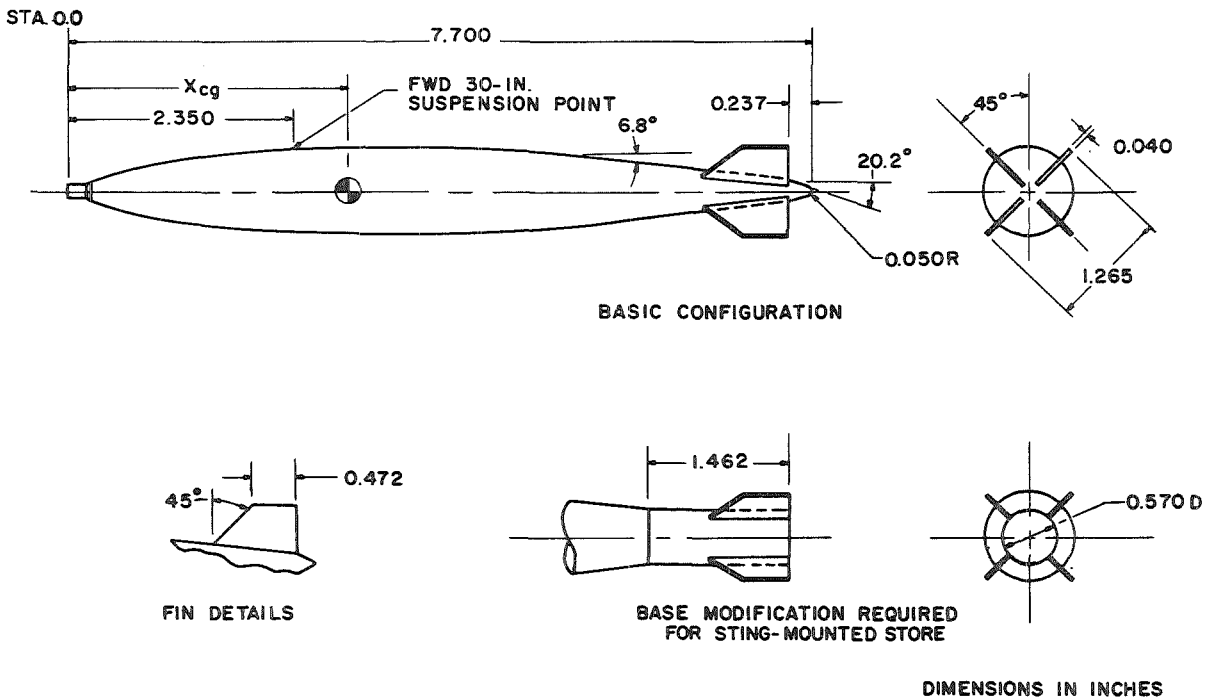

Figure 20. 0.05-Scale MK-84 LDGP bomb model.

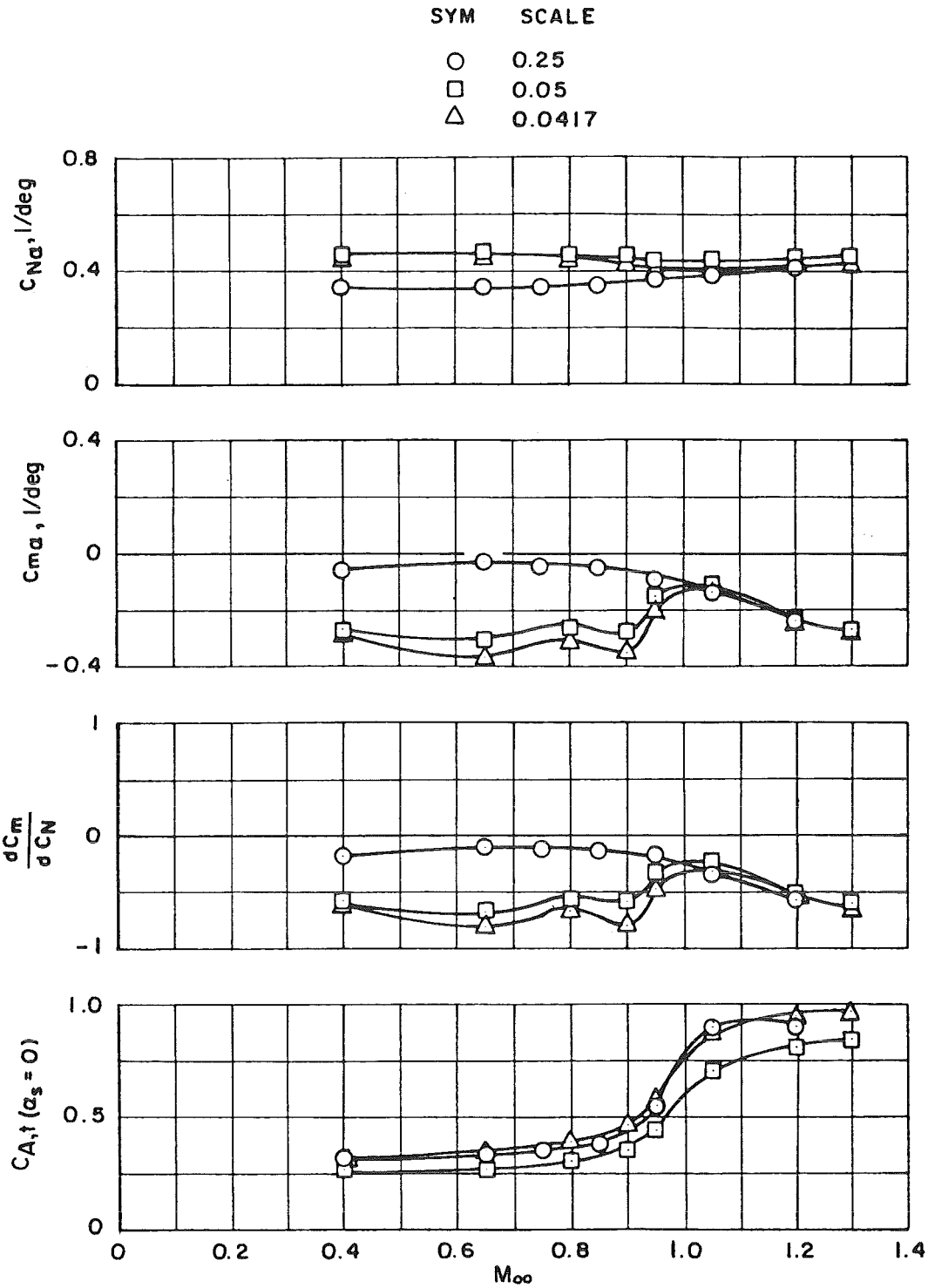

Figure 21. Variation of the zero-lift longitudinal stability derivatives and axial-force coefficients of a slender-finned bomb with Mach number.

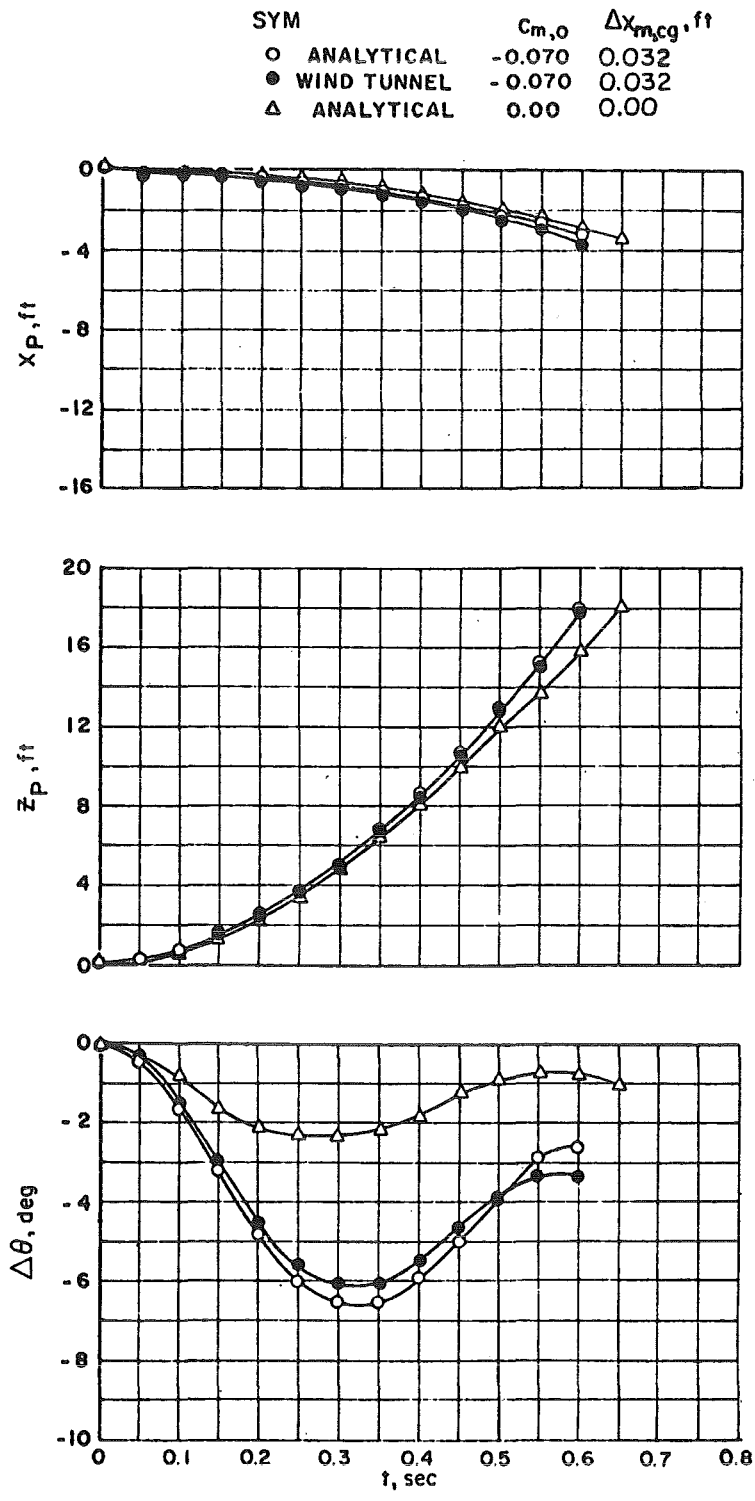

Figure 22. Effects of coefficient corrections on a typical trajectory of a slender-finned bomb.

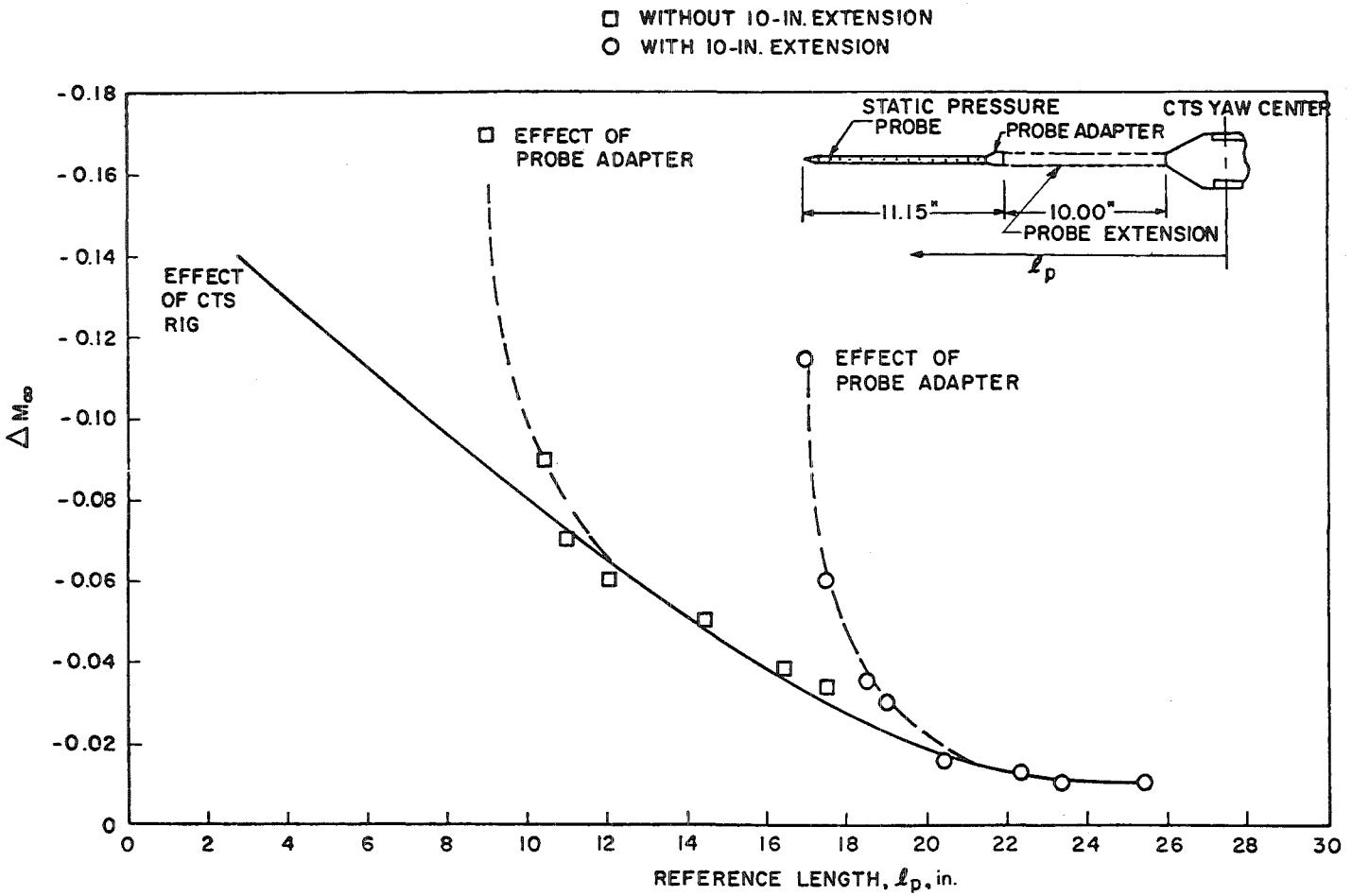

Figure 23. Effect of CTS rig on local Mach number distribution obtained from a CTS-mounted static probe.

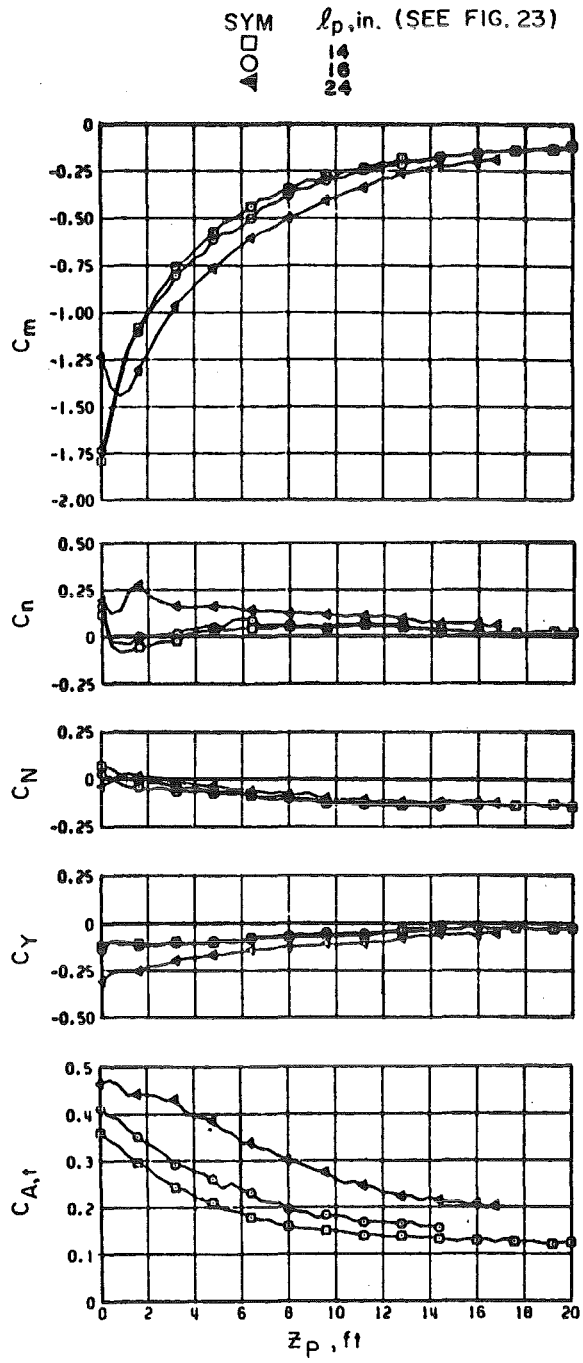

Figure 24. Typical variation of store aerodynamic coefficient data in the flow field of a supersonic fighter aircraft.

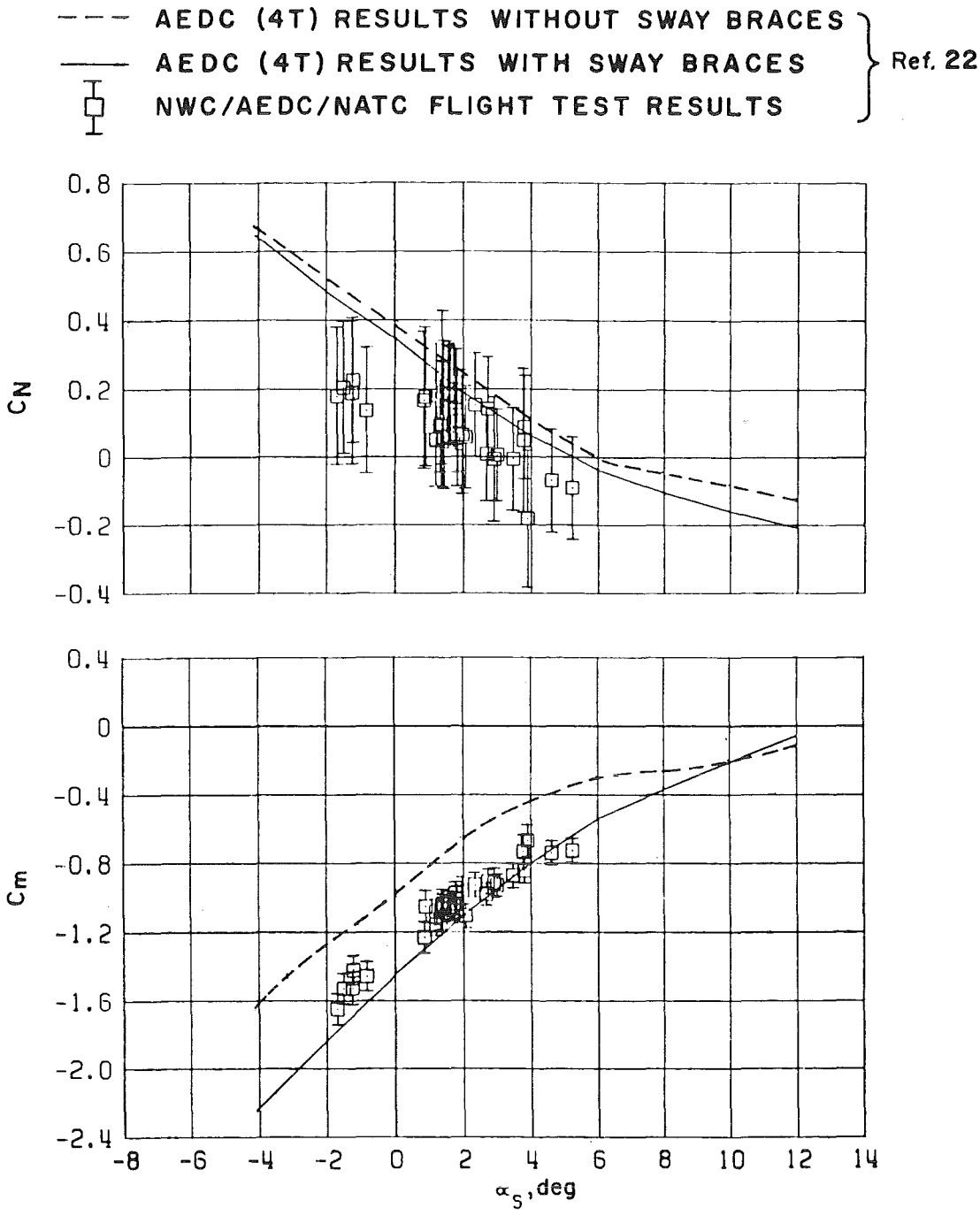

Figure 25. Effect of sway braces on the comparison of wind tunnel and in-flight measurements of captive-position store loads for the MK-83 low-drag bomb, M_∞ = 0.6, F-4C aircraft, left inboard pylon, TER position 1.

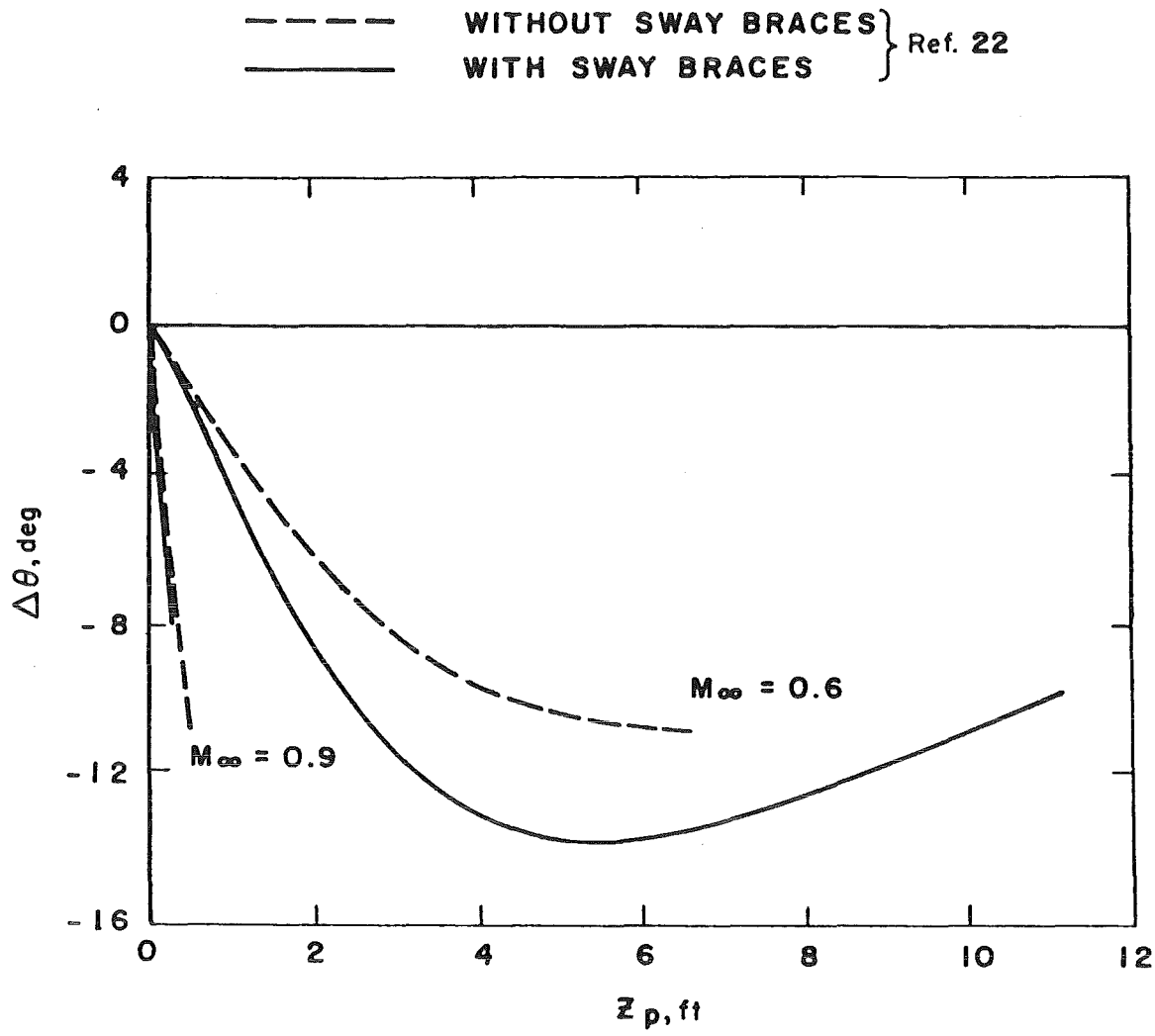

Figure 26. Effect of sway braces on separation trajectories of the MK-83 low-drag bomb from the F-4C Aircraft, left inboard pylon, TER station 1, level flight, 1,200-lb ejector force.

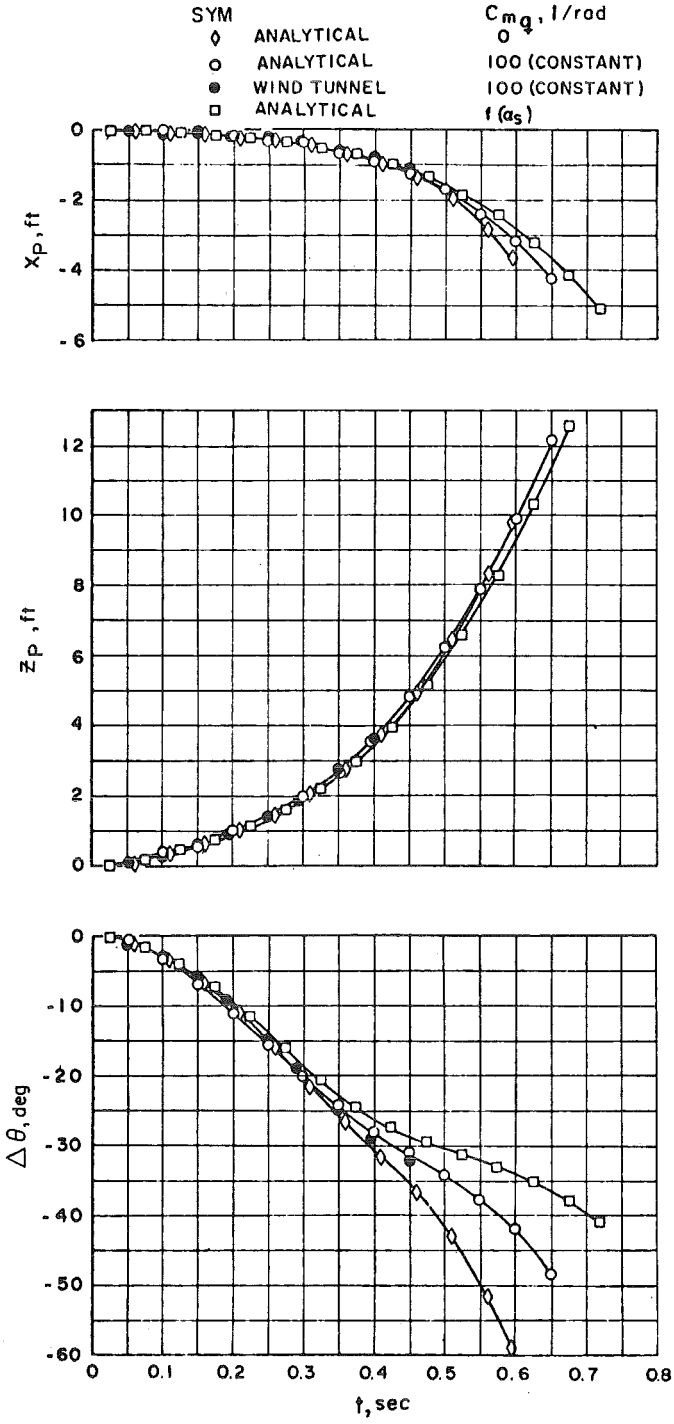

Figure 27. Effect of pitch-damping coefficient variations on the trajectory motion of a slender-finned bomb.

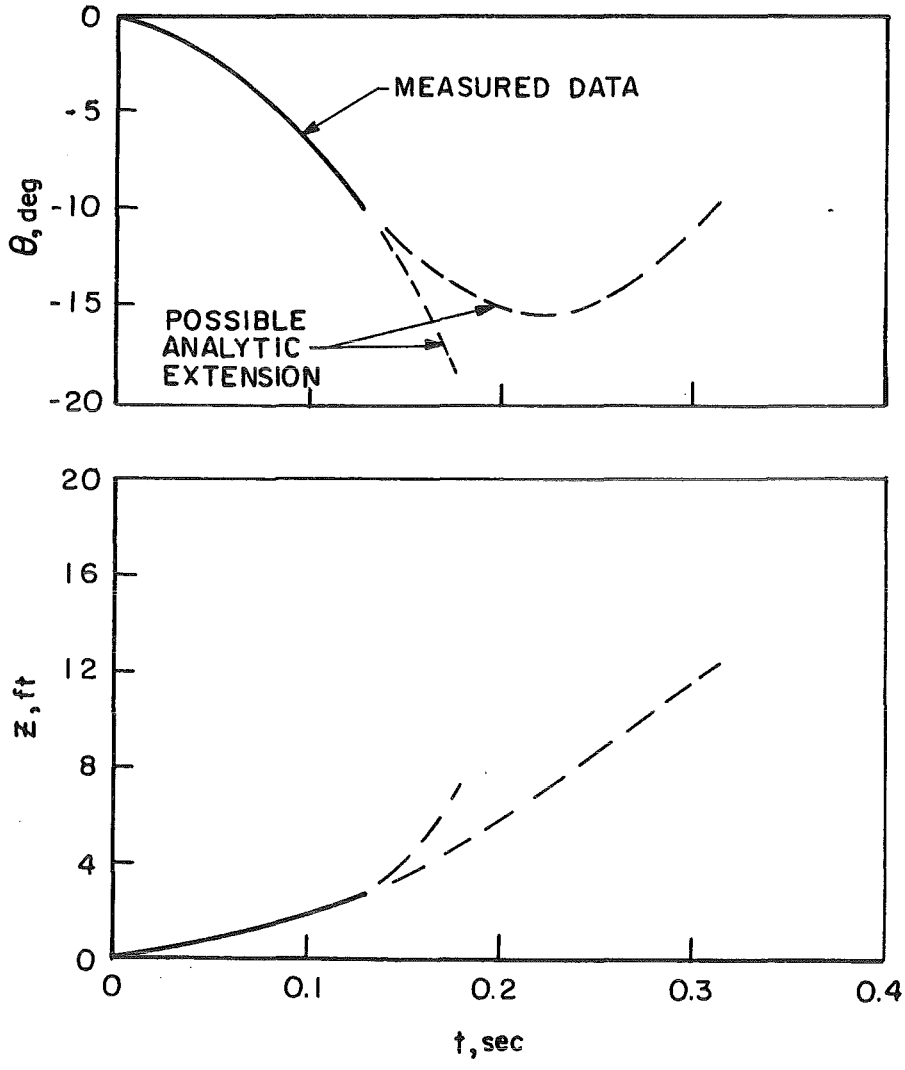

Figure 28. Potential extension of a foreshortened captive trajectory with the analytic simulation technique.

APPENDIX A
ANGULAR MOMENTUM

The angular momentum of a rotating rigid body about a point other than the mass center may be determined as follows[1]:

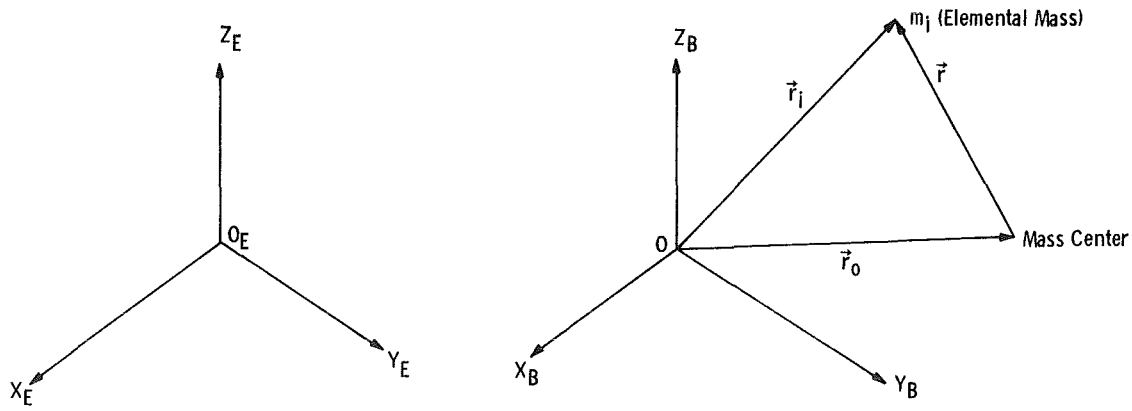

$O_E(X_E Y_E Z_E)$ is a space-fixed axis system.

X_B is parallel to X_E, Y_B is parallel to Y_E, and Z_B is parallel to Z_E at all times.

$\vec{v}_o$ is the velocity of point O (with respect to O_E).

$\vec{\omega}$ is the angular velocity about point O.

$$\vec{v}_i = \vec{v}_o + \vec{\omega} \times \vec{r}_i$$

$$\vec{r}_i = \vec{r}_o + \vec{r}$$

The angular momentum of the body about point O is:

$$\vec{H}_o = \Sigma \vec{r}_i \times m_i \vec{v}_i$$

[1]Etkin, Bernard. *Dynamics of Flight: Stability and Control.* John Wiley and Sons, Inc., New York, 1959, pp. 94-99, 442-443.

Substituting for $\vec{r}_i$ and $\vec{v}_i$, and expanding (noting that $\Sigma \vec{r} m_i \equiv 0$) gives:

$$\vec{H}_o = m\vec{r}_o \times \vec{v}_o + m\vec{r}_o \times (\vec{\omega} \times \vec{r}_o) + \Sigma \vec{r} \times m_i(\vec{\omega} \times \vec{r})$$

However, the last term in the above relation is defined as the angular momentum about the mass center ($\vec{H}$), such that

$$\vec{H}_o = m\vec{r}_o \times \vec{v}_o + m\vec{r}_o \times (\vec{\omega} \times \vec{r}_o) + \vec{H}$$

APPENDIX B
GENERALIZED MOMENT EQUATION AND ANGULAR ACCELERATIONS

For a nonrotating $X_BY_BZ_B$ axis system (as shown in Appendix A), the moment equation is:

$$\Sigma \vec{M}_o = \frac{d(\vec{H}_o)}{dt}$$

However, by letting the $X_BY_BZ_B$ axis system rotate (at angular velocity $\vec{\Omega}$), one obtains certain advantages, and the moment equation becomes:

$$\Sigma \vec{M}_o = \frac{\delta(\vec{H}_o)}{\delta t} + \vec{\Omega} \times \vec{H}_o$$

Substituting for $\vec{H}_o$ (from Appendix A) and expanding gives

$$\Sigma \vec{M}_o = \frac{\delta(\vec{H})}{\delta t} + \frac{\delta}{\delta t}(m\vec{r}_o \times \vec{v}_o) + \frac{\delta}{\delta t}\left[m\vec{r}_o \times (\vec{\omega} \times \vec{r}_o)\right]$$

$$+ \vec{\Omega} \times \vec{H} + \vec{\Omega} \times (m\vec{r}_o \times \vec{v}_o) + \vec{\Omega} \times \left(m\vec{r}_o \times (\vec{\omega} \times \vec{r}_o)\right)$$

For most store separation applications, the following criteria are valid:

1. The angular momentum about the mass center is $\vec{H} = I\vec{\omega}$

where

$$I = \begin{bmatrix} I_{XX} & -I_{XY} & -I_{XZ} \\ -I_{XY} & I_{YY} & -I_{YZ} \\ -I_{XZ} & -I_{YZ} & I_{ZZ} \end{bmatrix}$$

2. Fixing the rotating axis system with respect to the body gives

$$\vec{\Omega} = \vec{\omega} = \vec{i}p + \vec{j}q + \vec{k}r$$

$$\frac{\delta(\vec{\Omega})}{\delta t} = \frac{\delta(\vec{\omega})}{\delta t} = \vec{i}\dot{p} + \vec{j}\dot{q} + \vec{k}\dot{r}$$

$$\dot{I} = 0$$

3. Aligning the X_B-Z_B plane of the axis system in the body plane of symmetry gives

$$I_{XY} = I_{YZ} = 0$$

4. The distance from the rotation center to the mass center ($\vec{r}_o$) is nonzero only during staged release, but in any case, $\vec{r}_o$ is not time dependent.

$$\vec{r}_o = \vec{i}\, X_o + \vec{j}\, Y_o + \vec{k}\, Z_o$$

$$\frac{\delta(\vec{r}_o)}{\delta t} = 0$$

5. When $\vec{r}_o \neq 0$, the velocity and acceleration of the rotation center are

$$\vec{v}_o = \vec{i}\, v_{o,X} + \vec{j}\, v_{o,Y} + \vec{k}\, v_{o,Z}$$

$$\frac{\delta(\vec{v}_o)}{\delta t} = \vec{i}\, a_{o,X} + \vec{j}\, a_{o,Y} + \vec{k}\, a_{o,Z}$$

6. If $\vec{r}_o \neq 0$, the inertia about the rotation center may be defined as

$$\bar{I}_{XX} = I_{XX} + m(Y_o^2 + Z_o^2)$$

$$\bar{I}_{XY} = I_{XY} + mX_oY_o$$

$$\bar{I}_{XZ} = I_{XZ} + mX_oZ_o$$

$$\bar{I}_{YY} = I_{YY} + m(X_o^2 + Z_o^2)$$

$$\bar{I}_{YZ} = I_{YZ} + mY_oZ_o$$

$$\bar{I}_{ZZ} = I_{ZZ} + m(X_o^2 + Y_o^2)$$

$$\left[\bar{I}\right] = \begin{bmatrix} \bar{I}_{XX} & -\bar{I}_{XY} & -\bar{I}_{XZ} \\ -\bar{I}_{XY} & \bar{I}_{YY} & -\bar{I}_{YZ} \\ -\bar{I}_{XZ} & -\bar{I}_{YZ} & \bar{I}_{ZZ} \end{bmatrix}$$

7. The scalar components of $\vec{M}_o$, $\vec{H}$, and $\delta(\vec{H})/\delta t$ are defined as

$$\vec{M}_o = \vec{i}\, M_{o,X} + \vec{j}\, M_{o,Y} + \vec{k}\, M_{o,Z}$$

$$\begin{vmatrix} H_X \\ H_Y \\ H_Z \end{vmatrix} = \left[\bar{\bar{I}}\right] \begin{vmatrix} p \\ q \\ r \end{vmatrix}$$

$$\begin{vmatrix} \dot{H}_X \\ \dot{H}_Y \\ \dot{H}_Z \end{vmatrix} = \left[\bar{\bar{I}}\right] \begin{vmatrix} \dot{p} \\ \dot{q} \\ \dot{r} \end{vmatrix}$$

By applying the preceding criteria, one can determine the scalar components of the moment equation to be:

$$\Sigma M_{o,X} = \dot{H}_X + qH_Z - rH_Y + mX_o(qv_{o,Y} + rv_{o,Z}) + mY_o(a_{o,Z} - qv_{o,X}) - mZ_o(a_{o,Y} + rv_{o,X})$$

$$\Sigma M_{o,Y} = \dot{H}_Y + rH_X - pH_Z - mX_o(a_{o,Z} + pv_{o,Y}) + mY_o(pv_{o,X} + rv_{o,Z}) + mZ_o(a_{o,X} - rv_{o,Y})$$

$$\Sigma M_{o,Z} = \dot{H}_Z + pH_Y - qH_X + mX_o(a_{o,Y} - pv_{o,Z}) - mY_o(a_{o,X} + qv_{o,Z}) + mZ_o(pv_{o,X} + qv_{o,Y})$$

The moments about the X_B, Y_B, and Z_B axes at the rotation center are (see Fig. B-1):

$$\Sigma M_{o,X} = M_X + F_Z Y_o - F_Y Z_o + R_\ell$$

$$\Sigma M_{o,Y} = M_Y + F_X Z_o - F_Z X_o + R_m$$

$$\Sigma M_{o,Z} = M_Z + F_Y X_o - F_X Y_o + R_n$$

Substituting, then:

$$\dot{H}_X = M_X + F_Z Y_o - F_Y Z_o + R_\ell - qH_Z + rH_Y$$
$$- mX_o(qv_{o,Y} + rv_{o,Z}) - mY_o(a_{o,Z} - qv_{o,X}) + mZ_o(a_{o,Y} + rv_{o,X})$$

$$\dot{H}_Y = M_Y + F_X Z_o - F_Z X_o + R_m - rH_X + pH_Z$$
$$+ mX_o(a_{o,Z} + pv_{o,Y}) - mY_o(pv_{o,X} + rv_{o,Z}) - mZ_o(a_{o,X} - rv_{o,Y})$$

$$\dot{H}_Z = M_Z + F_Y X_o - F_X Y_o + R_n - pH_Y + qH_X$$
$$- mX_o(a_{o,Y} - pv_{o,Z}) + mY_o(a_{o,X} + qv_{o,Z}) - mZ_o(pv_{o,X} + qv_{o,Y})$$

The angular accelerations are then:

$$\begin{vmatrix} \dot{p} \\ \dot{q} \\ \dot{r} \end{vmatrix} = \left[\bar{I}\right]^{-1} \begin{vmatrix} \dot{H}_X \\ \dot{H}_Y \\ \dot{H}_Z \end{vmatrix}$$

where $[\bar{I}]^{-1}$ is the inverse of $[\bar{I}]$.

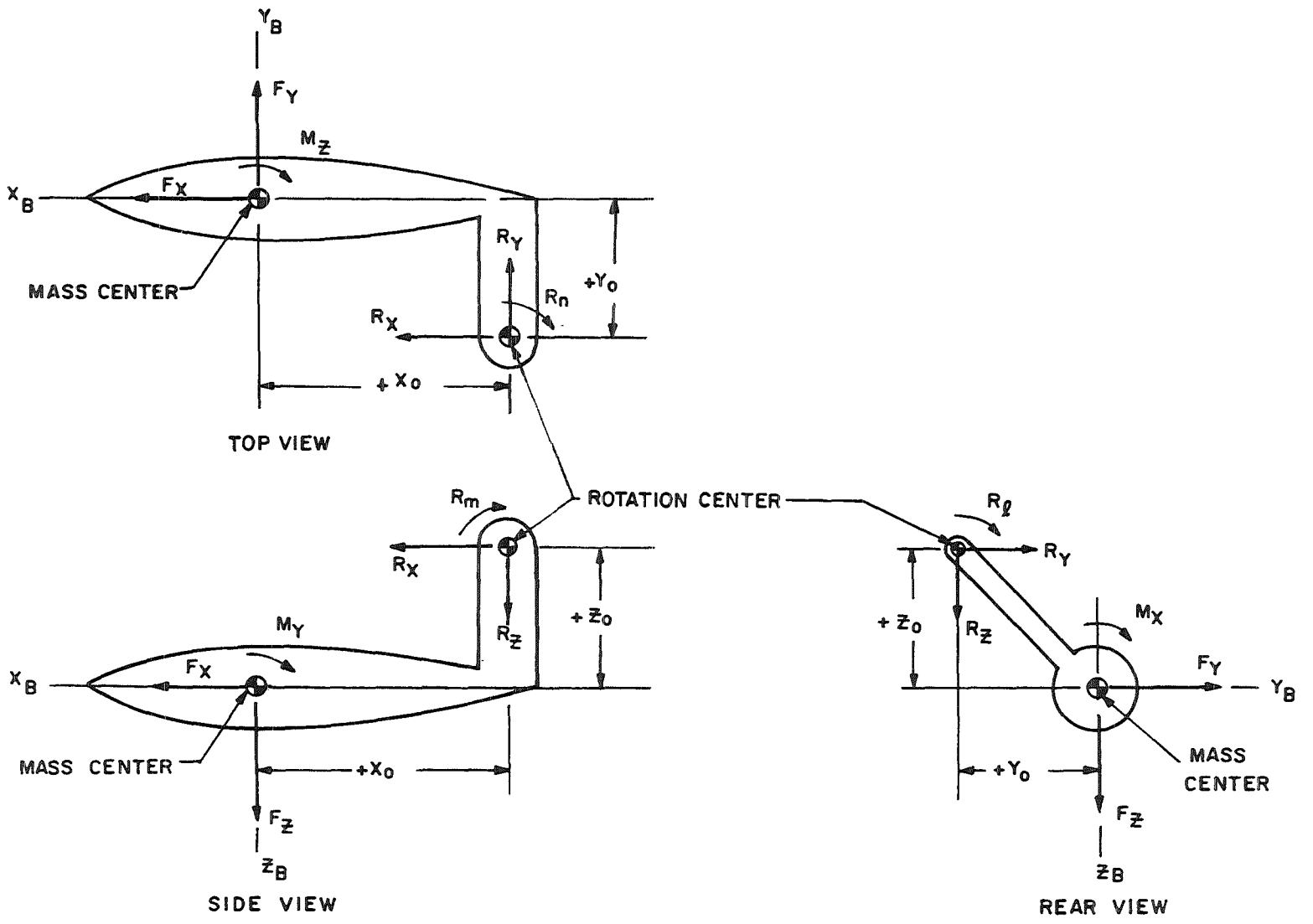

Figure B-1. Positive directions of full-scale forces and moments.

APPENDIX C
GENERALIZED FORCE EQUATION AND LINEAR ACCELERATIONS

The generalized force equation is:

$$\Sigma \vec{F} = \frac{d(m\vec{v})}{dt} = m \frac{d\vec{v}}{dt}$$

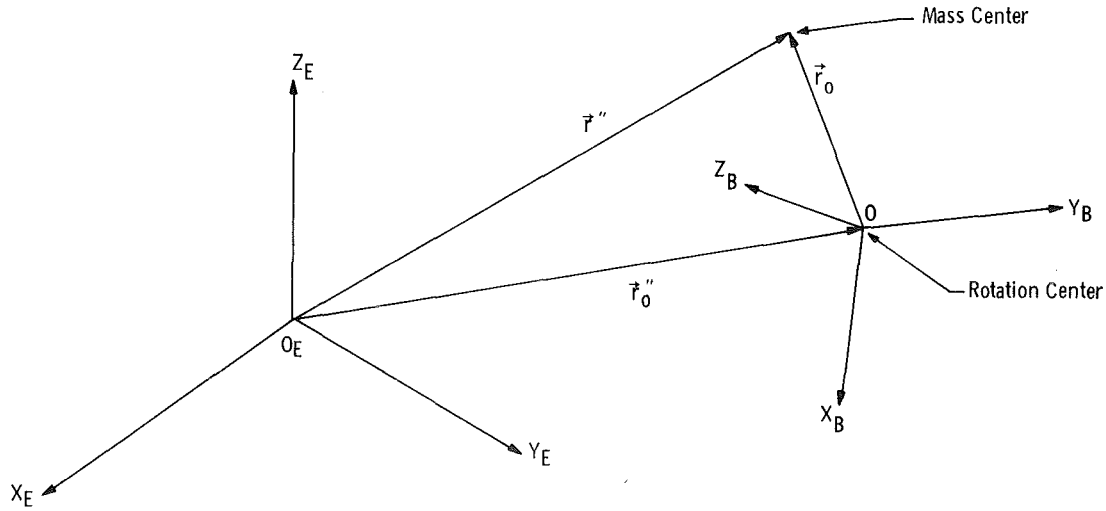

$O_E(X_E Y_E Z_E)$ is fixed frame of reference.

$O(X_B Y_B Z_B)$ is second frame of reference moving with a linear velocity $(\vec{v}_o)$ at the origin and at angular velocity $(\vec{\omega})$ with respect to the fixed frame.

The velocity at the mass center $(\vec{v})$ may be determined as:

$$\vec{v} = \frac{d(\vec{r}'')}{dt}$$

$$= \frac{d(\vec{r}_o'')}{dt} + \frac{d(\vec{r}_o)}{dt}$$

$$= \vec{v}_o + \frac{\delta}{\delta t}(\vec{r}_o) + \vec{\omega} \times \vec{r}_o$$

By defining:

$$\vec{v} = \vec{i}u + \vec{j}v + \vec{k}w$$

$$\vec{v}_o = \vec{i}v_{o,X} + \vec{j}v_{o,Y} + \vec{k}v_{o,Z}$$

$$\vec{r}_o = \vec{i}X_o + \vec{j}Y_o + \vec{k}Z_o$$

$$\vec{\omega} = \vec{i}p + \vec{j}q + \vec{k}r$$

$$\frac{\delta(\vec{r}_o)}{\delta t} = 0$$

The scalar components of velocity are:

$$u = v_{o,X} + qZ_o - rY_o$$

$$v = v_{o,Y} + rX_o - pZ_o$$

$$w = v_{o,Z} + pY_o - qX_o$$

The acceleration of the mass center may be determined to be:

$$\vec{a} = \frac{d(\vec{v})}{dt}$$

$$= \frac{\delta(\vec{v})}{\delta t} + \vec{\omega} \times \vec{v}$$

Substituting for $\vec{v}$ and expanding gives:

$$\vec{a} = \frac{\delta(\vec{v}_o)}{\delta t} + \frac{\delta^2(\vec{v}_o)}{\delta t^2} + \frac{\delta(\vec{\omega} \times \vec{r}_o)}{\delta t}$$

$$+ \vec{\omega} \times \vec{v}_o + \vec{\omega} \times \frac{\delta(\vec{r}_o)}{\delta t} + \vec{\omega} \times (\vec{\omega} \times \vec{r}_o)$$

Then by definition one arrives at:

$$\vec{a} = \vec{i}a_X + \vec{j}a_Y + \vec{k}a_Z$$

$$\frac{\delta(\vec{v}_o)}{\delta t} = \vec{i}a_{o,X} + \vec{j}a_{o,Y} + \vec{k}a_{o,Z}$$

$$\frac{\delta^2(\vec{r}_o)}{\delta t^2} = 0$$

$$\frac{\delta(\vec{\omega})}{\delta t} = \vec{i}\dot{p} + \vec{j}\dot{q} + \vec{k}\dot{r}$$

The scalar components of acceleration are then:

$$a_X = a_{o,X} + qv_{o,Z} - rv_{o,Y}$$
$$- X_o(q^2 + r^2) + Y_o(pq - \dot{r}) + Z_o(\dot{q} + pr)$$

$$a_Y = a_{o,Y} + rv_{o,X} - pv_{o,Z}$$
$$+ X_o(pq + \dot{r}) - Y_o(p^2 + r^2) + Z_o(qr - \dot{p})$$

$$a_Z = a_{o,Z} + pv_{o,Y} - qv_{o,X}$$
$$+ X_o(pr - \dot{q}) + Y_o(qr + \dot{p}) - Z_o(p^2 + q^2)$$

The scalar components of $\Sigma\vec{F}$ are (see Fig. B-1):

$$\Sigma\vec{F} = \vec{i}(F_X + R_X) + \vec{j}(F_Y + R_Y) + \vec{k}(F_Z + R_Z)$$

Therefore the scalar force equations are:

$$F_X + R_X = ma_X$$

$$F_Y + R_Y = ma_Y$$

$$F_Z + R_Z = ma_Z$$

For a free-falling body, the following equations are valid:

$$X_o = Y_o = Z_o = 0$$

$$R_X = R_Y = R_Z = 0$$

$$u = v_{o,X}, \; v = v_{o,Y}, \; w = v_{o,Z}$$

$$\dot{u} = a_{o,X}, \; \dot{v} = a_{o,Y}, \; \dot{w} = a_{o,Z}$$

The linear accelerations of the mass center are then:

$$\dot{u} = F_X/m + rv - qw$$

$$\dot{v} = F_Y/m + pw - ru$$

$$\dot{w} = F_Z/m + qu - pv$$

For a staged release ($\vec{r}_o \neq 0$), the terms $\dot{u}$, $\dot{v}$, $\dot{w}$ do not appear in the acceleration equations. However, by substituting one obtains:

$$a_X = \dot{u} + qw - rv$$

$$a_Y = \dot{v} + ru - pw$$

$$a_Z = \dot{w} + pv - qu$$

$$v_{o,X} = u - qZ_o + rY_o$$

$$v_{o,Y} = v - rX_o + pZ_o$$

$$v_{o,Z} = w - pY_o + qX_o$$

Then, the linear accelerations are:

$$\dot{u} = a_{o,X} + \dot{q}Z_o - \dot{r}Y_o$$

$$\dot{v} = a_{o,Y} + \dot{r}X_o - \dot{p}Z_o$$

$$\dot{w} = a_{o,Z} + \dot{p}Y_o - \dot{q}X_o$$

Note that for a staged release, the linear accelerations of the mass center are influenced by the applied forces only through coupling with the angular accelerations.

APPENDIX D
FULL-SCALE FORCE AND MOMENT EQUATIONS

For a free-falling store, components of the full-scale forces and moments acting through or about the store cg are described as follows:

Forces

$$F_X = \bar{W}_X - q_\infty A(C_{A,t} + C_{A,o}) + F_{T,X} + F_{E,X}$$

$$F_Y = \bar{W}_Y + q_\infty A(C_Y + C_{Y,o}) + F_{T,Y} + F_{E,Y}$$

$$F_Z = \bar{W}_Z - q_\infty A(C_N + C_{N,o}) + F_{T,Z} + F_{E,Z}$$

Moments

$$M_X = q_\infty A\ell_3 \left[C_\ell + C_{\ell,o} + C_{\ell_p} \left(p\ell_3/2U_R \right) \right] + M_{T,X} + M_{E,X}$$

$$M_Y = q_\infty A\ell_1 \left[C_m + C_{m,o} + C_{m_q} \left(q\ell_1/2U_R \right) \right] + M_{T,Y} + M_{E,Y}$$

$$M_Z = q_\infty A\ell_2 \left[C_n + C_{n,o} + C_{n_r} \left(r\ell_2/2U_R \right) \right] + M_{T,Z} + M_{E,Z}$$

Additional terms required to define the full-scale moments and forces which occur on staged release are given in Appendixes B and C, respectively.

NOMENCLATURE

A	Store full-scale reference area, ft^2
$\vec{a}$	Total acceleration of the store mass center, ft/sec^2
$a_{o,X}, a_{o,Y}$ $a_{o,Z}$	Accelerations of the store rotation center (if not coincident with the mass center) in the X_B, Y_B, and Z_B directions, respectively, ft/sec^2
a_X, a_Y, a_Z	Accelerations of the store mass center in the X_B, Y_B, and Z_B directions, respectively, ft/sec^2
$a_{Z,p}$	Acceleration of the aircraft in the Z_F direction, ft/sec^2 (see Fig. 12)
$C_{A,t}, C_N, C_Y$	Store measured (or predicted) axial-force, normal-force, and side-force coefficients, positive in the negative X_B, negative Z_B, and positive Y_B directions, respectively
$C_{A,o}, C_{N,o}$, $C_{Y,o}$	External input axial-force, normal-force, and side-force coefficients, respectively
C_ℓ, C_m, C_n	Store measured (or predicted) rolling-moment, pitching-moment, and yawing-moment coefficients, respectively; the positive vectors are coincident with the positive X_B, Y_B, and Z_B directions
$C_{\ell,o}, C_{m,o}$, $C_{n,o}$	External input rolling-moment, pitching-moment, and yawing-moment coefficients, respectively
$C_{\ell_p}, C_{m_q}, C_{n_r}$	Store roll-damping, pitch-damping, and yaw-damping derivatives, respectively, per radian
ΔC_m	Incremental value of pitching-moment coefficient used in the Ref. 8 flow-field math model
C_{m_α}	Pitching-moment coefficient derivative, per radian or per degree
C_{N_α}	Normal-force coefficient derivative, per radian or per degree

dC_m/dC_N	Static margin, reference lengths forward of the moment reference center
$\vec{F}$	Total force acting on the store, lb
F_{EI}	Total ejector force acting on the store, lb
$\Delta F'_{EI}$	Model ejector force augmentation to compensate for gravity deficiency, lb
$F_{E,X}, F_{E,Y}, F_{E,Z}$	Components of the ejector force acting on the store in the positive X_B, Y_B, and Z_B directions, respectively, lb
$F_{T,X}, F_{T,Y}, F_{T,Z}$	Components of the thrust force acting on the store in the positive X_B, Y_B, and Z_B directions, respectively, lb
F_X, F_Y, F_Z	Components of total force acting on a free-falling store in the positive X_B, Y_B, and Z_B directions, respectively, lb
g	Acceleration of gravity, ft/sec^2
$\Delta g'$	Model gravitational deficiency, ft/sec^2
$\vec{H}$	Angular momentum of a body rotating about its mass center, ft-lb-sec
$\vec{H}_o$	Angular momentum of a body rotating about a point other than its mass center, ft-lb-sec
H_X, H_Y, H_Z	Scalar components of the angular momentum ($\vec{H}$) about the X_B, Y_B, and Z_B axes, respectively, ft-lb-sec
h	Simulated pressure altitude, ft
I	Notation for the inertia matrix of a store which is calculated about the mass center (see Appendix B)
$\bar{I}$	Notation for the inertia matrix of a store which is calculated about a point (rotation center) other than the mass center (see Appendix B)

I_{XX}, I_{YY}, I_{ZZ}	Full-scale moments of inertia about the store X_B, Y_B, and Z_B axes, respectively, slug-ft^2, and referenced to the store mass center
$\bar{I}_{XX}, \bar{I}_{YY}, \bar{I}_{ZZ}$	Full-scale moments of inertia about the store X_B, Y_B, and Z_B directions, respectively, slug-ft^2, but referenced to a point (rotation center) other than the mass center
I_{XY}, I_{XZ}, I_{YZ}	Full-scale products of inertia in the store X_B-Y_B, X_B-Z_B, and Y_B-Z_B planes, respectively, slug-ft^2, and referenced to the store mass center
$\bar{I}_{XY}, \bar{I}_{XZ}, \bar{I}_{YZ}$	Full-scale products of inertia in the store X_B-Y_B,X_B-Z_B, and Y_B-Z_B planes, respectively, slug-ft^2, but referenced to a point (rotation center) other than the mass center
$\vec{i}, \vec{j}, \vec{k}$	Unit vectors along the store X_B, Y_B, and Z_B directions, respectively
ℓ_p	Probe extension length, in. (see Fig. 23)
ℓ_1, ℓ_2, ℓ_3	Store full-scale reference dimensions for pitching-moment, yawing-moment, and rolling-moment coefficients, respectively, ft
$M_{E,X}, M_{E,Y}, M_{E,Z}$	Components of ejector moment about the X_B, Y_B, and Z_B axes, respectively, ft-lb
$\vec{M}_o$	Total moment acting on the store, ft-lb
$M_{o,X}, M_{o,Y}, M_{o,Z}$	Scalar components of the total moment acting on the store about the X_B, Y_B, and Z_B axes, respectively, ft-lb
$M_{T,X}, M_{T,Y}, M_{T,Z}$	Components of the thrust moment acting on the store about the X_B, Y_B, and Z_B axes, respectively, ft-lb
M_X, M_Y, M_Z	Components of the total moment acting on a free-falling body about the X_B, Y_B, and Z_B axes, respectively, ft-lb
M_∞	Free-stream Mach number
ΔM_∞	Free-stream Mach number increment

m	Store mass, slugs
m_i	Store elemental mass, slugs
N_Z	Aircraft "g" loading factor
p,q,r	Store angular velocity about the X_B, Y_B, and Z_B axes, respectively; the positive vectors are coincident with the X_B, Y_B, and Z_B axes, rad/sec
q_p	Pitch rate of the aircraft during a pullup/pushover maneuver, rad/sec (see Fig. 12)
q_∞	Free-stream dynamic pressure, psf
R_ℓ, R_m, R_n	Full-scale body-axis restraining moments about the pivot (rotation center); the positive vectors are coincident with the positive X_B, Y_B, and Z_B directions, respectively, ft-lb
R_p	Effective rotation arm of the aircraft during a pullup/pushover maneuver, ft (see Fig. 12)
R_X, R_Y, R_Z	Full-scale body-axis pivot (rotation center) restraining forces, positive in the positive X_B, Y_B, and Z_B, directions, respectively, lb
$\vec{r}$	Distance from the mass center to an elemental mass, ft
$\vec{r}''$	Distance from the fixed frame of reference to the mass center, ft
$\vec{r}_i$	Distance from the rotation center to an elemental mass, ft
$\vec{r}_o$	Distance from the rotation center to the mass center, ft
$\vec{r}_o''$	Distance from the fixed frame of reference to the rotation center, ft
T_t	Free-stream total temperature, °R
T_∞	Free-stream static temperature, °R

t	Trajectory time from the instant of store release from the aircraft, sec
t'_E	Time of action of the model ejector, sec
U_A	Velocity of the aircraft at the simulated altitude, ft/sec
U_R	Total velocity of the full-scale store with respect to a space-fixed point, ft/sec
u,v,w	Velocities of the full-scale store relative to the origin of the flight-axis system in the positive X_B, Y_B, and Z_B directions, respectively, ft/sec
V_∞	Free-stream velocity, ft/sec
$\vec{v}$	Total velocity of the store mass center, ft/sec
$\vec{v}_i$	Velocity of the elemental mass with respect to a space-fixed point, ft/sec
$\vec{v}_o$	Velocity of the rotation center with respect to a spaced-fixed point, ft/sec
$v_{o,X}, v_{o,Y}, v_{o,Z}$	Scalar components of rotation center velocity ($\vec{v}_o$), positive in the positive X_B, Y_B, and Z_B directions, respectively, ft/sec
Wt	Full-scale store weight, lb
$\overline{W}_X, \overline{W}_Y, \overline{W}_Z$	Components of the full-scale store weight acting in the positive X_B, Y_B, and Z_B directions, respectively, lb (including effects of simulated dive or bank angles)
X,Y,Z	Separation distance of the store cg from the flight-axis system origin in the positive X_F, Y_F, and Z_F directions, respectively, ft, full scale
X_{cg}	Axial distance from the store nose to the cg location, ft, full scale
X_{El}	Distance from the mass center to the ejector line of action in the X_B direction, ft, positive forward

X_I, Y_I, Z_I	Separation of the store cg from the inertial-axis system origin in the positive X_I, Y_I, and Z_I directions, respectively, ft, full scale
X_o, Y_o, Z_o	Distances from the pivot (rotation center) to the store center of gravity along the X_B, Y_B, and Z_B axes, respectively, positive in the positive X_B, Y_B, and Z_B directions, ft, full scale
X_P, Y_P, Z_P	Separation distance of the store cg from the pylon-axis system origin in the positive X_P, Y_P, and Z_P directions, respectively, ft, full scale
$\Delta X_{m,cg}$	Axial distance from the store cg to the pitching-moment reference center, positive in the positive X_B direction, ft, full scale
$\Delta Z'$	Calculated adjustment to the observed store-model vertical displacement to correct for gravity deficiency and ejector-force augmentation effects, ft
α	Aircraft model angle of attack relative to the free-stream velocity vector, deg
α_s	Store model angle of attack, deg
α_{XY}	Sidewash angle with respect to the store longitudinal axis, positive inboard as seen by the pilot for aircraft left-wing data, deg
α_{XZ}	Upwash angle with respect to the store longitudinal axis, positive up as seen by the pilot, deg
$\Delta\alpha_s$	Incremental angle of attack on the store used in the Ref. 8 flow-field math model, deg or radians
γ	Simulated aircraft dive angle, positive for decreasing altitude, deg
θ	Angle between the store longitudinal axis and its projection in the X_F-Y_F plane, positive when the store nose is raised as seen by the pilot, deg (or radians)

θ_p	Rotation angle of the aircraft (flight-axis system) during a pullup/pushover maneuver, deg (see Fig. 12)
$\Delta\theta$	Angle between the store longitudinal axis and its projection in the X_P-Y_P plane, positive when the store nose is raised as seen by the pilot, deg
λ	Model scale factor
ϱ_∞	Free-stream density, slugs/ft^3
ϕ	Angle between the store lateral (Y_B) axis and the intersection of the Y_B-Z_B and X_F-Y_F planes, positive for clockwise rotation when looking upstream, deg
ψ	Angle between the projection of the store longitudinal axis in the X_F-Y_F plane and the X_F axis, positive when the store nose is to the right as seen by the pilot, deg
$\vec{\Omega}$	Angular velocity of the body-axis system, rad/sec
$\vec{\omega}$	Angular velocity of the body, rad/sec
$d(\vec{\ })/dt$	Total derivative of a vector parameter with respect to time such that $d(\vec{\ })/dt = \delta(\vec{\ })/\delta t + \vec{\Omega} \times (\vec{\ })$
$\delta(\vec{\ })/\delta t$	Partial derivative of a vector parameter with respect to time when the unit vectors have fixed directions, i.e., $\delta(\vec{\ })/\delta t = \vec{i}\,(\dot{\ })_X + \vec{j}(\dot{\ })_Y + \vec{k}(\dot{\ })_Z$
$\delta^2(\vec{\ })/\delta t^2$	Second partial derivative of a vector parameter with respect to time when the unit vectors have fixed directions, i.e., $\delta^2(\vec{\ })/\delta t^2 = \vec{i}\,(\ddot{\ })_X + \vec{j}\,(\ddot{\ })_Y + \vec{k}(\ddot{\ })_Z$
$(\dot{\ })$	A single dot denotes the first derivative of a scalar parameter with respect to time

$(\ddot{\ })$	A double dot denotes a second derivative of a scalar parameter with respect to time
$(\vec{\ })$	The arrow denotes a vector quantity
$(\ )'$	Primed quantities refer to model-scale dimensions or properties defined by the scaling laws or to wind tunnel operating parameters for the dynamic drop technique

INERTIAL-AXIS SYSTEM DEFINITIONS

Coordinate Directions

X_I	Parallel to the aircraft flight path direction at store release, positive forward as seen by the pilot
Y_I	Perpendicular to the X_I and Z_I directions, positive to the right as seen by the pilot
Z_I	Parallel to the aircraft plane of symmetry and perpendicular to the aircraft flight path direction at store release, positive downward as seen by the pilot

Origin

The inertial-axis system origin is coincident with the store cg at release and translates along the initial aircraft flight path direction at the free-stream velocity. The coordinate axes do not rotate with respect to the initial aircraft flight path direction.

FLIGHT-AXIS SYSTEM DEFINITIONS

Coordinate Directions

X_F	Parallel to the current aircraft flight path direction, positive forward as seen by the pilot
Y_F	Perpendicular to the X_F and Z_F directions, positive to the right as seen by the pilot

Z_F Parallel to the aircraft plane of symmetry and perpendicular to the current aircraft flight path direction, positive downward as seen by the pilot

Origin

The flight-axis system origin is coincident with the store cg at release. The origin is fixed with respect to the aircraft and thus translates along the current aircraft flight path at the free-stream velocity. The coordinate axes rotate to maintain alignment of the X_F axis with the current aircraft flight path direction.

PYLON-AXIS SYSTEM DEFINITIONS

Coordinate Directions

X_P Parallel to the store longitudinal axis at release and at constant angular orientation with respect to the current aircraft flight path direction, positive forward as seen by the pilot

Y_P Perpendicular to the X_P direction and parallel to the X_F-Y_F plane, positive to the right as seen by the pilot

Z_P Perpendicular to the X_P and Y_P directions, positive downward as seen by the pilot

Origin

The pylon-axis system origin is coincident with the flight-axis system origin and the store cg at release. It is fixed with respect to the aircraft and thus translates along the current aircraft flight path at the free-stream velocity. The coordinate axes rotate to maintain constant angular orientation with respect to the current aircraft flight path direction.

STORE BODY-AXIS SYSTEM DEFINITIONS

Coordinate Directions

X_B Parallel to the store longitudinal axis, positive direction is upstream at store release

Y_B Perpendicular to X_B and Z_B directions, positive to the right looking upstream when the store and aircraft are at zero yaw and roll angles

Z_B Perpendicular to the X_B direction and parallel to the aircraft plane of symmetry when the store and aircraft are at zero yaw and roll angles, positive downward as seen by the pilot when the store is at zero pitch and roll angles

Origin

The store body-axis system origin is coincident with the store cg at all times. The X_B, Y_B, and Z_B coordinate axes rotate with the store in pitch, yaw, and roll so that mass moments of inertia about the three axes are not time-varying quantities.